

**Early Synaptic Hippocampal Deficits In The Q175FDN Mouse
Model of Huntington Disease**

By:

Adam Shahin Ravalia

A thesis submitted to the school of graduate studies in partial fulfilment of the requirements for the degree of Master of Science in Medicine (Neuroscience)

Faculty of Medicine

Memorial University of Newfoundland

October 2019

St. John's

Newfoundland

Abstract

Huntington Disease (HD) is an inherited neurodegenerative disease caused by a CAG repeat expansion in the gene encoding the huntingtin protein. The resultant mutant huntingtin triggers numerous and severe neuronal abnormalities. Although motor deficits manifest during midlife, subtle cognitive aberrations can be detected prior to the onset of an overt behavioural phenotype. However, knowledge surrounding the cognitive deficits in the early stages of HD is scarce. Here, we studied hippocampal synaptic properties, including activity-dependent plasticity and nanoscale architecture in a mouse model of HD prior to the onset of motor symptoms. We focused on the hippocampus due to its involvement in cognitive function and the debilitating cognitive symptoms described by HD patients. Multi-electrode array recordings of synaptic activities revealed impairments in plasticity, while super-resolution microscopy elucidated clear alterations in synaptic nanoarchitecture of the hippocampus. Our data demonstrate detrimental effects of mHtt expression on hippocampal structure and function in presymptomatic HD.

Acknowledgements

First and foremost, I would like to extend my deepest, most sincere gratitude to my supervisor, Dr. Matthew Parsons for imparting his unfailing guidance, encouragement, and wisdom on both an academic and personal level. He has given much of his time to teach me valuable lessons, both scientific and in life, which will stay with me forever.

I would also like to thank my committee members, Dr. Michiru Hirasawa and Dr. Xihua Chen for their guidance and expertise throughout the duration of my M.Sc

I would like to thank all members of the Parsons lab, past and present, for always providing me with a lively and welcoming work environment. Particularly, Firoozeh Nafar has given me a tremendous amount of guidance, knowledge, and friendship and for that I would like to thank her.

To my family and friends (namely my cat, Frankie) the foundation of support you provide is something I will be forever grateful for.

Table of Contents

<i>Abstract</i>	<i>ii</i>
<i>Acknowledgements</i>	<i>iii</i>
<i>List of Tables</i>	<i>vii</i>
<i>List of Figures</i>	<i>vii</i>
<i>List of Abbreviations</i>	<i>ix</i>
<i>Co-Authorship Statement</i>	<i>xii</i>
<i>1-0 Introduction</i>	<i>1</i>
1-1 Overview of Huntington disease.....	1
1-2 Motor symptoms associated with Huntington Disease.....	2
1-3 Psychiatric and cognitive symptoms associated with Huntington Disease.....	3
1-4 The hippocampus.....	6
1-5 Early cognitive dysfunction in animal models of Huntington Disease.....	9
1-6 Synaptic plasticity & transmission.....	15
1-7 Dysfunction of the cortico-striatal synapse in prodromal Huntington Disease.....	20
1-8 Dysfunction of the hippocampus in prodromal Huntington Disease.....	22
1-9 Multi-electrode array electrophysiology.....	24
1-10 Super-resolution imaging.....	25
1-11 Hypothesis and aims.....	27

<i>2-0 Methods</i>	29
2-1 Animals	29
2-2 Slice preparation	29
2-3 Multi-electrode array electrophysiology	30
2-4 Chemical-LTP	31
2-5 Immunohistochemistry.....	32
2-6 Super-resolution imaging	33
2-7 Experimental design and statistics.	34
2-8 N-values	36
<i>3-0 Results</i>	37
3-1 Increased basal transmission in the hippocampus of presymptomatic Huntington disease mice revealed using multi-electrode array electrophysiology.....	37
.....	45
3-2 Deficits in hippocampal synaptic plasticity in presymptomatic Huntington disease mice revealed using multi-electrode array electrophysiology.	46
.....	52
3-3 Super-resolution radial fluctuation (SRRF) imaging of GluA2 and Synaptophysin across the stratum radiatum in WT and Heterozygous mice.....	53
3-4 SRRF imaging of GluA2 in proximal stratum radiatum in WT and heterozygous mice.....	54
3-5 SRRF imaging of GluA2 in distal stratum radiatum in WT and heterozygous mice.	59

3-6 SRRF imaging of synaptophysin in proximal stratum radiatum in WT and heterozygous mice.	63
3-7 SRRF imaging of Synaptophysin in distal stratum radiatum in WT and heterozygous mice.	67
.....	70
3-8 Nearest neighbour analysis of GluA2 and Synaptophysin along stratum radiatum in WT and heterozygous mice.	71
<i>4-0 Discussion</i>	77
4-1 Early synaptic deficits in HD	79
4-2 TBS and HFS LTP in presymptomatic HD	81
4-3 Pre and post-synaptic aberrations in early HD.....	83
4-4 Nanoscale investigation of synapses	85
4-5 Investigation of synaptic nanoarchitecture via super-resolution imaging	86
4-6 Early changes in synaptic nanoarchitecture in HD via SRRF	87
4-7 Caveats & Future Direction	93
4-8 Interpretations & Conclusion	94

List of Tables

Table 1. Relevant models of HD.....	12
-------------------------------------	----

List of Figures

Figure 1. Schematic of basal transmission and LTP induction.....	19
Figure 2. Schematic of MEA (MED64) hippocampal acute slice and electrode array placement	41
Figure 3. Input-Output (I/O) responses across stratum radiatum in WT and heterozygous mice.....	43
Figure 4. Input-Output (I/O) responses within genotype across stratum radiatum.....	45
Figure 5. HFS-LTP experiments across stratum radiatum in WT and heterozygous mice	51
Figure 6. TBS-LTP experiments across stratum radiatum WT and heterozygous mice....	53
Figure 7. SRRF imaging of GluA2 in proximal stratum radiatum in WT control, WT cLTP, Het Control, and Het cLTP tissue	58
Figure 8. SRRF imaging of GluA2 in distal stratum radiatum in WT control, WT cLTP, Het Control, and Het cLTP tissue	62
Figure 9. SRRF imaging of SYN in proximal stratum radiatum in WT control, WT cLTP, Het Control, and Het cLTP tissue	66

Figure 10. SRRF imaging of SYN in distal stratum radiatum in WT control, WT cLTP, Het Control, and Het cLTP tissue 70

Figure 11. NN analysis of SRRF images for GluA2 and SYN in proximal stratum radiatum in WT control, WT cLTP, Het Control, and Het cLTP tissue 74

Figure 12. NN analysis of SRRF images for GluA2 and SYN in distal stratum radiatum in WT control, WT cLTP, Het Control, and Het cLTP tissue 76

Figure 13. Summary of SRRF size, intensity, and density results 77

List of Abbreviations

aCSF: Artificial Cerebrospinal Fluid

AD: Alzheimer Disease

AMPA: *α*-amino-3-hydroxy-5-methyl-4-isoxazolepropionic receptor

BDNF: Brain-Derived Neurotrophic Factor

CAG: Cytosine, Adenine, Guanine

cLTP: Chemical Long Term Potentiation

CNS: Central Nervous System

CREB: cAMP Response Element Binding

DAPI: 4',6-diamidino-2-phenylindole

DG: Dentate Gyrus

EM-CCD: Electron-multiplying charge-coupled device

EPSPs: Excitatory Post-Synaptic Potentials

ERK: Extracellular Signal Regulated Kinase

fEPSP: Field Excitatory Post-Synaptic Potential

fMRI: Functional Magnetic Resonance Imaging

HD: Huntington Disease

Het: Heterozygous

HFS: High Frequency Stimulation

Htt: Huntingtin Protein

Hz: Hertz

IHC: Immunohistochemistry

I/O: Input/Output

JNK-MAPKs: c-JUN-N-terminal kinase-mitogen-activated protein kinases

KI: Knock-IN

LED: Light-emitting diode

LTD: Long Term Depression

LTP: Long Term Potentiation

MEA: Multi-Electrode Array

mHtt: Mutant Huntingtin Protein

mM: Millimolar

MRI: Magnetic Resonance Imaging

MSNs: Medium Spiny Neurons

NMDAR: N-Methyl-D Aspartate Receptor

NN: Nearest Neighbour

PALM: Photoactivated Localization Microscopy

PET: Positron Emission Tomography

PKA: Protein Kinase A

PSD: Post-Synaptic Density

RM: Repeated Measures

ROI: Region of Interest

SIM: Structured Illumination Microscopy

SRRF: Super Resolution Radial Fluctuation

STED: Stimulated Emission Depletion

STORM: Stochastic Optical Reconstruction Microscopy

SYN: Synaptophysin

TBS: Theta Burst Stimulation

UBC: University of British Columbia

UHDRS: Unified Huntington Disease Rating Scale

WT: Wild-type

μ l: Microliter

μ m: Micrometer

Co-Authorship Statement

All experiments were conducted by myself, Adam Ravalia. Electrophysiological and SRRF analyses were conducted by myself with the help of Dr. Matthew Parsons.

1-0 Introduction

1-1 Overview of Huntington disease

Huntington Disease (HD) is an autosomal dominant neurodegenerative disorder with midlife onset characterized by an array of motor, cognitive, and psychiatric symptoms. It affects approximately 1 in 10,000 people globally (Fisher and Hayden, 2014), with death usually occurring 12-15 years after motor symptom onset. HD is caused by a cytosine, adenine, and guanine (CAG) repeat expansion on chromosome 4, which translates into an aberrantly long polyglutamine tract at the N-terminus of the huntingtin protein (htt);(MacDonald et al., 1993; Ravikumar et al., 2004). The age of HD onset is inversely correlated with the length of the CAG repeat expansion. In patients who have 36-39 repeats, penetrance is variable, with full penetrance arising at 40 or more repeats (Ross et al., 2014). Moreover, age of onset as well as rate of progression of HD are likely to be influenced by environmental and genetic factors (Wexler et al., 2004). According to current criteria, onset is characterized as the point when a person develops explicit presence of otherwise unexplained extrapyramidal movement symptoms such as hyperkinetic “dancelike” movements known as chorea (Hogarth et al., 2005).

Htt is a cytoplasmic protein that is highly expressed in human tissue, particularly in the brain in areas such as the striatum and cerebral cortex. Unlike many other proteins of similar size (348 kDa), Htt is completely soluble and ubiquitously expressed both within and outside the central nervous system (CNS);(Cattaneo et al., 2005). Htt is imperative for embryonic development and plays a role in physiological intracellular processes such as gene transcription, protein and organelle trafficking, and mitochondrial

function (DiFiglia et al., 1995; Nasir et al., 1995; Cattaneo et al., 2005; Sepers and Raymond, 2014). Previous research indicates that mutant huntingtin (mHtt) protein's toxicity is directly related to the CAG repeat length described above (Andrew et al., 1993; Snell et al., 1993). More recently it has been suggested that loss of normal or wild-type (WT) huntingtin function may also contribute to the pathogenesis of HD. It is known that increased WT huntingtin expression improves CNS cell survival and helps to mitigate the effect of mutant protein (Rigamonti et al., 2000; Zuccato et al., 2001, 2003). Furthermore, total knock-out of WT huntingtin is lethal to mice in utero, and deletion of the WT allele in animal models of HD causes exacerbated neuropathology (Bates, 2003; Gauthier et al., 2004; Van Raamsdonk et al., 2005a).

1-2 Motor symptoms associated with Huntington Disease

The motor component of HD can broadly be divided into two categories. The first category encompasses involuntary movements, specifically chorea (Ross et al., 2014). HD is often referred to as Huntington chorea and chorea was first described by George Huntington in 1872 as “the name given to the disease on account of the dancing propensities of those who are affected by it” (Huntington, 1872). It can also be classified as the occurrence of rapid, irregular, and arrhythmic uncontrolled movement (Smith et al., 2000). Chorea is most prominent in adult-onset HD and gives the disease its stereotypical clinical manifestation of uncontrolled and sporadic movement. The second category involves impairment of voluntary movements and includes bradykinesia and rigidity. This aspect of the disease tends to appear in the late stages of HD and progresses more steadily than chorea (Rosenblatt et al., 2006). The motor dysfunction associated with HD stems

from significant and progressive atrophy of the basal ganglia, particularly the caudate nucleus and putamen, where the rate of atrophy is greater for patients with earlier onset of symptoms (Aylward et al., 1997). This atrophy involves loss of neurons in conjunction with astrogliosis (Vonsattel et al., 1985). Moreover, the involuntary movement component associated with HD is most often attributed to interruption of motor and cognitive basal ganglia loops. The loss of enkephalin-containing medium spiny neurons (MSNs) in the striatum that are part of the indirect pathway has been measured as decreased striatal dopamine D2 receptor binding with Positron Emission Tomography (PET);(Alexander et al., 1986; Reiner et al., 1988; Albin et al., 1989). Moreover, the preferential degeneration of MSNs in the indirect pathway from the caudate nucleus to the globus pallidus external reduces inhibitory control of the indirect pathway, resulting in choreic movements (Crook and Housman, 2012).

1-3 Psychiatric and cognitive symptoms associated with Huntington Disease

Although motor aberrations associated with HD do not usually manifest until the fourth or fifth decade of a patient's life, a wide array of research has shown that subtle abnormalities in psychiatric and cognitive functioning are present much earlier. This period of pre-motor symptomology is known as the prodrome (i.e. presymptomatic). The investigation into early psychiatric and cognitive symptoms of HD could help mitigate the detrimental effects on day-to-day functioning and quality of life. Psychiatric manifestations in HD include depression, apathy, irritability, obsessions, and occasionally psychosis (Paulsen et al., 2001; Julien et al., 2007; van Duijn et al., 2007). As previously stated, there is a direct association between the number of CAG repeats and age of onset

of motor symptoms in HD; however, there has been a reported unexplained temporal variability in the presentation and severity of psychiatric symptoms (Epping et al., 2016). To investigate this unexplained temporal variability, TRACK-HD was developed. TRACK-HD is a multinational longitudinal observational study in presymptomatic participants carrying the HD mutation designed similarly to a clinical trial. It employs rapid study design and data acquisition, stringent quality control, and blinded data analysis (Tabrizi et al., 2009). The primary aim of TRACK-HD is to provide advances in methodologies for disease-modifying clinical trials. TRACK-HD utilizes the known genetic cause of HD to optimize detection of psychiatric and cognitive changes in carriers of the HD gene who have yet to exhibit motor symptoms (Tabrizi et al., 2011). Interestingly, data from TRACK-HD indicated a significant increase in apathy over a 36-month period in pre-clinical HD mutation carriers. This is indicative of a more clear linear progression of psychiatric symptomology than previously understood (Tabrizi et al., 2013).

Cognitive impairments and how they relate to the pathophysiology and progression of HD are a little more widely studied than their psychiatric counterpart, however are still quite ambiguous. It is well known that cognitive impairments materialize years before the clinical diagnosis of HD, in the prodromal period. These impairments include poor performance on evaluations of attention, working memory, episodic memory, processing speed, psychomotor functions, emotional processing, and executive function (Paulsen et al., 2001; Johnson et al., 2007; Stout et al., 2007, 2011). There is no standard battery of testing for the cognitive assessment of HD, although many clinicians rely on the Unified Huntington Disease Rating Scale (UHDRS). This scale

includes the symbol digit modality test, the Stroop color word test, and a verbal fluency test (Huntington Study Group, 1996). Research suggests that cognitive impairment is one of the most debilitating aspects of the disease and is most highly associated with functional decline (Nehl et al., 2004; Paulsen, 2011). The cognitive symptoms associated with HD often develop approximately 15 years prior to the motor diagnosis and are tightly related to brain volume loss on Magnetic Resonance Imaging (MRI);(Aylward et al., 2011).

Many researchers attribute impairments in cognitive function in HD to dysfunction of the striatum and fronto-striatal circuits (Vonsattel et al., 1985; Snowden et al., 2002). One of the most common and persistent cognitive deficits observed in HD patients during pre-clinical stages is difficulty in tasks requiring a shift in strategy (Marder et al., 2000). Interestingly, this abnormal response is thought to stem from the inability to inhibit a previously learned response and is likely mediated by the interaction between striatal neurons and neighboring aspiny cholinergic interneurons (Swerdlow et al., 1995; Mink, 1996). Impairment in cortico-striatal function also holds true in neuro-imaging studies. A study employing functional MRI (fMRI) described decreased activity in both the frontal cortex and putamen of presymptomatic HD patients undergoing a serial reaction time test (Kim et al., 2004). At more advanced stages, dementia increasingly develops, resulting in alterations in a multitude of cognitive functions including slow information processing, depression, apathy, and changes in personality (Paulsen et al., 1995).

Along with the plethora of research surrounding the cortico-striatal system, it is also becoming increasingly evident that HD is a brain wide phenomenon, with emphasis

being placed on extrastriatal regions. HD patients in the prodromal period display significantly delayed response latencies on a pattern-recognition task in comparison to non-carriers (Lawrence et al., 1998). Furthermore, presymptomatic HD mutation carriers display aberrations in associative learning and spatial working memory on a foraging-for-reward task involving searching for tokens through a number of colored boxes (Lawrence et al., 2000; Berrios et al., 2002). These studies suggest an involvement of the hippocampus, a brain area imperative for cognitive function, specifically in learning and memory. As a result of the brain-wide nature of HD, researchers and clinicians alike are continuing to develop techniques such as powerful microscopy paradigms and cognitive clinical testing to further investigate outcomes related to HD that may offer insight into the cellular pathophysiology and subsequent progression of the disease. It is of utmost importance to identify the earliest detectable cellular abnormalities associated with HD, in order to initiate pre-clinical investigation into targeted treatments for the disease.

1-4 The hippocampus

The hippocampal formation, one of the most widely studied neuronal systems in the brain, is a seahorse shaped structure located deep in the medial temporal lobe (Bird and Burgess, 2008). There are three well-studied anatomical subdivisions of the hippocampus: CA1, CA3, and dentate gyrus (DG). The principle neurons in the CA regions are known as pyramidal neurons and they comprise about 90% of all neurons in these regions. Recently, it has been established that there is a high amount of heterogeneity among cell populations in the hippocampus, where a high degree of transcriptional variability across the long axis of hippocampus has been described

(Cembrowski et al., 2016). Specifically, excitatory pyramidal cells in CA1 and CA3, as well as granule cells, previously considered to be homogenous populations, show a striking degree of molecular diversity along the long axis (dorsal-ventral) obtained by examination of gene expression patterns (Thompson et al., 2008; Cembrowski et al., 2016). Notably, this dorsal-ventral heterogeneity can exhibit even further organizational boundaries. For example, CA3 pyramidal cells have been shown to form discrete subpopulations, with over 300 genes identified with robust regionalized expression patterns, while CA1 pyramidal cells and DG granule cells do not show the same subpopulation conformity (Thompson et al., 2008; Cembrowski et al., 2016).

The hippocampus is imperative for acquisition, temporary storage, and retrieval of explicit memory for facts and events (i.e. declarative memory);(Zola-Morgan and Squire, 1990). Patients with selective damage to the hippocampus exhibit impairments in acquiring new, consciously accessible memories while short-term memory, priming, and procedural learning that were acquired before the damage are often preserved (Zola-Morgan et al., 1986; Milner et al., 1998). It is becoming clear that the hippocampus plays a much more complex role in cognitive processes than its function in declarative memory; and has been highly implicated in spatial cognition. It was shown that rats placed in an open field to measure spatial memory exhibited high firing rates of particular cells, known as “place cells” in the hippocampus when in a particular place and orientation. Conversely, when the animal is in other locations in the open area, the same cells show no firing (O’Keefe and Dostrovsky, 1971). The hippocampus has also been implicated in temporal processing. For example, researchers have investigated hippocampal responses during trace-associative eyeblink conditioning. They wanted to assess hippocampal

neuronal firing patterns during the time period between an auditory cue and a delivered air puff to the eye. It was found that hippocampal pyramidal neurons fire repeatedly over the period of time between the conditioned stimulus (auditory cue) and unconditioned stimulus (puff to the eye), appearing to serve as a “time-keeping” or anticipatory role (McEchron and Disterhoft, 1997; McEchron et al., 2003). Moreover, the hippocampus has been implicated in the ability of rats to remember the sequences of odor presentation. It was found that hippocampal lesions produced an impairment in the ability of rats to remember the presentation of odors over an extended period of time, despite an intact ability to remember odors they recently encountered (Agster et al., 2002; Fortin et al., 2002). The hippocampus has also been implicated in formation of in-depth representations of complex environmental cues. A non-matching-to-sample test involving olfactory cues in small cups in numerous locations within an open field was conducted with rats. In this task, the animal had to learn that if the odor in any cup did not match the odor presented immediately previous to it, they would receive a reward. During this task, researchers observed hippocampal cells firing specifically to place, odor, as well as cells that fired selectively on an odor match or non-match (Wood et al., 1999). Again, this study helps to highlight the complex and multifaceted nature of the hippocampus.

Taking all these pieces of evidence into consideration, it is apparent that the hippocampus plays vital and complex roles in an array of cognitive processes. Unfortunately, hippocampal involvement in the highly burdensome cognitive deficits observed during the progression of HD has hardly been studied and requires much more in-depth and precise research. The hippocampus is of specific importance because the majority of hippocampal deficits in HD have been characterized only in late-stage

(symptomatic) models, therefore it is plausible that these deficits are manifesting much earlier on in disease progression when early cognitive deficits are seen. Utilizing novel and more sensitive measures to investigate the properties of hippocampus can help researchers determine whether the presymptomatic HD accompanies deficits in synaptic structure and/or plasticity in the hippocampus that are contributing to the pathophysiology of the disease.

1-5 Early cognitive dysfunction in animal models of Huntington Disease

The modelling and subsequent investigation of disease in animals is a hallmark of the scientific field. With rapid gestation and lifecycle periods, in combination with many similar anatomical and physiological features to humans, modelling and investigating human disease in a variety of animal species has led to many impactful scientific discoveries. In the case of HD, several different mouse models have been developed based on the known single gene mutation, which may recapitulate many critical neuroanatomical and physiological CNS features of HD patients (Dalley et al., 2004),. Many of these models exhibit significant similarities to the human disease, but are also significantly different (Brooks and Dunnett, 2013);(Table. 1). For the purposes of this thesis, we utilized a clinically relevant mouse model of HD, Q175FDN. This model of HD, specifically the heterozygous knock-in (KI) used for all experiments in this thesis, shows slowly progressing disease phenotype, expresses human *mhtt*, and closely resembles the genetic mutation that causes HD, and for this reason is a valuable model for pre-clinical investigation (Southwell et al., 2016). The Q175FDN model has an excised floxed neomycin (neo) cassette that is known to interfere with *mhtt* gene expression,

specifically causing partial loss of gene function, making the redesigned Q175FDN model a more relevant mouse line than its predecessors (Southwell et al., 2016). It is important to note that heterozygous Q175FDN mice do not exhibit any detectable behavioural deficits until 6 months of age (Southwell et al., 2016), and all of the experiments for this thesis were carried out at 3 months of age.

Table 1. Mouse models of Huntington Disease.

Table adapted from (Menalled and Chesselet, 2002; Gray et al., 2008; Menalled et al., 2012; Pouladi et al., 2013; Southwell et al., 2016).

Model	Transgene Product	Promotor	CAG Repeat Length	Earliest abnormal behaviour	Age at death
<i>Truncated N-terminal fragment models</i>	<i>Express shortened fragments of mhhtt and typically exhibit a rapid onset of symptoms.</i>				
R6/1	67 amino acids of N-terminal fragment (human <i>htt</i>)	1 kb human <i>htt</i> promoter	116	15-21 weeks (wheel clasping)	32-40 weeks
R6/2	67 amino acids of N-terminal fragment (human <i>htt</i>)	1 kb human <i>htt</i> promoter	144	5-6 weeks (motor deficits)	10-13 weeks
HD94	67 amino acids of N-terminal fragment (chimeric human <i>htt</i> :mouse <i>htt</i> exon 1)	CamkIIa	94	4 weeks (wheel clasping)	Normal lifespan
<i>Full-length models (knock in)</i>	<i>Transgenic models involve human mhhtt being inserted into the mouse genome. The mouse will express this mutant gene in addition to two normal copies of endogenous mouse htt.</i>				
HdhQ92	Full-length chimeric human <i>htt</i> exon 1:mouse <i>htt</i>	Endogenous mouse <i>htt</i> promoter	92	Not observed (up to 17 months)	Normal lifespan
HdhQ111	Full-length chimeric human <i>htt</i> exon 1: mouse <i>htt</i>	Endogenous mouse <i>htt</i> promoter	111	24 months (gait deficits)	Normal lifespan
Hdh94	Full-length chimeric human <i>htt</i>	Endogenous mouse <i>htt</i> promoter	94	2 months (mild hyperkinesia)	Normal lifespan

	exon1: mouse <i>htt</i>				
zQ175	Full-length chimeric human <i>htt</i> exon1: mouse <i>htt</i>	Endogenous mouse <i>htt</i> promoter	188	4 weeks (homozygous-grip strength) 4.5 months (heterozygous-reduced rearing in open field)	Significantly reduced lifespan reported (sudden death from seizures in homozygous)
*Q175FDN	Full-length chimeric human <i>htt</i> exon1: mouse <i>htt</i> – excised neo cassette from Q175F mice generating a new line	Endogenous mouse <i>htt</i> promoter	>200	3 months (homozygous-object recognition/object location deficits) 6 months (object recognition deficits)	Homozygous-death observed at 9 months Heterozygous death observed at 13 months
<i>Full-length models (transgenic)</i>	<i>Created using yeast artificial chromosome (YAC) or bacterial artificial chromosome (BAC) technology. Such models express human genomic mutant <i>htt</i> transgenes. Behavioural and neurodegenerative phenotypes tend to be more severe than KI models</i>				
YAC128	Full-length human <i>htt</i>	Human <i>htt</i> promoter and regulatory elements (24 kb upstream, 117 kb downstream)	128	6 months (rotarod deficits)	Not reported
YAC72	Full-length human <i>htt</i>	Human <i>htt</i> promoter and regulatory elements	72	7 months (hyperkinesia)	Not reported
BACHD	Full-length human <i>htt</i>	Human <i>htt</i> promoter and regulatory elements (20 kb upstream, 50 kb downstream)	97	2 months (subtle rotarod deficits)	Not reported

*** Q175FDN heterozygous mice used for all reported experiments in this thesis**

As previously mentioned, increased focus in both basic research and clinical settings is being placed upon identifying and characterizing cognitive abnormalities associated with HD. However, this area of HD is still remarkably understudied in relation to its reported burden on family members and caretakers, as well as the burden on the HD patient themselves. Cognitive decline in HD is highly associated with loss of functionality, and can be predictive of institutionalization (Paulsen, 2011). In mouse models of HD, the most widely reported behavioural deficit associated with cognition error is in reversal learning. Specifically, these mice show significant deficits in learning to efficiently locate a submerged platform after the location of the platform shifted during Morris water maze tasks (Murphy et al., 2000; Brooks et al., 2012). The neurological circuitry underlying this deficit is well known to be associated with the hippocampus as well as the anterior cingulate and orbitofrontal cortices. This may mediate a positive-feedback response in the fronto-striatal-thalamic loop (Clarke et al., 2008; Hampshire et al., 2012; Klanker et al., 2013). Furthermore, visual discrimination learning and tactile-dependent learning, both of which are mediated by hippocampal function, are significantly altered in the R6/1 model HD mice (Mazarakis et al., 2005; Giralt et al., 2009). Landmark studies have demonstrated that transcription of the pro-survival factor brain-derived neurotrophic factor (BDNF) is increased by Htt and reduced by mHtt (Zuccato et al., 2001, 2003). BDNF has emerged as an important regulator of synaptic plasticity and is expressed in areas of the brain imperative to cognitive function such as the neocortex, hippocampus, cerebellum, and amygdala (Kawamoto et al., 1996; Kafitz et al., 1999). Reduced BDNF expression is observed in the striatum of presymptomatic YAC72 HD mice (Zuccato et al., 2001).

Cognitive testing designed to assess dysfunction in HD mice has revealed impaired hippocampal function. Specifically, spatial learning and navigation memories are abnormal in R6/1, R6/2, and Hdh^{Q7/Q111} mouse models of HD. Hippocampal protein kinase A (PKA) activity contributes to R6/1 and R6/2 abnormalities. Increased PKA activity results in the hyper-phosphorylation of several membranous PKA substrates, occluding normal PKA-dependent processes, thus contributing to the deficits in learning and memory observed (Giralt et al., 2011). Furthermore, PKA pathway aberrations in Hdh^{Q7/Q111} mice are associated with reduced hippocampal expression of cAMP response element binding (CREB) binding protein and diminished levels of histone H3 acetylation (Giralt et al., 2012). Neuronal CREB-mediated transcription regulates synaptic plasticity, mitochondrial function, and cell survival (Harjes and Wanker, 2003). In addition, in a study examining neurogenesis in the sub-ventricular zone and sub-granular zone of DG, hippocampal cell proliferation and neurogenesis were significantly reduced in R6/2 HD mice when compared to wild-type (WT) controls (Gil et al., 2005). Although the cellular and synaptic underpinnings of cognitive dysfunction are well documented in early-to-late symptomatic HD, with the majority of research being completed at this symptomatic stage, there is a substantial gap in the literature in relation to the earliest synaptic abnormalities that appear in the hippocampus of presymptomatic HD mutation carriers.

1-6 Synaptic plasticity & transmission

Synaptic plasticity, the activity-dependent modification of synapses, is an efficacious mechanism for shaping and adjusting the response properties of neurons (Abbott and Nelson, 2000). Long-term potentiation (LTP) and long-term depression

(LTD) of synaptic strength provide the framework for the majority of models of learning and memory. LTP was first described in 1973 when brief trains of high-frequency stimulation (HFS) were delivered to monosynaptic excitatory pathways in rabbit hippocampus and resulted in a sustained increase in the strength of synaptic transmission (Bliss and Lømo, 1973). LTP is expressed as a continual increase in the size of the evoked response, recorded from an individual neuron or populations of neurons (fig. 1).

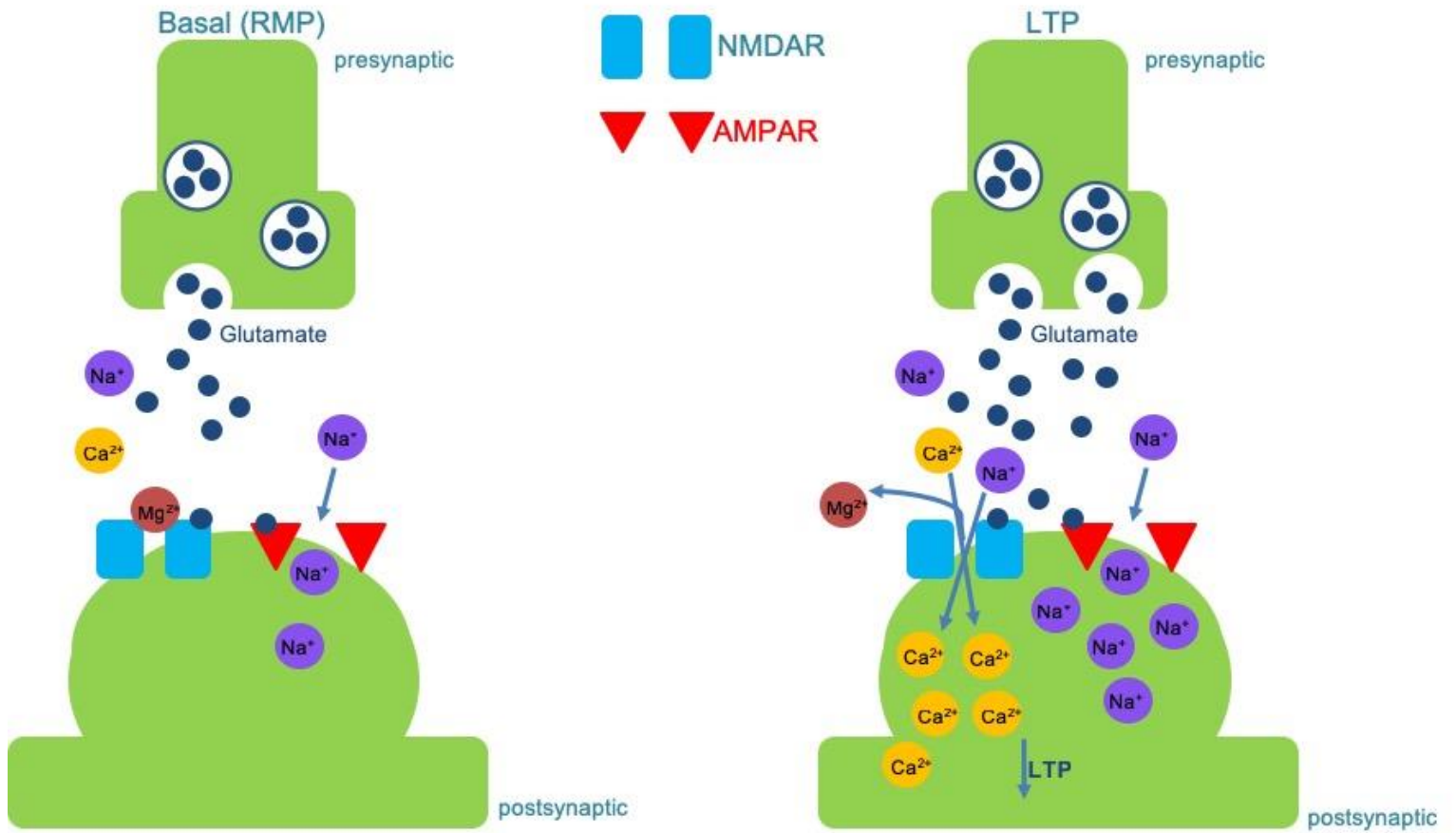
It is widely accepted that many forms of LTP induction require the activation of postsynaptic *N*-Methyl-*D*-Aspartate receptors (NMDARs), a subtype of glutamate receptor. Although NMDAR-independent LTP is also a widely established phenomenon (Komatsu et al., 1991; Kanterewicz et al., 2000), here the focus will be on NMDAR-dependent LTP. NMDAR activation requires depolarization of the postsynaptic cell, which is accomplished by repetitive and tetanic stimulation of synapses (Nicoll and Malenka, 1995). During fast excitatory synaptic transmission, glutamate binds to α -amino-3-hydroxy-5-methyl-4-isoxazolepropionic receptors (AMPA) which are ion channels permeable to monovalent cations (Na^+ , K^+) and provide the majority of inward current associated with post-synaptic responses. Furthermore, AMPARs that lack the specific subunit GluA2 are also permeable to the divalent cation Ca^{2+} (Man, 2011). The influx of positive current generated causes the postsynaptic cell to depolarize, allowing Mg^{2+} to dissociate from its position blocking the channel of NMDARs, granting Ca^{2+} to enter the cell. The subsequent rise in intracellular Ca^{2+} activates the downstream cellular pathways such as PKA and calpain that increase synaptic efficacy, resulting in LTP (Lu et al., 2001).

LTP can be induced in many ways, most often by delivering tetanic stimulation to the neuronal pathway of interest (Bliss and Collingridge, 1993). The two most common forms of LTP induction by means of tetanic stimulation are theta-burst stimulation (TBS) and HFS. TBS most often consists of 10 bursts of 4-5 pulses at 100 Hz delivered at 200 millisecond intervals (Abraham and Huggett, 1997). TBS is a physiologically-relevant stimulation paradigm and mimics two aspects of hippocampal physiology: spike discharges of pyramidal neurons and regulation of these cells during hippocampal theta rhythm (4-12 Hz);(Buzsáki, 2002; Larson and Munkácsy, 2015). HFS protocols are most typically executed at 100 Hz for 1 second (Bliss and Collingridge, 1993). Although widely used and extremely effective, HFS lacks the same physiological relevance as TBS (Albeni et al., 2007). LTP can also be induced chemically (cLTP) in a number of ways. The most common method involves bathing organotypic slices in glycine, a NMDAR co-agonist, as well as artificial cerebrospinal fluid (aCSF) containing no magnesium. The lack of Mg^{2+} in this solution removes the Mg^{2+} from NMDAR receptors, allowing the influx of positive cations. (Otmakhov et al., 2004; Kopec et al., 2006). Although LTP is triggered within seconds for the protocols we describe above, it can last for hours in vitro and up to days in vivo (Malenka and Nicoll, 1999).

Figure 1. Schematic of basal transmission and LTP induction.

Image on the left depicts synaptic transmission during basal conditions. RMP stands for “resting membrane potential”. In this image, we can see that the post-synaptic side is not depolarized therefore the Mg^{2+} block remains in the NMDAR and LTP cannot occur.

Image on the right depicts synaptic transmission during LTP induction. Here, the post-synaptic cell has depolarized sufficiently to cause the Mg^{2+} block to be removed from the NMDAR triggering an influx of Ca^{2+} and subsequent LTP. Adapted from (Malenka and Nicoll, 1999).



1-7 Dysfunction of the cortico-striatal synapse in prodromal Huntington Disease

Electrophysiological studies in striatal slices derived from HD mouse models have revealed clear evidence for early neuronal dysfunction. For example, striatal neurons of presymptomatic R6/2 mice showed increased cell-membrane input resistance, lower stimulus intensity to evoke action potentials, and reduced paired-pulsed facilitation in comparison to WT controls (Klapstein et al., 2001). Furthermore, in presymptomatic 1-month old YAC128 mice, pre-synaptic glutamate release and AMPAR-mediated synaptic currents were significantly increased, corresponding to an increased responsiveness of MSNs to cortical stimulation. Increased glutamate release could contribute to increased neuronal excitotoxicity and subsequent damage of the striatum (Joshi et al., 2009).

Many studies have also observed early alterations in NMDAR activity in the striatum of HD mice. A significant alteration in NMDAR-mediated transmission in presymptomatic HD mice is seen as the persistent reduction of Mg^{2+} sensitivity. As previously mentioned, when the cell membrane is hyperpolarized or at rest, NMDAR channels are blocked by Mg^{2+} . In a subset of striatal cells in an R6/2 model of HD however, NMDARs are activated at more hyperpolarized potentials, which could be detrimental to cell function (Starling et al., 2005). Moreover, there is a distinct link between the NMDAR subunit GluN2B, which is enriched in the striatum, and the effects of mHtt (Landwehrmeyer et al., 1995; Li et al., 2003). It has been suggested that GluN2B containing NMDARs are preferentially linked to cell death signaling pathways when compared with GluN2A containing NMDARs (Tu et al., 2010). Overexpression of the GluN2B subunit in HD mice has been shown to exacerbate HD-like pathology (Heng et al., 2009). In addition to subunit composition, the subcellular localization of NMDARs is

thought to play a pivotal role in determining whether the downstream intracellular signaling cascades promote cell-survival or stimulate cell death. This “localization hypothesis” posits that the activation of synaptic NMDARs promotes cell survival, while activation of extrasynaptic NMDARs promotes cell death (Hardingham et al., 2002). This hypothesis involves the concept that depending where in the cellular domain the receptor is located relative to the synapse, it will activate distinct downstream signaling cascades related to cell survival and plasticity, or cell death. A major outcome of synaptic NMDAR activation is increased phosphorylation and activity of an important transcriptional regulator CREB (Hardingham et al., 2001). Synaptic transmission promotes the expression of a multitude of anti-apoptotic, anti-oxidant, and pro-survival proteins including BDNF (Favaron et al., 1993; Hansen et al., 2004; Papadia et al., 2008). Conversely, increased extrasynaptic NMDAR expression, current, and associated reductions in CREB activation were observed in the striatum of YAC128 mice. In this case, extrasynaptic NMDAR activation promotes cell death (Milnerwood et al., 2010). Activation of extrasynaptic NMDARs results in CREB deactivation, release of apoptotic factors such as a result of mitochondrial calcium overload, and activation of cell death signaling p38 and c-JUN-N-terminal kinase-mitogen-activated protein kinases (JNK-MAPKs);(Ivanov et al., 2006; Papadia et al., 2008; Hardingham and Bading, 2010; Parsons and Raymond, 2014). Furthermore, it has been suggested that GluN2B containing receptors are found predominately at extrasynaptic locations (Barria and Malinow, 2002). These findings suggest that glutamate release probability, receptor subcellular localization, and downstream signaling cascades are altered in the cortico-striatal system at an early age in HD (Milnerwood and Raymond, 2007).

1-8 Dysfunction of the hippocampus in prodromal Huntington Disease

Although aberrations in synaptic transmission are well documented in the cortico-striatal system in prodromal HD, research surrounding early synaptic dysfunction in hippocampus is largely incomplete. There is however, some documented research classifying other types of deficits in the hippocampus of HD mice. Specifically, it was found that in newborn R6/2 mice, cell proliferation was compromised and granule cells had shorter apical dendrites, and DG neurons had a lesser degree of dendritic branching than in WT controls (Phillips et al., 2005). Furthermore, the number of BrdU⁺ cells, a marker that detects proliferating cells, was significantly decreased in the DG of R6/1 mice when compared to WT controls. Moreover, R6/1 mice had smaller and irregularly shaped cell-bodies, shorter dendrites, and migrated shorter distances into the granule cell layer when compared to WT controls (Lazic et al., 2006). Additionally, it was found that in symptomatic R6/2 mice, both synaptic plasticity and spatial cognition are impaired. Weakened coupling between excitatory post-synaptic potentials (EPSPs) and the generation of action potentials was observed. Additionally, in a Morris water maze task, R6/2 mice control mice swam back to the area of the removed platform while HD mice swam in a random manner with no reference to the platform's location (Murphy et al., 2000). It was also found that aggregation of neuronal intracellular inclusions, a hallmark of many polyglutamine repeat diseases, appear and increase with age in CA3, CA1, and DG of R6/2 HD mice (Morton et al., 2000).

In human studies, although sparse, there is evidence for prodromal hippocampal abnormalities. For example, hippocampal volume was reduced by up to 9% in a cohort of presymptomatic HD patients measured by high-resolution T1 weighted brain scans

(Rosas et al., 2003). In a TRACK-HD study examining early atrophy in a multitude of brain areas, hippocampal atrophy (up to 10% reduction in volume) was observed in “preHD-B” patients who were closer than 10.8 years to disease onset. TRACK-HD reports that early atrophy of the hippocampus rapidly becomes more severe as the disease moves into manifest stages and correlates with clinical measures (Bogaard et al., 2011). In another study, researchers employed techniques previously used in mouse models of HD to presymptomatic HD patients. Here, patients had to learn the location of a submerged hidden platform relative to external cues on the wall in a virtual Morris water maze task. Patients in the prodromal stage of HD were unable to learn the location of the platform as quickly as age-matched controls (Begeti et al., 2016).

Hippocampal dysfunction in the early to late onset stages of HD, in both animal and human studies, has been reported but hippocampal dysfunction in the HD prodrome is still widely understudied. In order to make progress in the pursuit to ameliorate HD, more in-depth investigation of the prodromal hippocampus is required. To begin more thorough investigation of the presymptomatic HD hippocampus, more sensitive pre-clinical techniques may help to identify early deficits and help to develop more targeted therapeutics for the disease. There has been evidence showing that early intervention can delay or reverse HD progression. For example, low-dose treatment with the weak NMDAR antagonist memantine from 2 months of age reversed neuropathological and behavioural deficits in YAC128 mice when assessed at 12 months (Okamoto et al., 2009). Although deficits in the presymptomatic phase are not severe enough to require treatment, it is well known that early synaptic deficits are a prerequisite for cell death, thereby intervening early on in disease progression may allow for the slowing or cessation of cell

death later on in disease progression (Milnerwood and Raymond, 2010). For the purposes of this thesis, we employ multi-electrode array electrophysiology in order to investigate the electrophysiological properties of a large area of the hippocampus simultaneously. We also employ super-resolution microscopy to investigate nanoscale changes in synaptic architecture in the presymptomatic HD hippocampus.

1-9 Multi-electrode array electrophysiology

When examining heterogenous cell populations like those that makeup the hippocampal formation, understanding how these cells function together as a whole can be pivotal to gaining further insight into how a brain area operates in both healthy and diseased brains. One method for examining the electrical properties and functional connectivity of large cell populations is microelectrode array electrophysiology. Application of microelectrode arrays (MEAs) to acute brain tissue was first reported when it was shown that an array could both stimulate and record from multiple sites on hippocampal slice preparations (Novak and Wheeler, 1988). Based on these findings, a more sophisticated MEA with a larger area and more effective hydrophilic electrode coating was developed (Oka et al., 1999). This MEA, known as the MED system, was the earliest version of the MEA used to investigate synaptic deficits in HD for this thesis. Although many other MEAs exist, the MED system offers proficiency in recording brain activity from multiple areas simultaneously.

Although there is a substantial gap in the literature surrounding presymptomatic synaptic deficits in HD, and virtually no research in this area utilized MEAs, the MED system has been used to investigate cellular anomalies in hippocampus in other

neurodegenerative diseases such as Alzheimer Disease (AD). Here, researchers utilized the MED64 system to record field EPSP (fEPSP) deficits in the hippocampus of AD mice (Wang et al., 2018). Furthermore, the MED64 system was used to detect LTP deficits in a double transgenic model (5XFAD) of AD (Zhen et al., 2017). Furthermore, it was found utilizing the MED64 system that overexpression of cancerous inhibitor of PP2A (CIP2A), PP2A being a phosphatase known to play a key role in tau hyperphosphorylation in AD, led to a significant impairment of LTP at the Schaffer collateral synapse (Shentu et al., 2018). Although the argument could be made that similar results as described above could be achieved via conventional electrophysiological techniques, having the ability to record from multiple sites across a heterogenous population of cells can offer insight into how these cell groups are collectively affected in a disease state, thus increasing the potential to develop targeted pharmacological intervention for specific cell populations in these conditions. Therefore, the present thesis used MEA electrophysiology, namely the MED64 system, to examine synaptic transmission in the hippocampus, and more specifically to detect the earliest synaptic deficits detectable in the Q175FDN mouse model of HD.

1-10 Super-resolution imaging

For hundreds of years, light microscopy has helped researchers to understand the precise function of cells. For example, approximately 300 years ago Antoine Van Leeuwenhook used his self-ground optical lenses to discover bacteria and kickstart the field of microbiology. About 200 years after that, Ramon y Cajal used light microscopes

to investigate Golgi stained brains and create drawings of neurons and hypotheses surrounding information flow in the CNS (Huang et al., 2010).

Unfortunately, the resolution for optical microscopy is limited by the diffraction or “spreading out” of light when it passes through a small aperture or is focused on a very small area. Due to the fact that this property is intrinsic to all light waves, breaking this diffraction barrier has been deemed impossible until recent super resolution microscopy techniques were developed (Huang et al., 2010). Recently, several novel fluorescence microscopy techniques have greatly surpassed the diffraction limit of image resolution. In general, all of these approaches generate diffraction unlimited images by using the physical properties of fluorescent probes to differentiate light emission from two nearby molecules that are within the diffraction limit. Although it is outside the scope of this thesis to go into each technique with immense detail, some examples of these techniques are: stimulated emission depletion (STED);(Klar and Hell, 1999), structured illumination microscopy (SIM);(Klar et al., 2000), stochastic optical reconstruction microscopy (STORM);(Rust et al., 2006), and photoactivated localization microscopy (PALM);(Betzig et al., 2006). Although these techniques are revolutionary and extremely efficient, they often come with fiscal setbacks and complicated optical setups that are not attainable for the average neuroscience research lab.

Recently however, a new super resolution microscopy technique has been introduced that can be utilized with virtually any conventional wide-field microscope. This technique, known as super resolution radial fluctuation (SRRF), is executed via an open source ImageJ plugin that is capable of achieving spatial resolutions of up to 50 nm (Gustafsson et al., 2016). SRRF follows similar principles to STORM but generates a

super resolution reconstruction with the use of a series of images obtained from wide-field microscopy, conventional fluorophores, and low-intensity illumination (Gustafsson et al., 2016). In neuroscience, the appeal of super resolution imaging stems from investigation of the synapse and its nanoarchitecture. The average synaptic cleft ranges from 20-50 nm in size (Bergles et al., 1997), indicating that conventional fluorescence imaging of the synapse would be limited by the intrinsic diffraction limit of light. However, application of super resolution imaging techniques allows researchers to investigate the nanoarchitecture of the synapse and its associated proteins and transporters to gain more in-depth insight into the structure and function of the synapse in both healthy and diseased brains. The present thesis uses super-resolution imaging, specifically SRRF, to investigate synaptic architecture at the nanoscale level in pre symptomatic Q175FDN HD mice.

1-11 Hypothesis and aims

Despite clear evidence of early cognitive decline in HD, few studies have identified cellular/synaptic dysfunction in the prodromal HD hippocampus. This is likely due to previous techniques and methodology not being able to achieve the level of sensitivity required to study these dysfunctions underlying early cognitive decline. Aberrations in synaptic transmission detected via multielectrode array electrophysiology, in combination with changes in synaptic nanoarchitecture elucidated through novel super resolution fluorescent imaging techniques could provide much-needed insight into the cognitive deficits associated with prodromal HD.

I hypothesize that synaptic transmission in the hippocampus is significantly altered in presymptomatic HD mice when compared to WT littermate controls. Specifically, I expect to see an impairment and possible failure of LTP in the hippocampus of presymptomatic HD mice. Furthermore, I hypothesize that super-resolution imaging after cLTP will be sensitive to detect subtle alterations in synaptic architecture, namely the size, number, and the fluorescence intensity of protein clusters (nano-objects) in HD mice when compared to WT littermate controls. I expect that there will be basal differences in synaptic architecture between HD mice and WT controls, and these differences will be further exemplified when both genotypes undergo a plasticity (cLTP) protocol. I will investigate these hypotheses using the following specific aims:

- Specific aim 1: Characterize LTP using MEA electrophysiology in 3-month old Q175FDN HD mice and WT littermate controls.
- Specific aim 2: Investigate pre and post synaptic nanoarchitecture in 3-month old Q175FDN HD mice and WT littermate controls in both basal and LTP conditions by utilizing super resolution fluorescence microscopy, specifically SRRF.

2-0 Methods

2-1 Animals

All experiments were performed on acute brain slices obtained from male and female heterozygous Q175FDN mice (het), as well as wild-type littermates (WT). Breeder mice were obtained from University of British Columbia (UBC) and the colony was subsequently bred at Memorial University's animal care facility. Mice were group-housed in ventilated cage racks, were provided with standard chow and water *ab libitum*, and were maintained on a normal 12 hour light/dark cycle. All experimental procedures were approved by Memorial University's Institutional Animal Care Committee and were performed in accordance with the guidelines set by the Canadian Council on Animal Care.

2-2 Slice preparation

At 3 months of age (\pm 14 days), mice were anesthetized with isoflurane and decapitated, and the brain was quickly removed and immersed in ice-cold oxygenated (95% O₂/5% CO₂) slicing solution consisting of (in mM) 125 NaCl, 2.5 KCl, 25 NaHCO₃, 1.25 NaH₂PO₄, 2.5 MgCl₂, 0.5 CaCl₂, and 10 glucose. Transverse brain slices at 350 μ m containing hippocampus were obtained with a Leica VT1000 vibratome. Slices were then placed in artificial cerebrospinal fluid (aCSF) containing (in mM) 125 NaCl, 2.5 KCl, 25 NaHCO₃, 1.25 NaH₂PO₄, 1 MgCl₂, 2 CaCl₂, and 10 glucose. Slices were recovered in oxygenated aCSF for 90 min at room temperature before electrophysiological experimentation and for 180 min at room temperature before c-LTP protocol.

2-3 Multi-electrode array electrophysiology

Slices were transferred to the recording chamber of the MED64 system (Alpha MED Scientific), known as the MED probe. The MED probe contains multiple microelectrodes embedded in the center of a transparent glass plate. For our experiments, we utilized the MED-RG501A probe (2x8 microelectrode array; 16 total electrodes) and the MED-R515A probe (8x8 microelectrode array; 64 total electrodes). Each electrode is 10 mm in depth, and they are each 300 μm apart. Average input impedance of the electrodes is 100 M Ω . The surface of the MED probe was treated with 0.1% polyethylenimine, a cationic polymer, in 0.15 M borate buffer, pH 8.4, overnight at room temperature. The majority of materials that make up the MED probe are hydrophobic. To counteract this, coating the probe with a hydrophilic buffer allowed the tissue to sit near the electrodes. The probe surface was subsequently rinsed 3 times with sterile distilled water to remove the buffer. A peristaltic pump (Gilson Minipuls 3) was used to perfuse oxygenated (95% O₂ / 5% CO₂) aCSF to the probe containing the slice at a flow rate of 2 ml/min. aCSF was maintained at 23°C using an in-line heater and temperature controller (MED-CP04). One side of the acute hippocampal slice was adhered to the multi-electrode array by placing a small rectangular mesh, and a metal harp on the opposite side of the slice. If no response was elicited from one side, the slice was flipped in an attempt to elicit a response from that side.

The stimulating electrode was selected in relation to its position in the Schaffer collateral pathway within the stratum radiatum. Mobius software (Alpha Med Scientific) was used to send triggering stimulus through the digital outputs of MED64 main and head

amplifiers (MED-A64MD1A/ MED-A64HE1S) for precise control over stimulating and recording via the 64-electrode array. Basal field potential responses were evoked using basal stimulation (stimulation intensity was manipulated until it evoked 30-40% of the maximal response during input-output (I/O)) at 20s intervals and simultaneously recorded at 63 (8x8 electrode), or 15 (2x8 electrode) sites until a minimum of 10 minutes of stability were achieved.

Upon achieving a stable baseline, the MED64 system was utilized to deliver tetanic stimulation to induce LTP. Two different tetanic stimulation paradigms were used to induce different forms of LTP. HFS (1s at 100 Hz) and TBS (10 bursts of 4 pulses at 5 Hz with each burst consisting of 4 pulses at 100 Hz). After tetanic stimulation, slices were continued to be perfused with aCSF for 60 minutes, while reverting back to basal stimulation evoking responses via single pulses every 20 seconds to measure changes induced by LTP. “%LTP” was defined as average of responses from 55-60 minutes post-tetanic stimulation and was then expressed as an average percentage of the 10 minute baseline period.

2-4 Chemical-LTP

cLTP was induced in brain slices from 3-month old heterozygous Q175FDN HD mice, as well as WT littermates. cLTP protocol was based on previous work in stratum radiatum where LTP was induced chemically (Lin et al., 2008; Makino and Malinow, 2009; Zhou et al., 2018). Here, we chose to use cLTP over electrical stimulation so that we could induce LTP in the entire acute slice and then follow the necessary steps to visualize changes via fluorescence microscopy. cLTP was induced by bathing 350 μm acute slices

for 10 minutes in 0-Mg²⁺ aCSF containing (in mM) 125 NaCl, 2.5 KCl, 25 NaHCO₃, 1.25 NaH₂PO₄, 2 CaCl₂, and 10 glucose, followed by a 3 minute incubation in 0-Mg²⁺ aCSF combined with 200 μM glycine. Slices were then transferred to a recovery well containing regular aCSF for 10 minutes. Control slices were also bathed in 0-Mg²⁺ aCSF for 10 minutes followed by regular aCSF for 3 minutes, and then transferred to another well containing regular aCSF for 10 minutes to follow the same experimental manipulation (sham) as the chemical-LTP treated slices except for glycine. Both cLTP and control slices were oxygenated throughout the entire experimental procedure. Following treatment, slices were subjected to immunohistochemistry (IHC) and subsequent super-resolution imaging.

2-5 Immunohistochemistry

Immediately following the recovery period of the cLTP protocol, slices were fixed by immersion in 4% paraformaldehyde overnight at 4°C and then cryoprotected in 30% sucrose for a minimum of 24 hours. The acute slices were re-sectioned (16 μm) with a cryostat (Leica CM3050 S);(-23°C) and placed on glass slides (Fisherbrand Superfrost Plus 1.0 mm) and stored at -80°C for long-term storage if slides were not utilized right away. Slides were then retrieved from -80°C and warmed at 37°C on a slide warmer for 20 minutes. While warming, a Dako pen (S2002, Dako Denmark, Denmark) was used to draw a hydrophobic barrier around sections of the slide to contain the antibodies once they were applied. Following this, the slides were washed in 0.01M PBS for 5 minutes. This step was repeated for a total of three times.

Slides were then incubated in blocking serum (0.01M PBS with 5% BSA) for 1 hour. After blocking, slides were incubated in primary antibody (rabbit monoclonal anti-GluA2, 1:500, Neuromab) overnight at 4°C. On day two, slides were incubated in secondary antibody (Alexa fluor 488-conjugated goat anti-rabbit IgG 1:500, Life Technologies Corporation) at room temperature for 2 hours. All remaining procedures were carried out in opaque slide holders as well as in reduced lab lighting to prevent photobleaching of the secondary antibody fluorophores. Next, slides were blocked with blocking solution containing Triton X-100 (0.25%) for 1 hour at room temperature to permeabilize the cell membrane and allow antibody penetration into the cell. Slides were then incubated in another primary antibody (rabbit monoclonal anti-Synaptophysin, 1:1000, Abcam,) overnight at 4°C. On day 3, the slides were washed three times in PBS and then incubated in a secondary antibody (Alexa fluor 594-conjugated goat anti-mouse 1:500, Life Technologies Corporation) at room temperature for 2 hours. Finally, slides were cover-slipped using Dako mounting medium containing DAPI. Once dry (1-2 days storage at room temperature), slides were transferred to a slide box and placed in 4°C for long-term storage. To control for variation in staining intensities, all immunohistochemistry was carried out in one batch.

2-6 Super-resolution imaging

Imaging of CA1 stratum radiatum hippocampus of re-sectioned (16 μ m) mouse hippocampal slices was performed using an EM-CCD camera (Andor, iXon Ultra 897, DU-897U-CSO-#BV) and Olympus BX51 microscope. Precise control of LED illumination source (Prior, Lumen 300) was controlled manually by switching the LED

illumination source on and off when needed. The region of interest (ROI) was identified and selected through a 4x objective (Olympus, 0.28NA) to ensure a wide-field view of the slice and specifically the Schaffer collateral pathway. Furthermore, one ROI was selected at a proximal area of CA1 (approximately 150-450 μm from CA3 cell bodies) and one was selected from a distal area of CA1 (approximately 500-800 μm from CA3 cell bodies). Once the ROI was selected, a 60x objective (Olympus, 1.40NA) was positioned to capture the images required for super-resolution imaging. 60x imaging was completed through an objective that required oil immersion (Zeiss, Immersol 518F, Batch no: 170704). Images were acquired with Ander Solis software, capturing 100 images over approximately 10 seconds, to yield a final super-resolution image. Acquisition settings were as follows: Exposure time, 0.1s; number of accumulations, 1; accumulation cycle time, 0.118s (8.45 Hz); kinetic series length, 100; kinetic cycle time, 0.118s (8.45 Hz); shift speed, 0.3; vertical clock voltage amplitude, normal; readout rate, 17MHz at 16-bit; pre-amplifier gain, gain 1; output amplifier, electron multiplying; electron multiplier gain level, 2. Standard filter cubes were used for GFP and mCherry to yield green and red images, respectively.

2-7 Experimental design and statistics.

The statistical tests used include: one-way ANOVA, one-way repeated measures (RM) ANOVA, two-way ANOVA, linear regression, and T-test. Post hoc tests included Tukey, Bonferroni and Dunnett tests. The statistical test used for each experiment is stated within the results section. P values of < 0.05 were considered significant. Where indicated, “N” and “n” refer to the number of animals and slices used in each experiment,

respectively. Furthermore, bilinear interpolation via ImageJ was used to create the 2-dimensional plots of hippocampal LTP.

Super resolution images were analyzed using the “NanoJSRRF” plugin in Fiji (Fiji is just ImageJ). The analysis was completed in an automated series of steps in Fiji. Initially, the 512x512 series of 100 images were cropped to 128x128 (equivalent to a field of view of 34x34 μm). Next, a drift correction (to increase resolution and correct for fluorophore fluctuation across images during acquisition) was completed. Next, this cropped series of images was run through the NanoJSRRF plugin, creating a super-resolution image. In conjunction with SRRF analysis, chromatic aberration correction (to correct for the tendency of a lens to erroneously focus colors to different points) was performed. At this point, the colour of the images was changed to reflect their respective fluorophores with GluA2 images being converted to green and Synaptophysin (SYN) to red. Furthermore, these images were merged to create a composite image for representative purposes. The corrected individual images (GluA2 & SYN) were then converted to 8-bit (binary) in order to run auto local thresholding to separate puncta from background information. Specifically, “Bernsen” auto local thresholding was determined to reflect to most accurate puncta cut-off measures for the specific antibodies utilized for the purposes of this thesis. Bernsen’s local thresholding method is a form of binarization commonly used for image segmentation for converting grayscale images to binary. From this binary image, Fiji generated a list of the puncta in each image while simultaneously measuring the area of each puncta, allowing us to determine puncta size. This list of puncta was then overlaid onto the original SRRF image, where Fiji determines the mean fluorescent intensity of each puncta based on the chromatic properties. Furthermore,

puncta density was determined by dividing the number of puncta per image by the area of the image (34x34 μm).

Nearest Neighbor (NN) analysis was carried out via Nano-J Core “Nearest Neighbor” analysis to generate Voronoi plots and an excel spreadsheet generated by the Parsons lab for numerical NN analysis. Specifically, this NN analysis determined the exact center (centroid) of each GluA2 puncta and subsequently measured its distance from the centroid of the nearest SYN puncta to measure any changes in protein position amongst the different conditions. NN analysis via Nano-J Core also generated Voronoi diagrams to visualize puncta distance for representative purposes. From this, it was possible to determine where puncta were located based on their corresponding distances from one another.

2-8 N-values

For electrophysiological experiments “N” refers number of animals used in the experiment, and “n” refers to number of acute slices. For super resolution (SRRF) experiments, “N” refers to number of animals, “n” refers to number of acute slices, “n¹” refers to number of 16 μm resections, and “n²” refers to number of nano-objects analyzed.

3-0 Results

3-1 Increased basal transmission in the hippocampus of presymptomatic Huntington disease mice revealed using multi-electrode array electrophysiology

The phenotypic presentation of a wide array of neurodegenerative disease are often rooted in deficits in synaptic transmission and LTP (Selkoe, 2002). Cellular disturbances are well characterized in HD. For example, neurotransmitter release probability, receptor subcellular localization and/or downstream signaling cascades are altered in the cortico-striatal system at an early age in HD mice (Milnerwood and Raymond, 2007; Milnerwood et al., 2010; Parsons and Raymond, 2014). However, in order to understand LTP and its mechanisms in HD, we first need to investigate basal transmission to fully understand communication at the synapses of interest. One prior study showed no significant difference in I/O curves between WT and HD mice at the Schaffer collateral synapse (Usdin et al., 1999); however, a more recent investigation found increased basal connectivity (i.e. larger I/O responses) in R6/2 mice at 6 weeks of age (Beaumont et al., 2014). Here, to determine whether any basal differences in synaptic transmission exist between WT and Q175FDN HD mice, we examined the I/O relationship of hippocampal Schaffer collateral synapses in response to increasing stimulus intensity of single electrical stimuli. As expected, there was a significant effect of stimulus intensity on the response size, where the slope of fEPSCs grew larger as the stimulus intensity increased at every location examined. At 150 μm away from the stimulating electrode (see fig.2 for MEA schematic), there was no significant effect of genotype and no significant interaction effect was observed. (fig. 3a), RM two-way

ANOVA, $p_{(\text{stim intensity})} < 0.001$, $p_{(\text{genotype})} = 0.354$, $p_{(\text{interaction})} = 0.462$, WT: n=17, Het: n=18). At 300 μm , while there was no significant genotype effect, we did observe a significant interaction effect, reflecting the larger fEPSP to higher stimulus intensities in heterozygous mice (fig. 3b, RM two-way ANOVA, $p_{(\text{genotype})} = 0.354$, $p_{(\text{stim intensity})} < 0.001$, $p_{(\text{interaction})} = 0.003$, WT: n=17, Het: n=18). At 450 μm , similar to 300 μm , a significant interaction effect was observed. Interestingly, at this distance, a significant genotype effect emerged, with mean fEPSP being larger in heterozygous mice compared to WT littermates (fig. 3c, RM two-way ANOVA, $p_{(\text{genotype})} = 0.025$, $p_{(\text{stim intensity})} < 0.001$, $p_{(\text{interaction})} < 0.001$, WT: n=17, Het: n=18). At 600 μm , the significant effect of genotype was no longer apparent, although a significant interaction effect was again observed (fig. 3d, RM two-way ANOVA, $p_{(\text{genotype})} = 0.054$, $p_{(\text{stim intensity})} < 0.001$, $p_{(\text{interaction})} < 0.001$, WT: n=17, Het: n=18). Finally, at 750 μm , there was no significant effect of genotype and the significant interaction effect noted at other distances was no longer observed (fig. 3e, RM two-way ANOVA, $p_{(\text{genotype})} = 0.426$, $p_{(\text{stim intensity})} < 0.001$, $p_{(\text{interaction})} = 0.856$, WT: n=17, Het: n=18). These data are indicative of a clear difference in basal transmission between WT and HD mice at specific distances along stratum radiatum in the hippocampus. Increased basal excitatory transmission is observed in the HD hippocampus. The discrepancies from previous research reporting either no change (Usdin et al., 1999) or in agreement showing an increase (Beaumont et al., 2014) in basal transmission may stem from the precise location of the recording electrode within the stratum radiatum. Recently, it has been established that there is a high level of heterogeneity amongst cell populations in the hippocampus, with some transcriptional heterogeneity observed along

the proximal-distal axis (Cembrowski et al., 2016). These varying results may reflect the heterogeneity found across the long axis of hippocampus (Cembrowski et al., 2016).

To help visualize how I/O responses varied from proximal to distal recording sites within each genotype, I/O data were also grouped into two graphs, one each for WT and het, displaying the evoked response differences across stratum radiatum (fig. 4). Here, WT mice showed a significant effect of stimulus intensity, electrode position, and a significant interaction (fig. 4a, RM two-way ANOVA, $p_{(\text{stim intensity})} < 0.001$, $p_{(\text{position})} < 0.001$, $p_{(\text{interaction})} < 0.001$, $n=17$). These results held true for the heterozygous group (fig. 4b, $p_{(\text{stim intensity})} < 0.001$, $p_{(\text{position})} = 0.007$, $p_{(\text{interaction})} < 0.001$, $n=18$). Here, these results display the decrease in basal synaptic transmission in both genotypes as stimulation propagates along the proximal-distal axis of hippocampus.

In summary, while examining basal synaptic transmission along the proximal-distal axis of hippocampus in WT and heterozygous mice, we observed an increase in synaptic transmission in the heterozygotes which became more apparent in the medial-distal areas (300-600 μm) of the Schaffer collateral pathway of hippocampus. These results are indicative of clear aberrant basal synaptic signaling in the presymptomatic HD mice.

Figure 2: Schematic of MEA (MED64) hippocampal acute slice placement on to electrode array.

Representative image of an acute slice from a Q175FDN mouse adhered to a MED64 8x8 electrode array, with the hippocampus positioned directly on to the array. The electrodes are arranged in a grid with 150 μm distance between neighboring electrodes. Orange arrow and circle represent typical location of stimulation electrode, purple arrow and circle represent typical proximal recording site (300 μm), red arrow and circle represent typical distal recording site (750 μm). Electrode immediately to the left of the purple circle represents typical site for 150 μm , electrodes immediately to the right of the purple circle represents typical recording site at 450 μm , and electrodes immediately to the left of the red circle represents typical recording site at 600 μm .

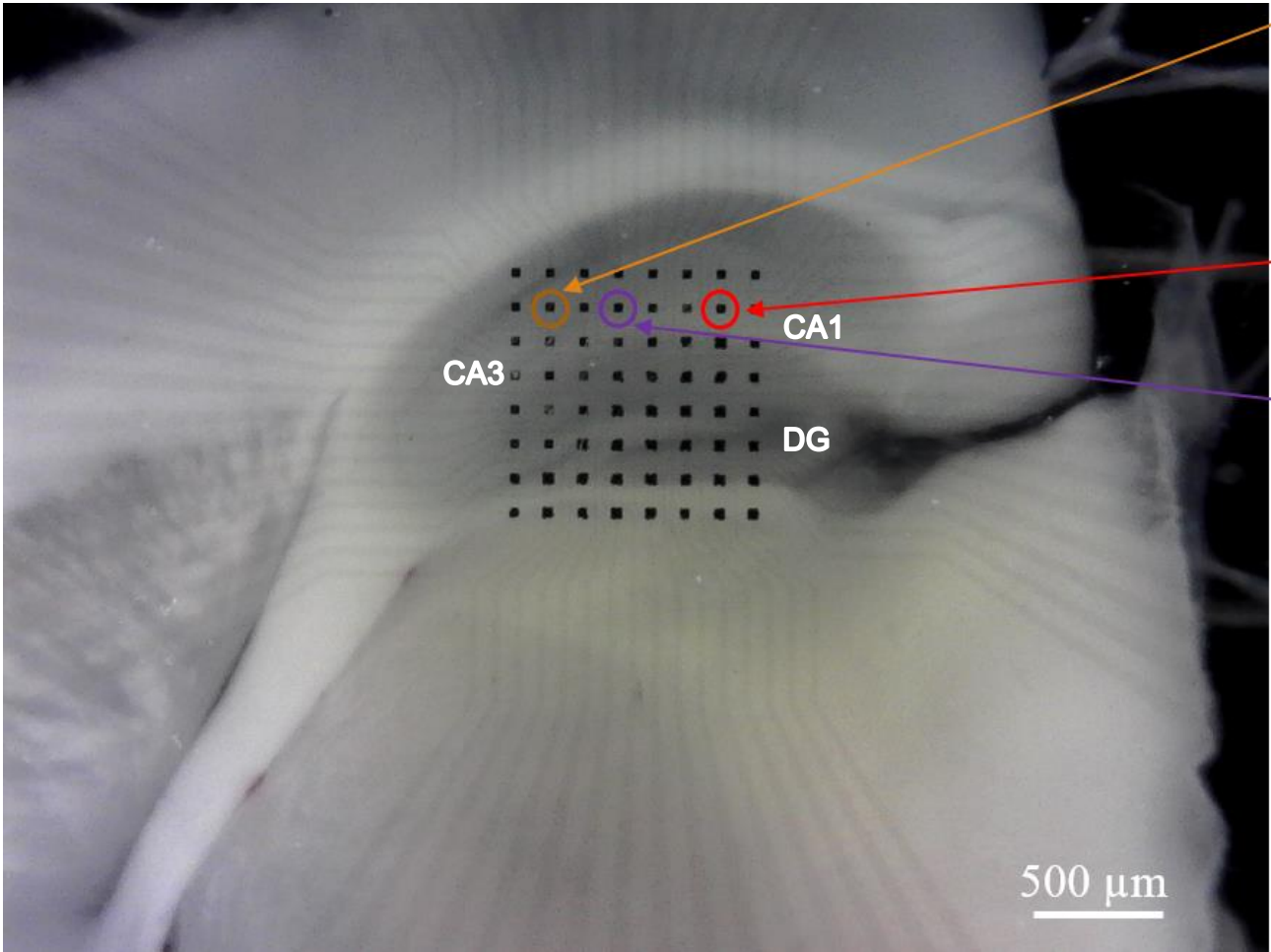


Figure 3: Input-Output (I/O) responses across stratum radiatum in WT and heterozygous mice.

(A) I/O graph displaying the slope of evoked fEPSP (field excitatory post-synaptic potential) response over stimulus intensity for the recording electrode 150 μm (toward CA1) away from the stimulating electrode. (B) I/O graph displaying slope of evoked EPSP response over stimulus intensity for the recording electrode 300 μm away from the stimulating electrode. (C) I/O graph displaying slope of evoked EPSP response over stimulus intensity for the recording electrode 450 μm away from the stimulating electrode. (D) I/O graph displaying slope of evoked EPSP response over stimulus intensity for the recording electrode 600 μm away from the stimulating electrode. (E) I/O graph displaying slope of evoked EPSP response over stimulus intensity for the recording electrode 750 μm away from the stimulating electrode. WT displayed in purple, Het displayed in pink.

* $p < 0.05$, *** $p < 0.005$

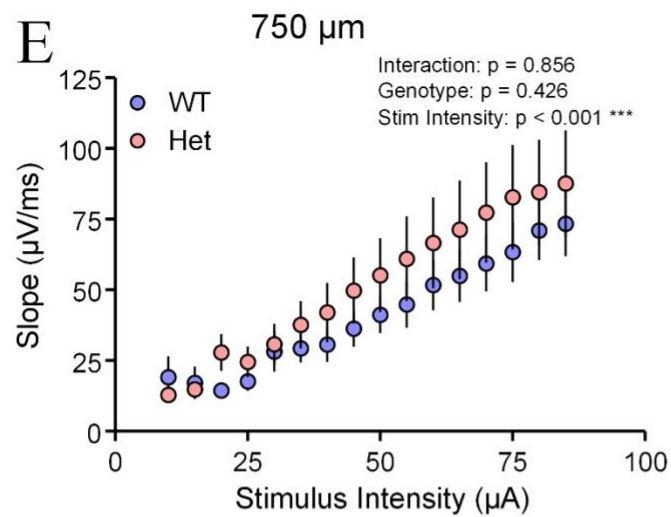
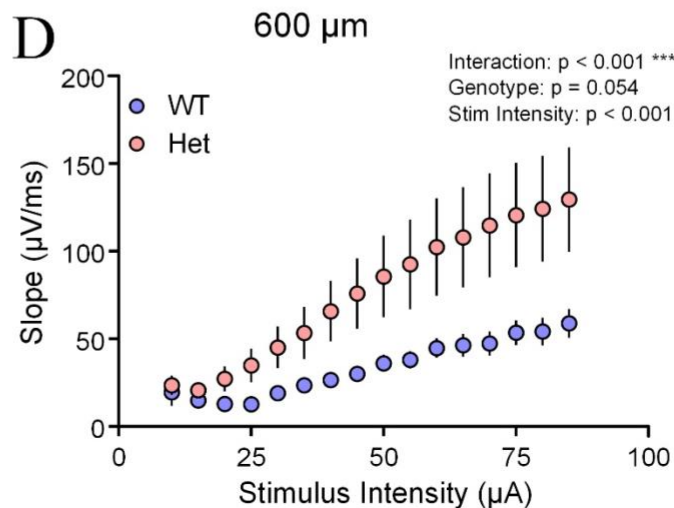
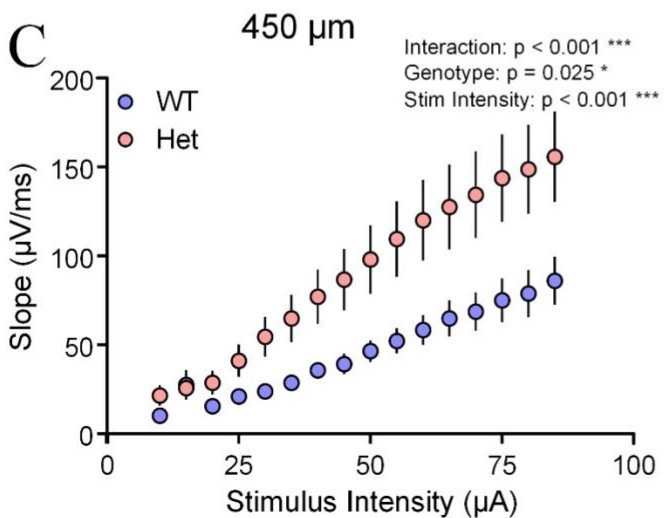
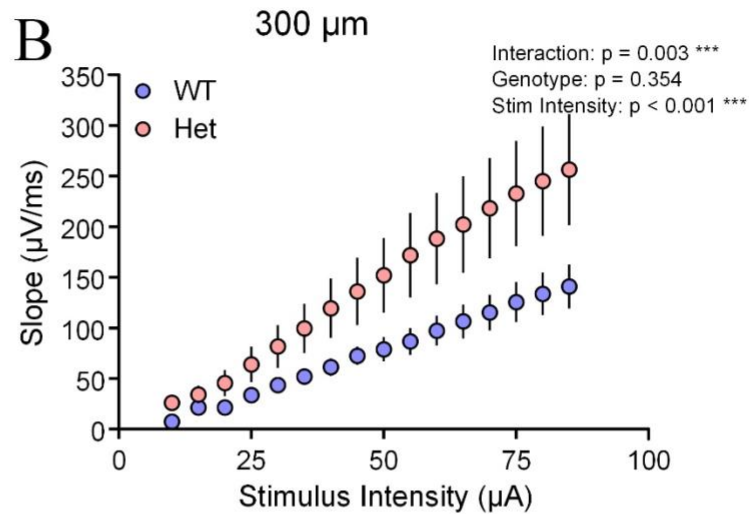
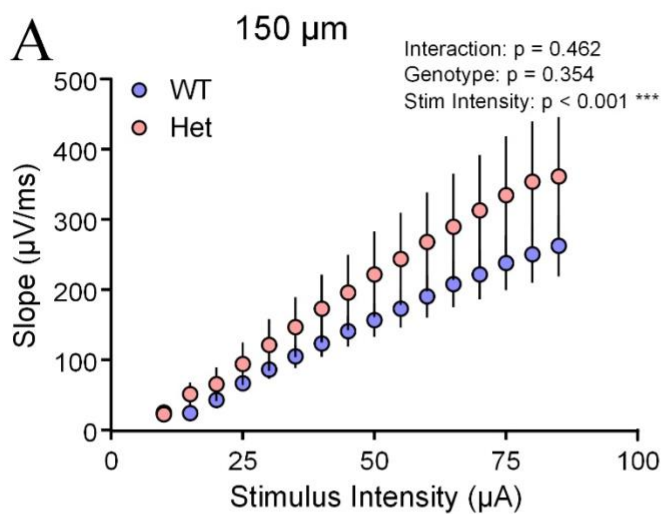
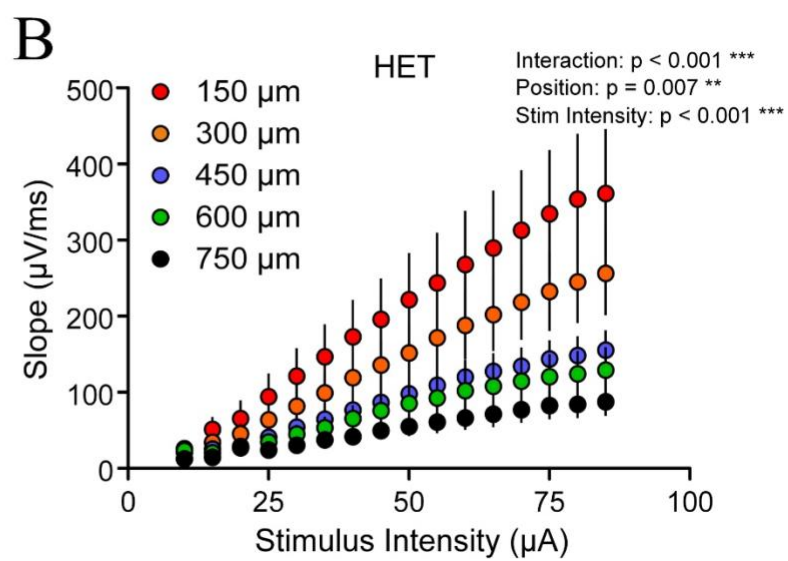
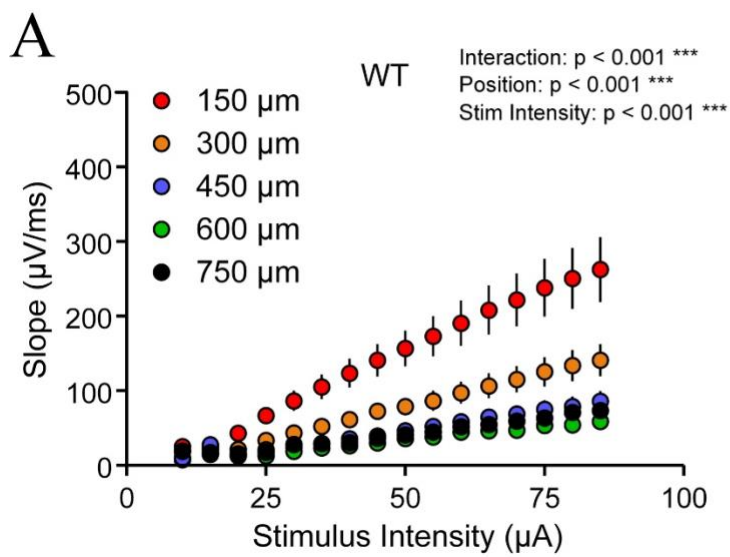


Figure 4: Input-Output (I/O) relationship within genotype across stratum radiatum.

(A) I/O relationship at each recording electrode across the proximal-distal axis of hippocampus for WT mice. (B) I/O curves displaying each electrode across the proximal-distal axis of hippocampus for Het mice. 150 μm away from the stimulating electrode in red, 300 μm away in orange, 450 μm away in purple, 600 μm away in green, and 750 μm away in black.

** $p < 0.01$, *** $p < 0.001$



3-2 Deficits in hippocampal synaptic plasticity in presymptomatic Huntington disease mice revealed using multi-electrode array electrophysiology.

Synaptic deficits including alterations in paired-pulse facilitation, AMPAR- and NMDAR-mediated synaptic transmission, and glutamate release are well documented in the striatum of both prodromal and symptomatic HD (Klapstein et al., 2001; Starling et al., 2005; Joshi et al., 2009; Parsons et al., 2016). Cellular deficits such as reduced dendritic spine size, deficits in cell proliferation, and weakened “gain” or coupling between EPSPs and action potentials (Murphy et al., 2000; Phillips et al., 2005; Lazic et al., 2006) have been characterized in the hippocampus of early HD. However, there remains a substantial gap in the literature with respect to the earliest aberrations in hippocampal synaptic transmission in presymptomatic HD.

Here, in an attempt to detect some of the earliest synaptic aberrations with putative relevance to the early cognitive deficits observed in HD patients (Tabrizi et al., 2009), we utilized a highly sensitive electrophysiological paradigm in the MED64 system (Oka et al., 1999). The MED64 system was used to examine activity-dependent synaptic plasticity in presymptomatic HD mice via two well-established LTP induction paradigms, HFS and TBS. It has been shown in the hippocampus that successful LTP consolidation by these two induction paradigms occurs via distinct mechanisms. Specifically, TBS-LTP requires activation of calpain-1 and extracellular signal regulated kinases (ERK), while HFS-LTP relies on protein-kinase A (PKA) phosphorylation and does not require ERK activation (Selcher et al., 2003; Zhu et al., 2015).

In these experiments, the slope of the fEPSP was measured and LTP was defined as a slope at least 20% larger than baseline that sustained for 60 minutes. Slices from 3-

months old WT and het mice that received HFS-LTP was observed across stratum radiatum as expected (fig. 5). However, no significant differences were detected between WT (N=5, n=10) and heterozygous (N=5, n=9) mice delivered HFS-LTP with respect to genotype, recording electrode position relative to the stimulating electrode, or interaction (fig. 5 a-f) (RM two-way ANOVA, $p_{(\text{genotype})} = 0.740$, $p_{(\text{position})} = 0.170$, $p_{(\text{interaction})} = 0.682$). Bonferroni post-hoc tests $p > 0.05$ for all positions. Specifically, at 150 μm WT HFS-LTP was $44.1 \pm 6.50\%$ of baseline values and het HFS-LTP was $45.1 \pm 12.1\%$ (t-test, $p = 0.950$). At 300 μm , WT HFS-LTP was $44.6 \pm 6.00\%$ and het HFS-LTP was $48.0 \pm 12.0\%$ (t-test, $p = 0.814$). At 450 μm , WT HFS-LTP was $50.6 \pm 6.00\%$ and het HFS-LTP was $44.5 \pm 10.0\%$ (t-test, $p = 0.630$). At 600 μm , WT HFS-LTP was $41.1 \pm 11.4\%$ and het HFS-LTP was $32.5 \pm 8.80\%$ (t-test, $p = 0.552$). At 750 μm , WT HFS-LTP was $42.6 \pm 10.5\%$ and het HFS-LTP was $39.9 \pm 8.10\%$ (t-test, $p = 0.463$). To better visualize the effect of HFS on fEPSC amplitude LTP throughout the stratum radiatum, we used bilinear interpolation (ImageJ) to generate 2D heatmaps that display the magnitude of synaptic responses at 55-60 minutes post-tetanic stimulation across the electrodes that were located in stratum radiatum (fig. 5g). These heatmaps provide a visual of the results described above by displaying low %LTP in cool colours (black/blue) and high %LTP in warm colours (red/yellow/orange) to topographically describe the LTP observed. These data indicate that HFS-LTP is unaffected at 3 months in this model of HD.

Interestingly, and in stark contrast to HFS, brain slices from 3-month old het mice that were delivered TBS showed significant impairments of LTP compared to age-matched WT at electrodes distal to the stimulating electrode, and a significant interaction effect was observed (fig. 6); (WT N=4, n=7, het N=5, n=9; RM two-way ANOVA,

$p_{(\text{genotype})} = 0.058$, $p_{(\text{position})} = 0.005$, $p_{(\text{interaction})} = 0.029$). Specifically, at 150 μm WT TBS-LTP was $55.9 \pm 6.80\%$ and het TBS-LTP was $57.6 \pm 10.2\%$ (t-test, $p = 0.897$). At 300 μm , WT TBS-LTP was $60.6 \pm 8.00\%$ and het TBS-LTP $38.3 \pm 10.6\%$ (t-test, $p = 0.133$). At 450 μm , WT TBS-LTP was $66.5 \pm 10.6\%$ and het TBS was $33.4 \pm 7.40\%$ (t-test, $p = 0.02$). At 600 μm , WT TBS-LTP was $55.2 \pm 10.6\%$ and het TBS was $23.4 \pm 7.80\%$ (t-test, $p = 0.03$). Finally, at 750 μm , WT TBS-LTP was $41.5 \pm 7.70\%$ and het TBS-LTP was $21.6 \pm 6.50\%$ (t-test, $p = 0.06$). These data indicate that functional impairments of excitatory synapses in the hippocampus exist at presymptomatic stage of HD. While there were statistically significant deficits in TBS-LTP, no apparent deficits in HFS-LTP were found. These results suggest that the signaling pathways involved in the consolidation of TBS-LTP may be affected earlier in the time course of the disease than those involved in HFS-LTP consolidation in the HD hippocampus.

Figure 5: HFS induces similar LTP across stratum radiatum in WT and heterozygous mice.

(A) LTP in WT (purple) and Het (pink) mice at 150 μm away from the stimulating electrode. In representative traces for panel A-E, black trace represents fEPSPs before LTP induction and red trace represents fEPSP recorded 55-60 minutes after LTP induction. HFS was applied to all electrodes at time 0. (B) LTP in WT and Het at 300 μm away from the stimulating electrode. (C) LTP in WT and Het at 450 μm away from the stimulating electrode. (D) LTP in WT and Het at 600 μm away from the stimulating electrode. (E) LTP in WT and Het at 750 μm away from the stimulating electrode. (F) % change in fEPSC slope from baseline in the last 5 minutes of the experiment (minute 55-60) in WT and Het at each electrode. (G) 2D heatmap generated by bi-linear interpolation of 16 electrodes of the MEA displaying %LTP across the stratum radiatum of hippocampus. “Stim” refers to the stimulating electrode site in the MEA.

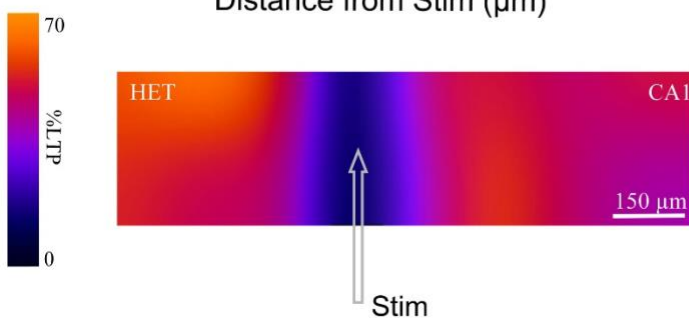
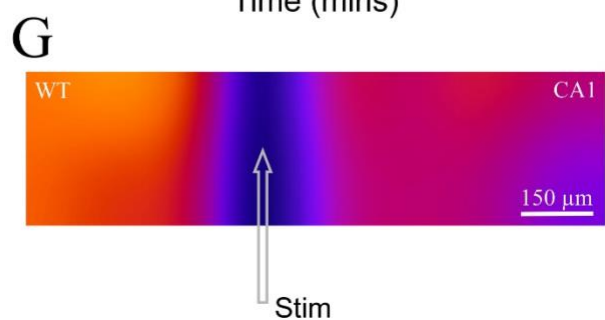
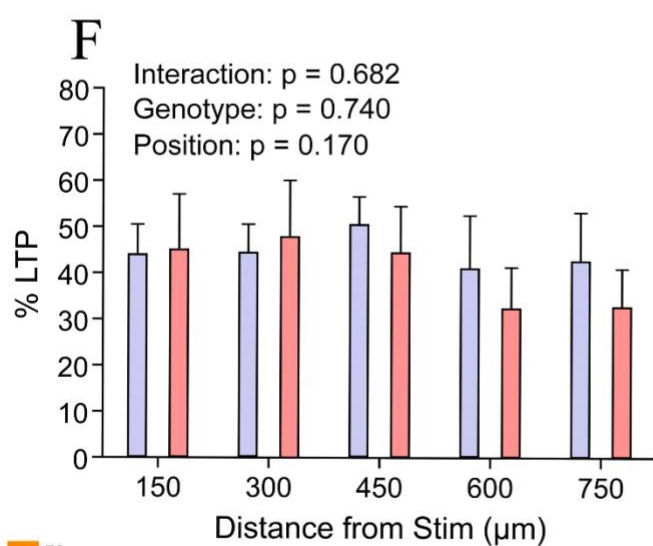
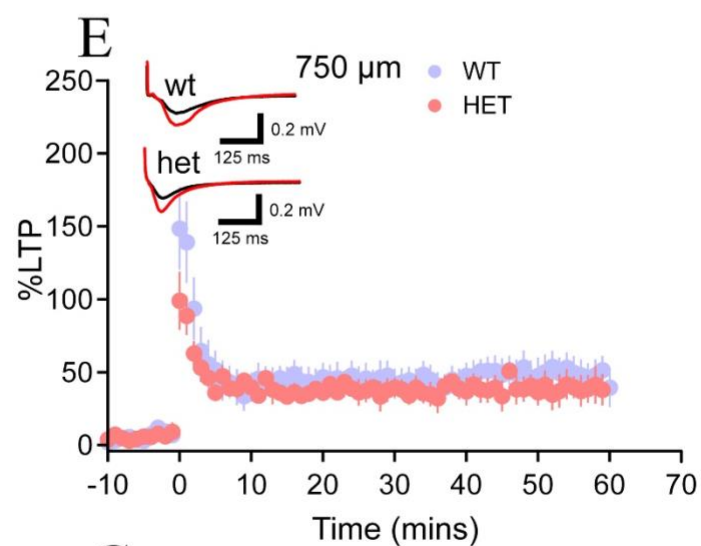
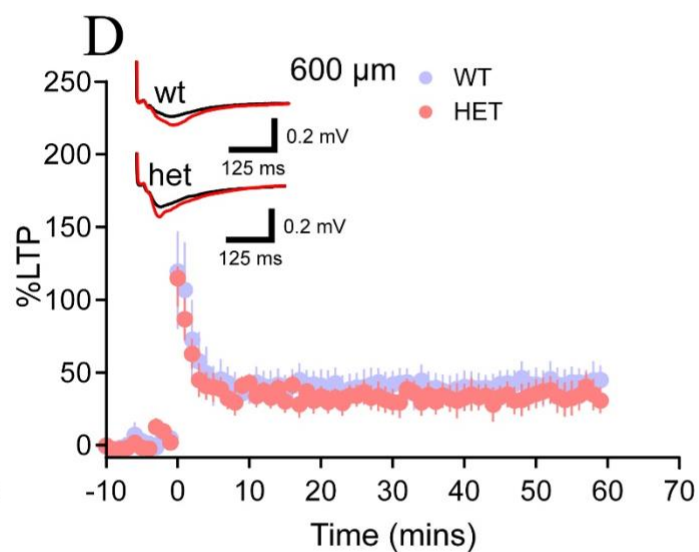
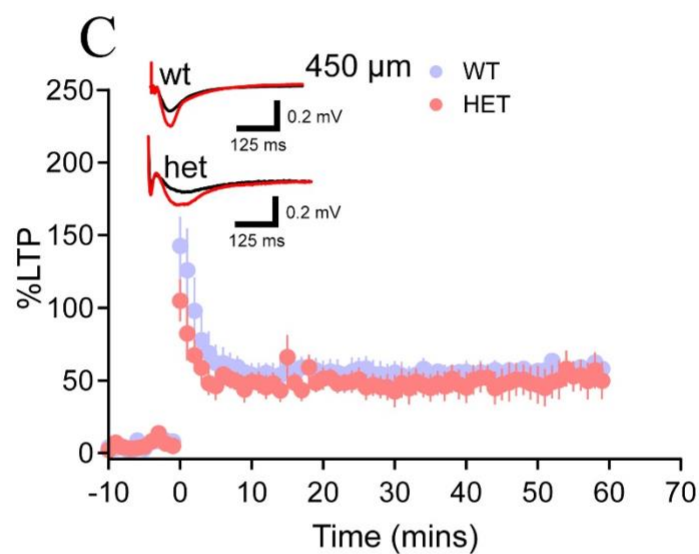
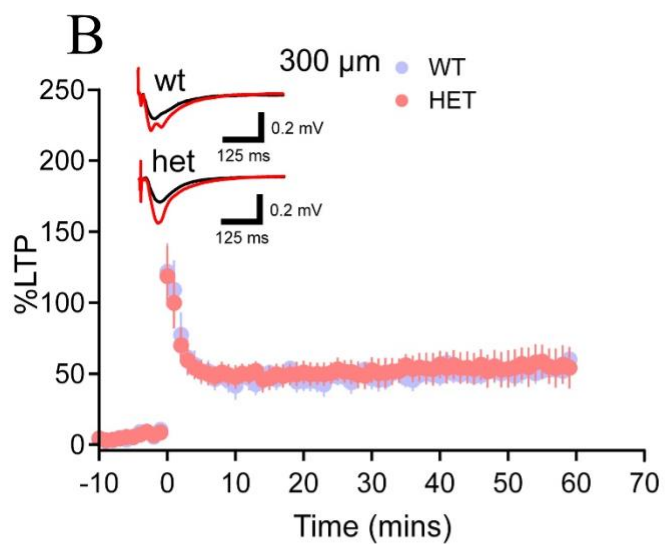
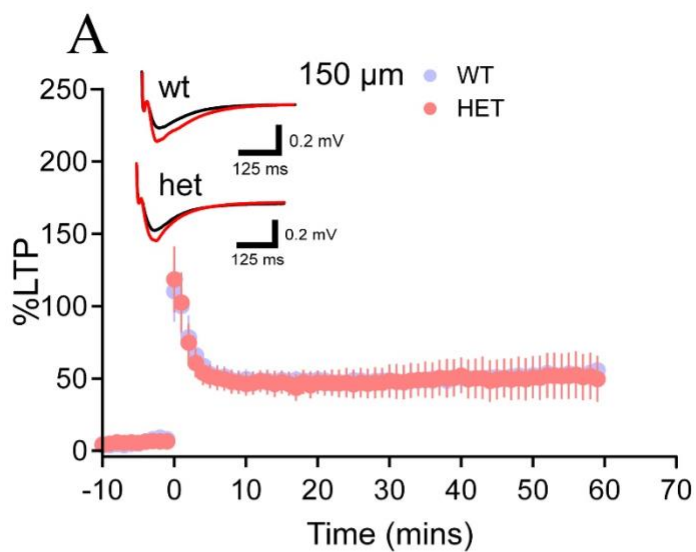
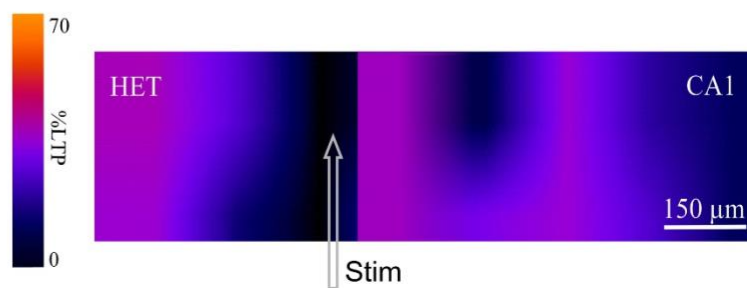
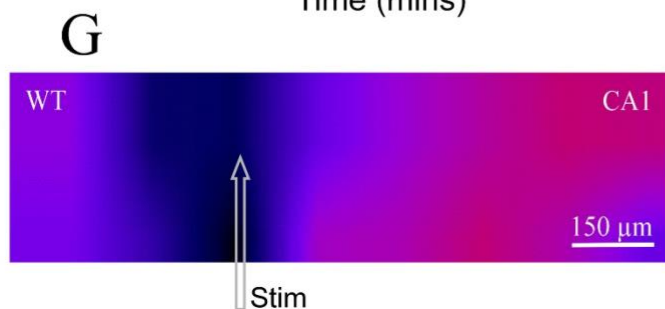
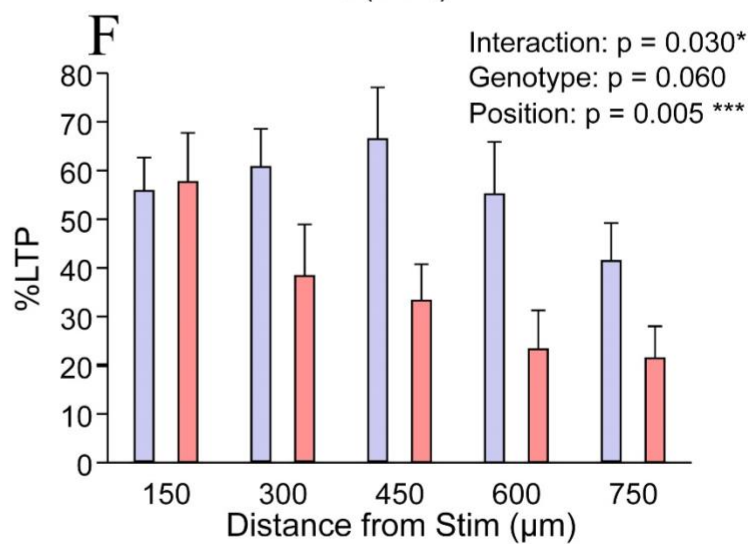
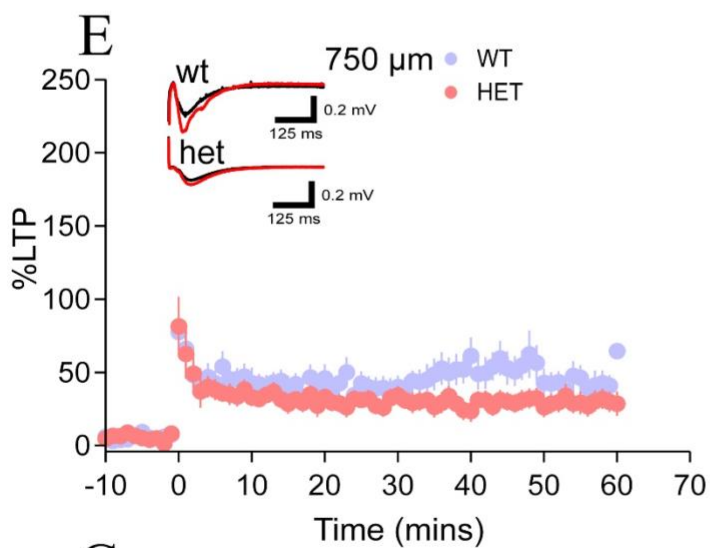
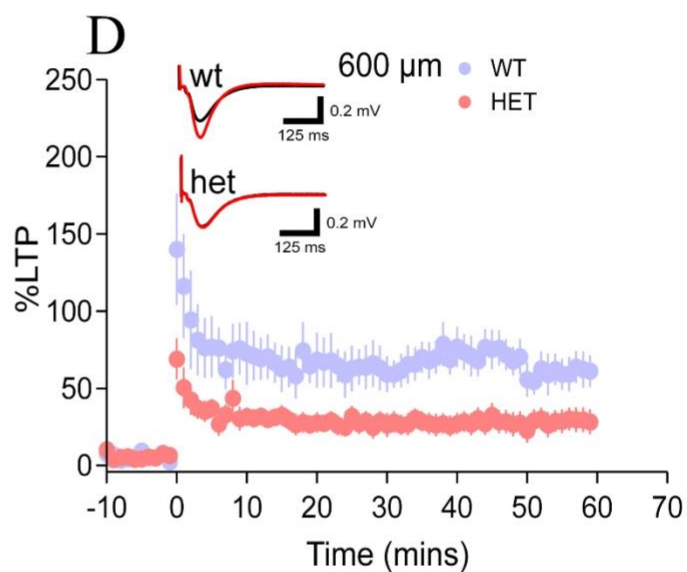
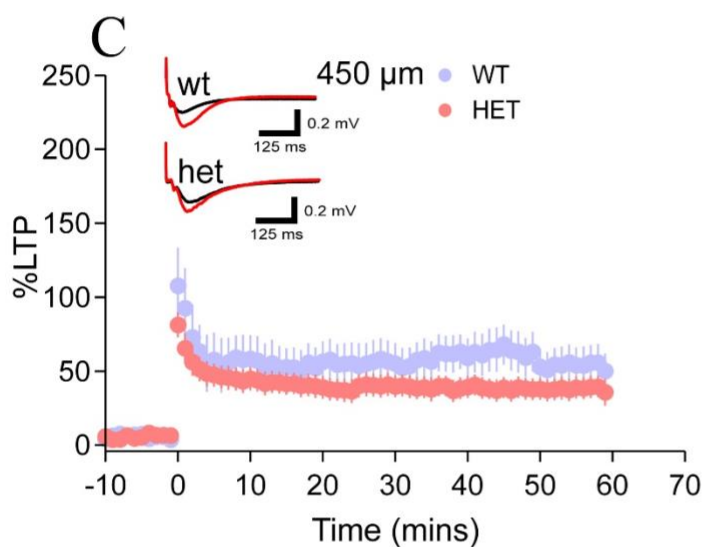
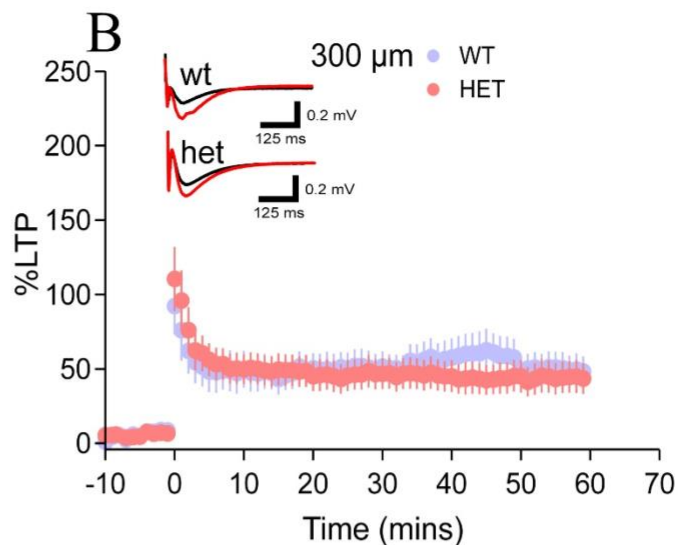
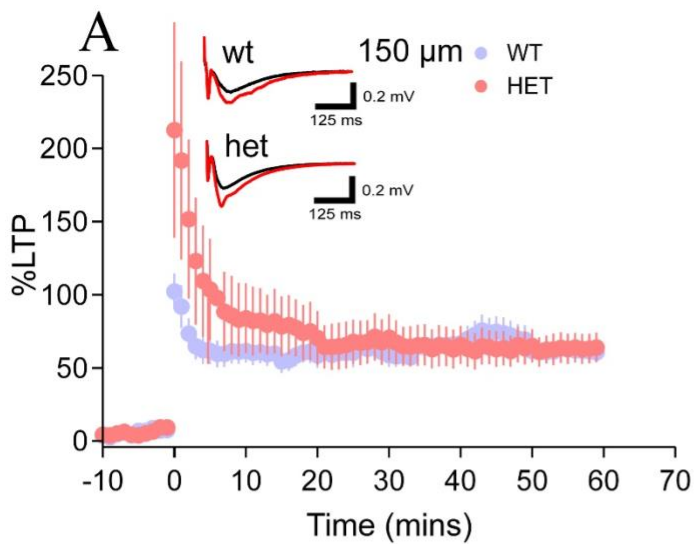


Figure 6: TBS-LTP in stratum radiatum is impaired in heterozygous HD mice.

(A) LTP in WT (purple) and Het (pink) mice at 150 μm away from the stimulating electrode. In representative traces for all panels, black represents pre-LTP induction and red represents 55-60 minutes post-LTP induction. (B) LTP in WT and Het at 300 μm away from the stimulating electrode. (C) LTP in WT and Het at 450 μm away from the stimulating electrode. (D) LTP in WT and Het at 600 μm away from the stimulating electrode. (E) LTP in WT and Het at 750 μm away from stimulating electrode. (F) %LTP increase from baseline in the last 5 minutes of the experiment (minute 55-60 post LTP) in WT and Het at each electrode. (G) 2D heatmap generated by bi-linear interpolation of 16 electrodes of the MEA displaying %LTP across the proximal distal-axis of hippocampus. “Stim” refers to the stimulating electrode site in the MEA.



3-3 Super-resolution radial fluctuation (SRRF) imaging of GluA2 and Synaptophysin across the stratum radiatum in WT and Heterozygous mice.

Until recently, visual investigation of the nanoarchitecture of the synapse using light microscopy was hindered by the intrinsic diffraction barrier of light as it passes through a small aperture or is focused on a very small area (Huang et al., 2010). However, novel techniques in microscopy have been developed to surpass this diffraction barrier, allowing imaging and investigation of nano-objects that exist beyond the approximate 200 nm diffraction limit of light microscopy. Due to the novel nature of these techniques, synaptic nanoarchitecture has not been widely studied in HD brains. From our MEA electrophysiology results, we determined that aberrations in synaptic transmission, specifically in LTP induced by physiologically relevant stimulus (TBS), are apparent in presymptomatic HD mice. Though these findings are novel and intriguing, MEA electrophysiology only samples synaptic responses at the cell population level, and does not distinguish between functional and structural changes.

In order to probe the observed TBS-LTP anomaly further and investigate presymptomatic HD at the synaptic/subcellular level, we sought to bridge the gap between electrophysiological properties and subcellular level alterations in architecture by utilizing SRRF imaging techniques. In this study, we focused on two major proteins that constitute the excitatory synapse: the AMPAR receptor subunit GluA2 (fig. 7,8) and the pre-synaptic vesicular glycoprotein SYN (fig. 9,10) along the stratum radiatum. To investigate alterations in synaptic protein distribution associated with synaptic plasticity, subsets of acute hippocampal tissue from WT and HD mice underwent cLTP. We also further investigated GluA2 and SYN by utilizing a nearest neighbour (NN) analysis

paradigm to assess any changes in how the pre and post-synaptic architecture may change spatially with respect to one another in presymptomatic HD. Here, we examined the movement of clusters of GluA2 and SYN proteins known as nano-objects based on their nearest neighbour in WT control, WT cLTP, Het control, and Het cLTP tissue (fig. 11,12).

3-4 SRRF imaging of GluA2 in proximal stratum radiatum in WT and heterozygous mice.

In proximal stratum radiatum (i.e. 150-450 μm away from CA3 cell bodies, fig. 3) we found a significant difference in GluA2 size between genotypes (fig. 7a,b);(one-way ANOVA, $p < 0.001$). More specifically, in basal conditions, Het GluA2 size was significantly larger than WT GluA2 size. As expected (Hruska et al., 2018), cLTP significantly increased GluA2 size in WT tissue. In contrast, cLTP resulted in a significant reduction in GluA2 size in hippocampal tissue obtained from HD mice (post-hoc Tukey tests for WT control vs. WT cLTP, $p < 0.001$; WT control vs. Het control, $p < 0.001$; WT control vs. Het cLTP, $p < 0.001$; WT cLTP vs. Het control, $p < 0.001$; WT cLTP vs. Het cLTP, $p = 0.003$; Het control vs. Het cLTP, $p < 0.001$; WT control: $N=3$, $n=5$, $n^1=10$, $n^2=5869$; WT cLTP: $N=3$, $n=6$, $n^1=12$, $n^2=7003$; Het control: $N=3$, $n=6$, $n^1=12$, $n^2=7319$; Het cLTP: $N=3$, $n=6$, $n^1=12$, $n^2=6758$). The decrease in size observed in Het tissue after cLTP was robust and is a complete reversal from what we observed in WT tissue.

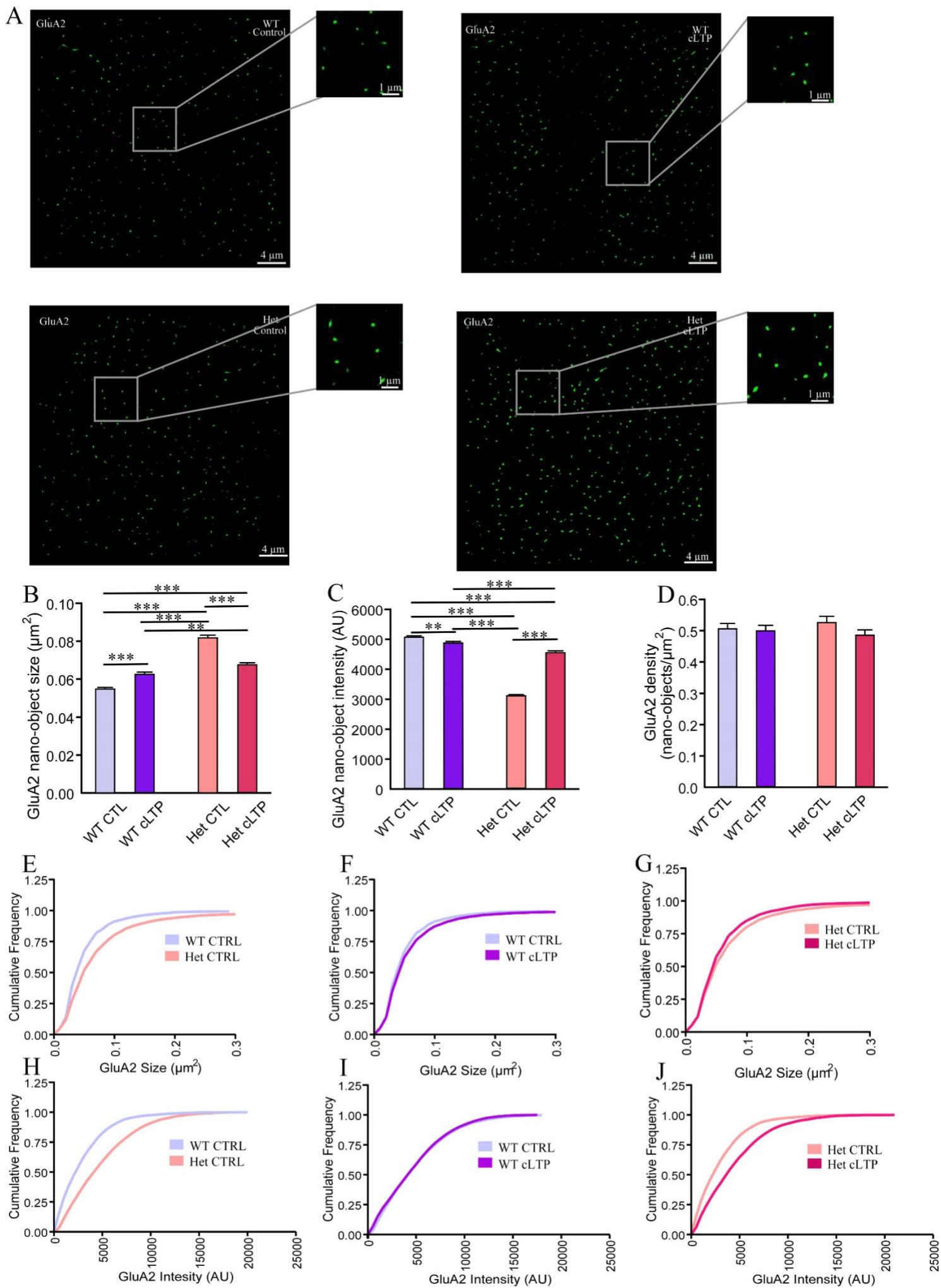
Changes in fluorescence intensity in super-resolution microscopy are often indicative of nanoscale reorganization (Huang et al., 2010), specifically clustering or

dispersing of nano-objects. Here, we observed a significant difference in GluA2 intensity between genotypes (Fig. 7c, one-way ANOVA, $p < 0.001$). More specifically, in basal conditions, Het GluA2 intensity was significantly lower than that in WT. Furthermore, cLTP induced a modest but significant reduction in GluA2 intensity in WT tissue. This observation in combination with the GluA2 size result indicates that larger puncta may represent more dispersed, and therefore less intense, nano-objects. Moreover, cLTP significantly increased GluA2 intensity in Het tissue. (post-hoc Tukey tests for WT control vs. WT cLTP, $p = 0.008$; WT control vs. Het control, $p < 0.001$; WT control vs. Het cLTP, $p < 0.001$; WT cLTP vs. Het control, $p < 0.001$; WT cLTP vs. Het cLTP, $p < 0.001$; Het control vs. Het cLTP, $p < 0.001$; WT control: $N=3$, $n=5$, $n^1=10$, $n^2=5869$; WT cLTP: $N=3$, $n=6$, $n^1=12$, $n^2=7003$; Het control: $N=3$, $n=6$, $n^1=12$, $n^2=7319$; Het cLTP: $N=3$, $n=6$, $n^1=12$, $n^2=6758$). When measuring GluA2 density, which is indicative of the number of nano-objects per given area (fig. 7d, number of nano-objects per image) we found no significant difference in proximal areas of hippocampus (one way ANOVA, $p = 0.415$; post-hoc Tukey tests for WT control vs. WT cLTP, $p = 0.999$; WT control vs. Het control, $p = 0.870$; WT control vs. Het cLTP, $p = 0.842$; WT cLTP vs. Het control, $p = 0.677$; WT cLTP vs. Het cLTP, $p = 0.948$; Het control vs. Het cLTP, $p = 0.353$; WT control: $N=3$, $n=5$, $n^1=10$; WT cLTP: $N=3$, $n=6$, $n^1=12$; Het control: $N=3$, $n=6$, $n^1=12$; Het cLTP: $N=3$, $n=6$, $n^1=12$). From these results as a whole, it is apparent that there are basal differences in post-synaptic nanoarchitecture between WT and het tissue. Furthermore, after cLTP there are significant alterations in the nanoarchitecture of GluA2 in proximal areas of hippocampus. Specifically, it is evident that in WT tissue, cLTP causes GluA2 puncta to increase in size (fig. 7b,e,f,g) in conjunction with a decrease in fluorescence

intensity (fig. 7c,h,i,j) with no overall change in the number of puncta (fig. 7d). However, in het tissue, cLTP causes GluA2 puncta to decrease in size while their corresponding fluorescence intensity decreases with no overall change in the number of puncta. These results indicate that there are significant alterations at a presymptomatic HD in nanoscale organization of excitatory synapses in the hippocampus.

Figure 7: GluA2 expression before and after LTP induction in proximal stratum radiatum from WT and Het mice

(A) Representative SRRF images in proximal stratum radiatum of GluA2 in all conditions. Top left: WT control, top right: WT cLTP, bottom left: Het control, bottom right: Het cLTP. (B) GluA2 size for all conditions. (C) GluA2 fluorescent intensity for all conditions. AU stands for arbitrary units. (D) GluA2 density (nano-objects/per μm^2) for WT control, WT cLTP, Het control, and Het cLTP. (E) Cumulative frequency graph for GluA2 size comparing WT control and Het control tissue. (F) Cumulative frequency graph for GluA2 size comparing WT control and WT cLTP tissue. (G) Cumulative frequency graph for GluA2 size comparing Het control and Het cLTP tissue. (H) Cumulative frequency graph for GluA2 intensity comparing WT control and WT cLTP tissue. (I) Cumulative frequency graph for GluA2 intensity comparing WT control and WT cLTP tissue. (J) Cumulative frequency graph for GluA2 intensity comparing Het control and Het cLTP tissue.



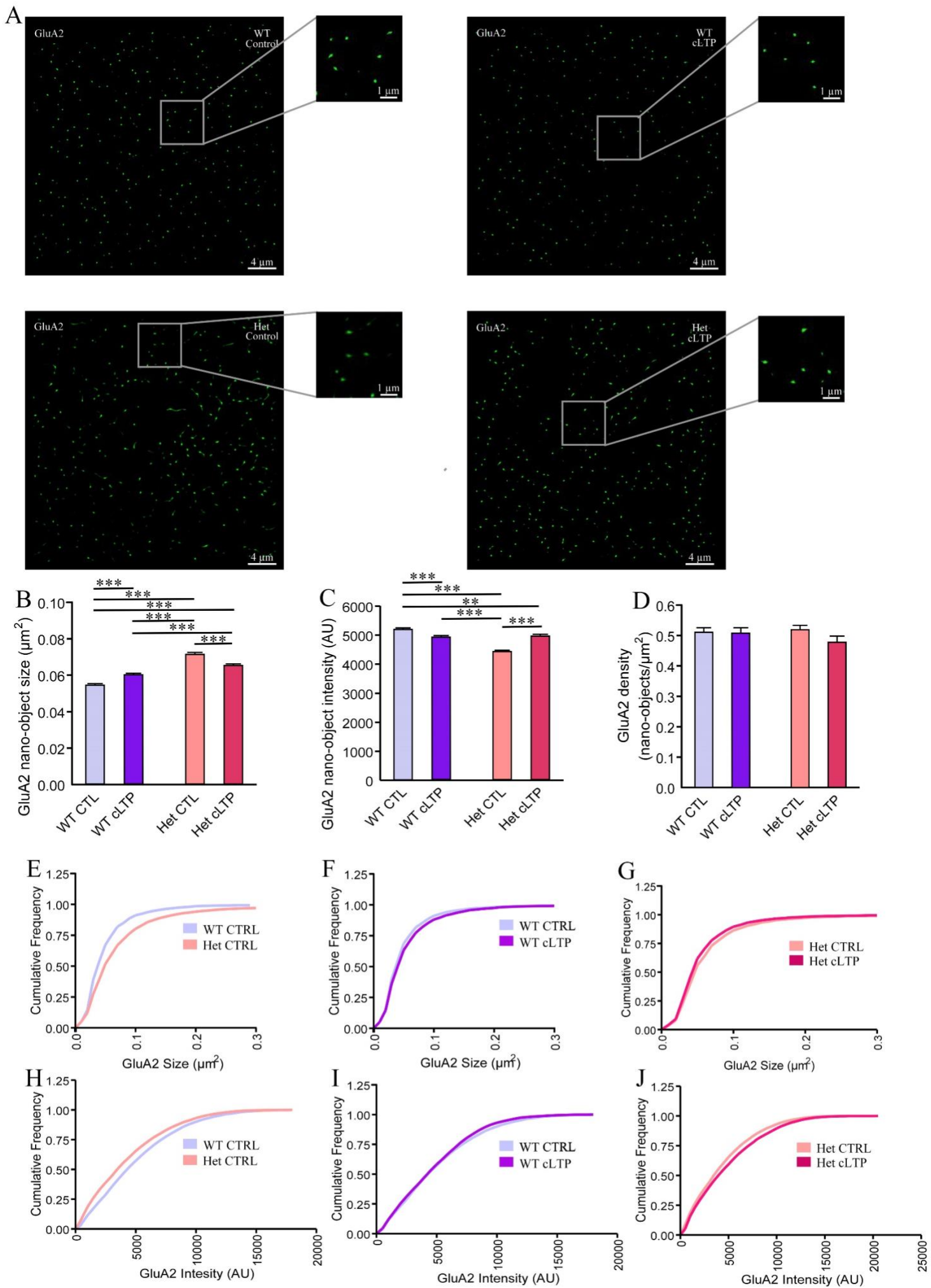
3-5 SRRF imaging of GluA2 in distal stratum radiatum in WT and heterozygous mice.

In distal stratum radiatum (i.e. 500-800 μm away from CA3 cell bodies), similar to proximal, we observed a significant difference in GluA2 size (fig. 8b);(one-way ANOVA, $p < 0.001$). More specifically, het control GluA2 size was significantly larger than WT control GluA2 size. Furthermore, cLTP significantly increased GluA2 size in WT tissue, while cLTP significantly reduced GluA2 size in het tissue (post-hoc Tukey tests for WT control vs. WT cLTP, $p < 0.001$; WT control vs. Het control, $p < 0.001$; WT control vs. Het cLTP, $p < 0.001$; WT cLTP vs. Het control, $p < 0.001$; WT cLTP vs. Het cLTP, $p = 0.001$; Het control vs. Het cLTP, $p < 0.001$; WT control: $N=3$, $n=5$, $n^1=10$, $n^2=5921$; WT cLTP: $N=3$, $n=6$, $n^1=12$, $n^2=6514$; Het control: $N=3$, $n=6$, $n^1=12$, $n^2=6606$; Het cLTP: $N=3$, $n=6$, $n^1=12$, $n^2=6662$). When measuring GluA2 fluorescent intensity (fig. 8c), we found a significant difference (one-way ANOVA, $p < 0.001$). More specifically, het basal intensity was significantly decreased when compared to WT basal tissue. Furthermore, cLTP significantly reduced GluA2 intensity in WT tissue, while cLTP significantly increased GluA2 intensity in Het tissue. (post-hoc Tukey tests for WT control vs. WT cLTP, $p = 0.001$; WT control vs. Het control, $p = 0.0019$; WT control vs. Het cLTP, $p < 0.001$; WT cLTP vs. Het control, $p < 0.001$; WT cLTP vs. Het cLTP, $p = 0.0019$; Het control vs. Het cLTP, $p < 0.001$; WT control: $N=3$, $n=5$, $n^1=10$, $n^2=5921$; WT cLTP: $N=3$, $n=6$, $n^1=12$, $n^2=6514$; Het control: $N=3$, $n=6$, $n^1=12$, $n^2=6606$; Het cLTP: $N=3$, $n=6$, $n^1=12$, $n^2=6662$). When measuring GluA2 density (fig. 8d, number of nano-objects per area) we found no significant difference (one way ANOVA, $p = 0.340$; post-hoc Tukey tests for WT control vs. WT cLTP, $p = 0.999$; WT control vs. Het control, $p =$

0.990; WT control vs. Het cLTP, $p = 0.529$; WT cLTP vs. Het control, $p = 0.968$; WT cLTP vs. Het cLTP, $p = 0.597$; Het control vs. Het cLTP, $p = 0.328$ WT control: $N=3$, $n=5$, $n^1=10$; WT cLTP: $N=3$, $n=6$, $n^1=12$; Het control: $N=3$, $n=6$, $n^1=12$; Het cLTP: $N=3$, $n=6$, $n^1=12$). From these data, we can infer that after cLTP there are significant alterations in the nanoarchitecture of GluA2 in distal stratum radiatum. The similar changes that we observed in both proximal and distal areas of hippocampus in terms of size (fig. 8b,e,f,g), intensity (fig. 8c,h,i,j), and density (fig. 8d) are indicative of spatially sustained alterations of post-synaptic nanoarchitecture in the stratum radiatum of presymptomatic HD.

Figure 8: GluA2 expression before and after LTP induction in distal stratum radiatum from WT and Het mice

(A) Representative SRRF images in distal stratum radiatum of GluA2 in all conditions. Top left: WT control, top right: WT cLTP, bottom left: Het control, bottom right: Het cLTP. (B) GluA2 size for all conditions. (C) GluA2 fluorescent intensity for all conditions. AU stands for arbitrary units (D) GluA2 density (nano-objects/per μm^2) for WT control, WT cLTP, Het control, Het cLTP. (E) Cumulative frequency graph for GluA2 size comparing WT control and Het control tissue. (F) Cumulative frequency graph for GluA2 size comparing WT control and WT cLTP tissue. (G) Cumulative frequency graph for GluA2 size comparing Het control and Het cLTP tissue. (H) Cumulative frequency graph for GluA2 intensity comparing WT control and WT cLTP tissue. (I) Cumulative frequency graph for GluA2 intensity comparing WT control and WT cLTP tissue. (J) Cumulative frequency graph for GluA2 intensity comparing Het control and Het cLTP tissue.



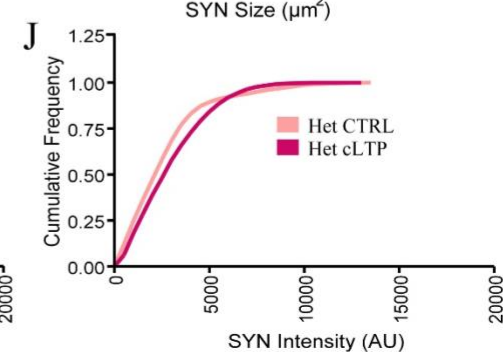
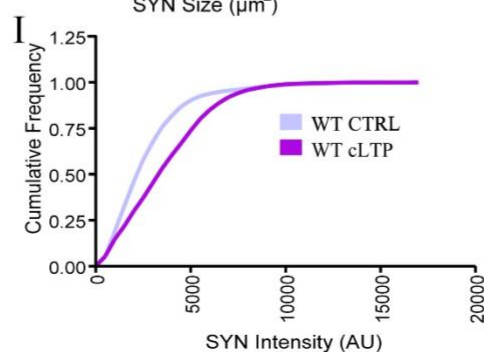
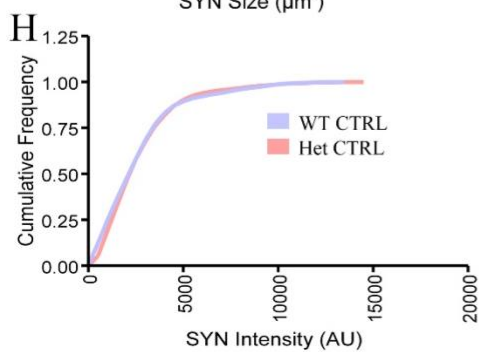
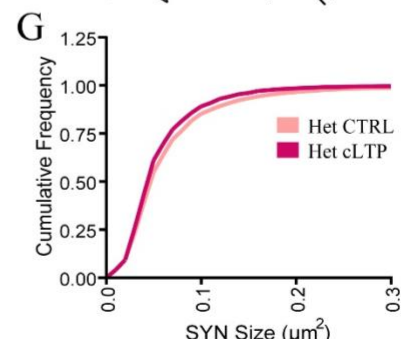
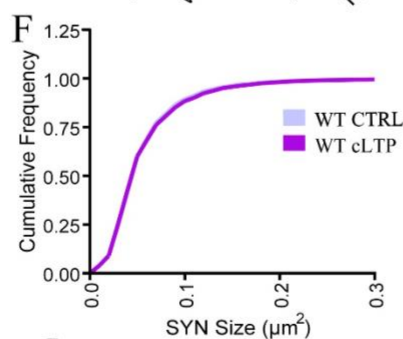
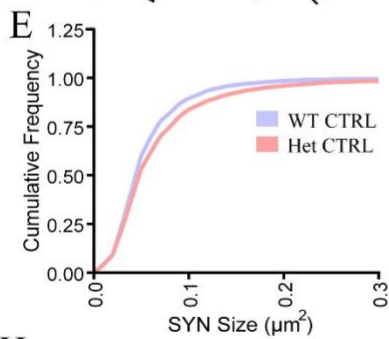
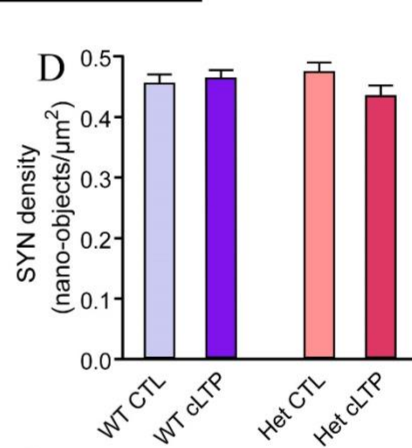
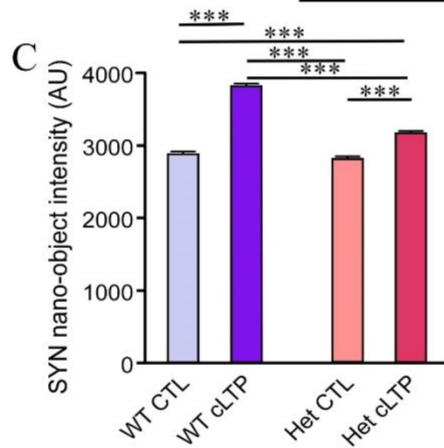
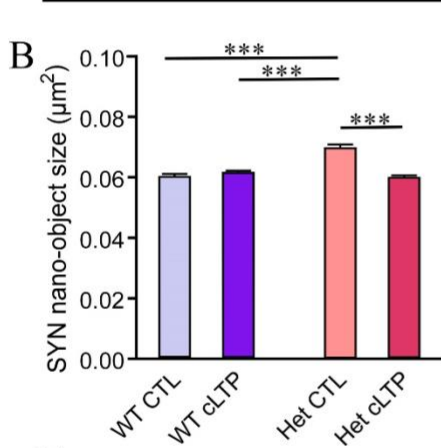
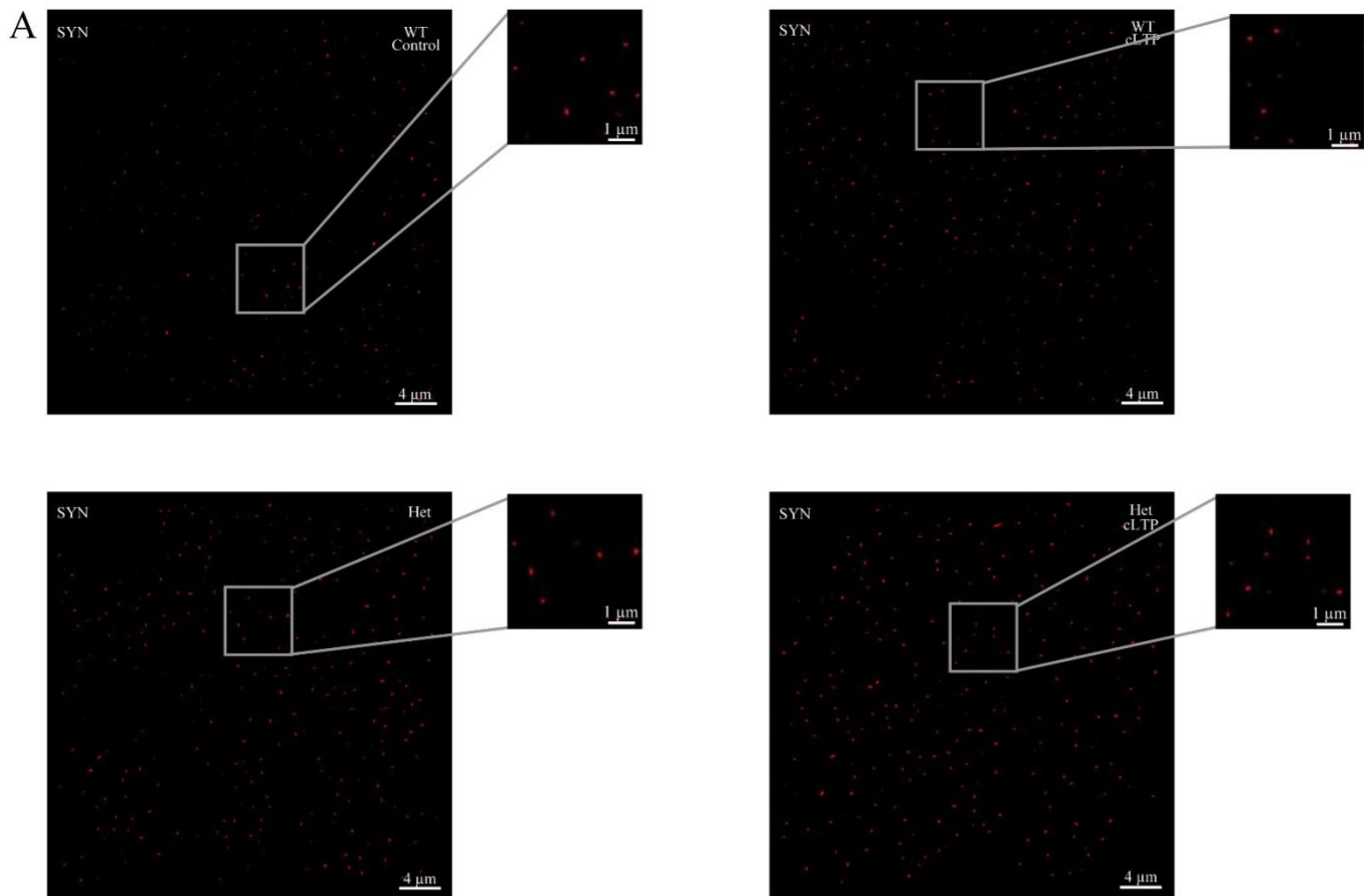
3-6 SRRF imaging of synaptophysin in proximal stratum radiatum in WT and heterozygous mice.

In proximal stratum radiatum (i.e. 150-450 μm away from CA3 cell bodies) when investigating SYN (fig. 9, we found a significant difference in SYN size (fig. 9b);(one-way ANOVA, $p < 0.001$). More specifically, in basal conditions, het control SYN size was significantly larger than WT control SYN size. Furthermore, cLTP significantly reduced SYN size in het tissue but had no effect on WT tissue (post-hoc Tukey tests for WT control vs. WT cLTP, $p = 0.688$; WT control vs. Het control, $p < 0.001$; WT control vs. Het cLTP, $p = 0.980$; WT cLTP vs. Het control, $p < 0.001$; WT cLTP vs. Het cLTP, $p = 0.385$; Het control vs. Het cLTP, $p < 0.001$; WT control: $N=3$, $n=5$, $n^1=10$, $n^2=5272$; WT cLTP: $N=3$, $n=6$, $n^1=12$, $n^2=6784$; Het control: $N=3$, $n=6$, $n^1=12$, $n^2=6588$; Het cLTP: $N=3$, $n=6$, $n^1=12$, $n^2=6050$). The change in SYN size is indicative of a pre-synaptic alteration in nanoarchitecture of presymptomatic HD mice. Furthermore, we found a significant difference in SYN intensity (fig.10c, one-way ANOVA, $p < 0.001$). Firstly, there was no observed difference in basal intensity between WT and HD mice. cLTP significantly increased SYN intensity in both WT and Het tissue, however the increase in het tissue was not as large as the increase in WT tissue (post-hoc Tukey tests for WT control vs. WT cLTP, $p < 0.001$; WT control vs. Het control, $p = 0.365$; WT control vs. Het cLTP, $p < 0.001$; WT cLTP vs. Het control, $p < 0.001$; WT cLTP vs. Het cLTP, $p < 0.001$; Het control vs. Het cLTP, $p < 0.001$; WT control: $N=3$, $n=5$, $n^1=10$, $n^2=5272$; WT cLTP: $N=3$, $n=6$, $n^1=12$, $n^2=6784$; Het control: $N=3$, $n=6$, $n^1=12$, $n^2=6588$; Het cLTP: $N=3$, $n=6$, $n^1=12$, $n^2=6050$). When measuring SYN density (fig. 9d, number of nano-objects per image), similar to our GluA2 results, we found no significant difference

between genotypes or treatment conditions in proximal stratum radiatum (one way ANOVA, $p = 0.275$; post-hoc Tukey tests for WT control vs. WT cLTP, $p = 0.979$; WT control vs. Het control, $p = 0.809$; WT control vs. Het cLTP, $p = 0.779$; WT cLTP vs. Het control, $p = 0.954$; WT cLTP vs. Het cLTP, $p = 0.500$; Het control vs. Het cLTP, $p = 0.231$; WT control: $N=3$, $n=5$, $n^1=10$; WT cLTP: $N=3$, $n=6$, $n^1=12$; Het control: $N=3$, $n=6$, $n^1=12$; Het cLTP: $N=3$, $n=6$, $n^1=12$). Here, we surmise that after cLTP there are significant alterations in the puncta properties of SYN in relation to size (fig. 9b,e,f,g) and intensity (fig. 9c,h,i,j), suggesting pre-synaptic alterations. Distinct changes were found in nanoarchitecture of the hippocampal synapses of HD mice in comparison to WT, which may underlie functional differences.

Figure 9: SYN expression before and after LTP induction in proximal stratum radiatum from WT and Het mice

(A) Representative SRRF images in proximal stratum radiatum of SYN before (control) or after cLTP induction in WT or het. Top left: WT control, top right: WT cLTP, bottom left: Het control, bottom right: Het cLTP. (B) SYN size for all conditions. (C) SYN fluorescent intensity for all conditions. AU stands for arbitrary units (D) SYN density (nans-objects/per μm^2) for WT control, WT cLTP, Het control, and Het cLTP. (E) Cumulative frequency graph for SYN size comparing WT control and Het control tissue. (F) Cumulative frequency graph for SYN size comparing WT control and WT cLTP tissue. (G) Cumulative frequency graph for SYN size comparing Het control and Het cLTP tissue. (H) Cumulative frequency graph for SYN intensity comparing WT control and WT cLTP tissue. (I) Cumulative frequency graph for SYN intensity comparing WT control and WT cLTP tissue. (J) Cumulative frequency graph for SYN intensity comparing Het control and Het cLTP tissue.



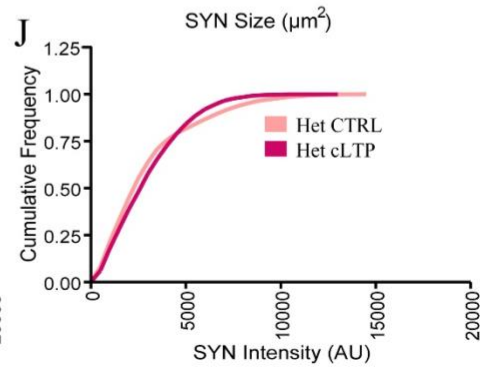
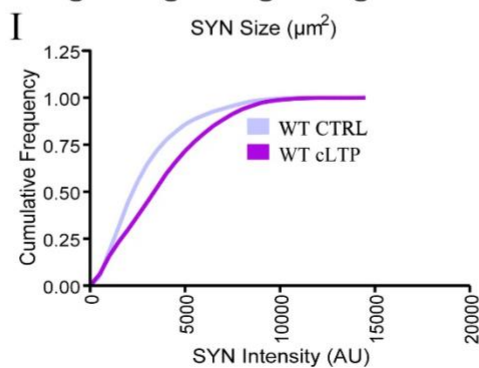
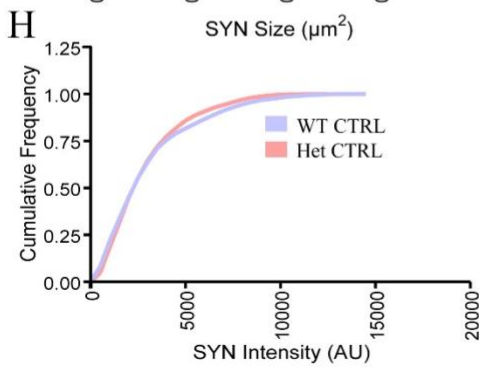
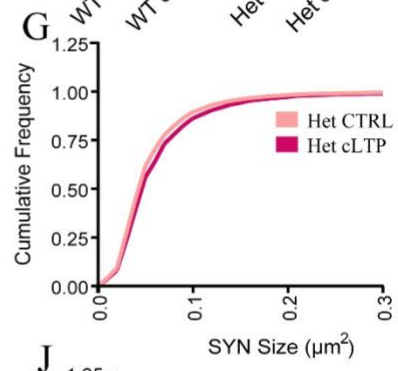
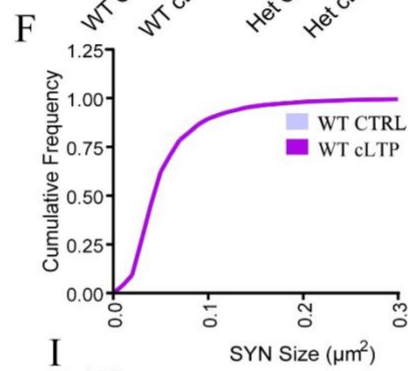
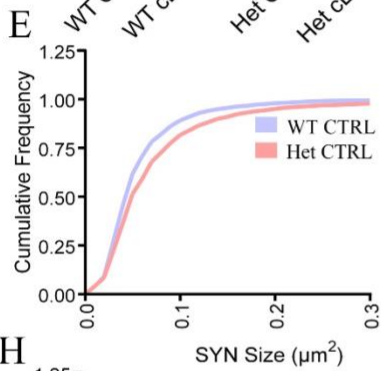
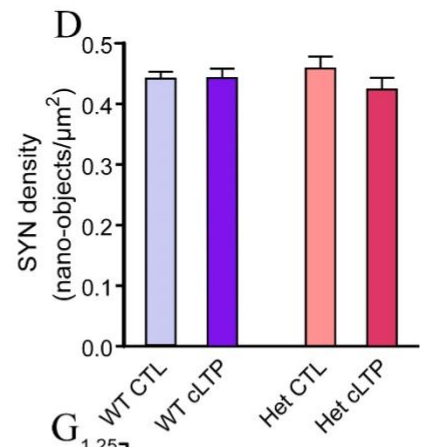
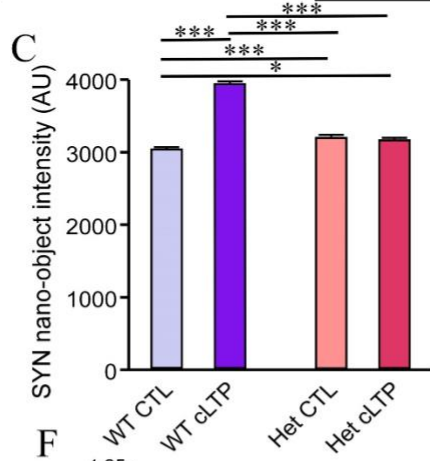
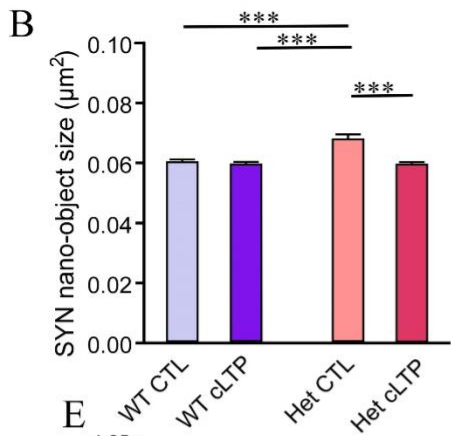
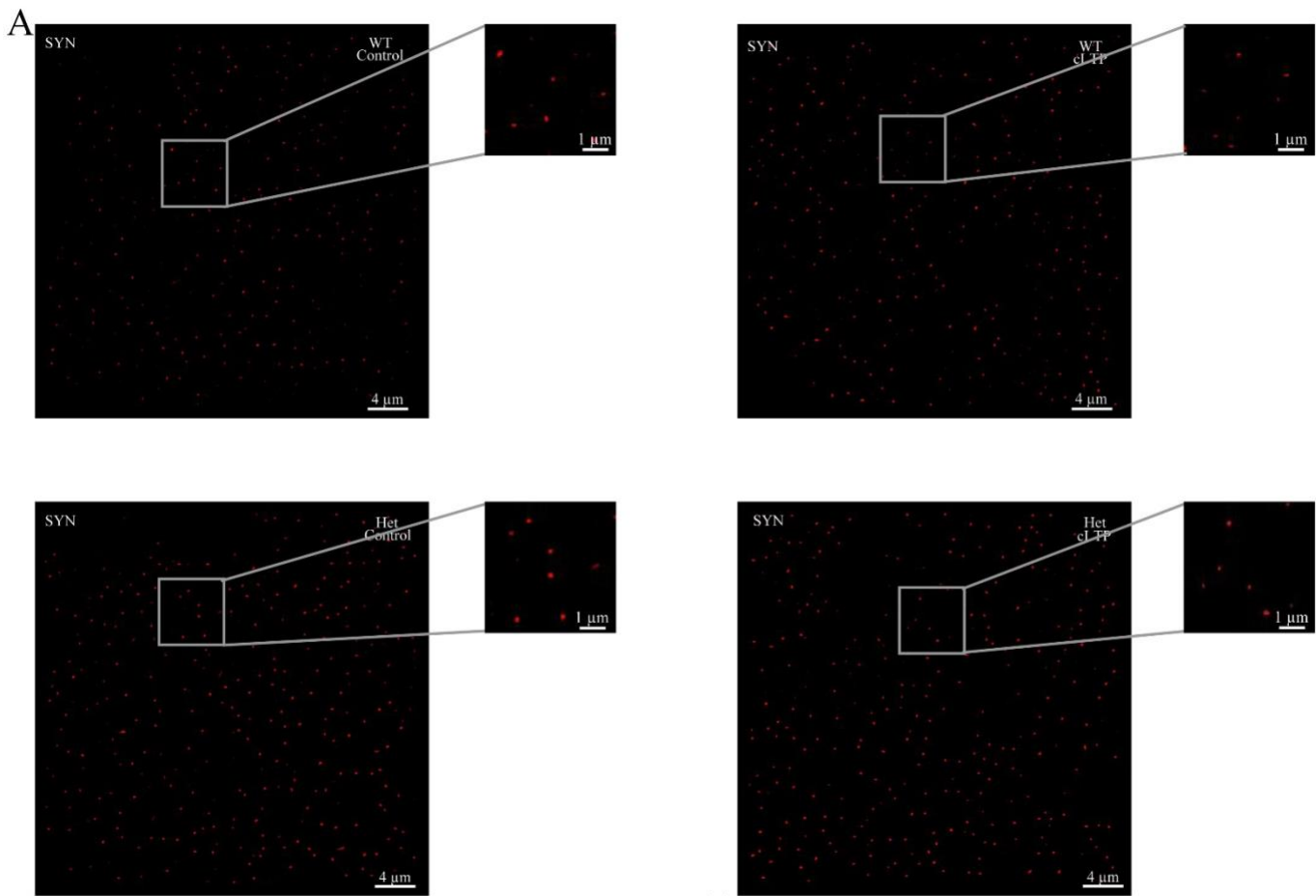
3-7 SRRF imaging of Synaptophysin in distal stratum radiatum in WT and heterozygous mice.

In distal stratum radiatum (i.e. 500-800 μm away from CA3 cell bodies);(fig. 10), we found a significant difference in SYN size (fig. 10b);(one-way ANOVA, $p < 0.001$). More specifically, in similar fashion to proximal areas, het SYN size in the basal condition (control) was significantly larger than WT control SYN size. Furthermore, cLTP significantly reduced SYN size in het tissue but had no effect in WT tissue (post-hoc Tukey tests for WT control vs. WT cLTP, $p = 0.935$; WT control vs. Het control, $p < 0.001$; WT control vs. Het cLTP, $p = 0.913$; WT cLTP vs. Het control, $p < 0.001$; WT cLTP vs. Het cLTP, $p = 0.100$; Het control vs. Het cLTP, $p < 0.001$; WT control: $N=3$, $n=5$, $n^1=10$, $n^2=5117$; WT cLTP: $N=3$, $n=6$, $n^1=12$, $n^2=6146$; Het control: $N=3$, $n=6$, $n^1=12$, $n^2=5830$; Het cLTP: $N=3$, $n=6$, $n^1=12$, $n^2=5892$). It is clear from these results that the pre-synaptic alterations in SYN size described above are apparent across stratum radiatum in presymptomatic HD mice. In addition, we found a significant difference in SYN intensity (fig. 10c, one-way ANOVA, $p < 0.001$). More specifically, cLTP significantly increased SYN intensity in WT tissue but showed no significant effect in Het tissue (post-hoc Tukey tests for WT control vs. WT cLTP, $p < 0.001$; WT control vs. Het control, $p = 0.009$; WT control vs. Het cLTP, $p = 0.011$; WT cLTP vs. Het control, $p < 0.001$; WT cLTP vs. Het cLTP, $p < 0.001$; Het control vs. Het cLTP, $p = 0.881$; WT control: $N=3$, $n=5$, $n^1=10$, $n^2=5117$; WT cLTP: $N=3$, $n=6$, $n^1=12$, $n^2=6146$; Het control: $N=3$, $n=6$, $n^1=12$, $n^2=5830$; Het cLTP: $N=3$, $n=6$, $n^1=12$, $n^2=5892$). When measuring SYN density (fig. 10d, number of nano-objects per image) we found no significant differences in distal stratum radiatum within genotypes or treatment conditions (one-way

ANOVA, $p = 0.559$; post-hoc Tukey tests for WT control vs. WT cLTP, $p > 0.999$; WT control vs. Het control, $p = 0.916$; WT control vs. Het cLTP, $p = 0.878$; WT cLTP vs. Het control, $p = 0.912$; WT cLTP vs. Het cLTP, $p = 0.854$; Het control vs. Het cLTP, $p = 0.481$; WT control: $N=3$, $n=5$, $n^1=10$; WT cLTP: $N=3$, $n=6$, $n^1=12$; Het control: $N=3$, $n=6$, $n^1=12$; Het cLTP: $N=3$, $n=6$, $n^1=12$). From these results, it is apparent that in distal stratum radiatum, SYN size is not affected after cLTP in WT tissue and is significantly decreased after cLTP in het tissue (fig.11 b,e,f,g). Unlike in proximal areas of hippocampus however, cLTP seems to have no effect on het SYN intensity in distal areas (fig.11 c,h,i,j) indicating that the phenomenon experienced in proximal areas of stratum radiatum in het mice does not translate to distal areas. Similar to GluA2, we observe no discernable difference in SYN density (fig.11 d) in any of the conditions.

Figure 10: SYN expression before and after LTP induction in distal stratum radiatum from WT or Het mice

(A) Representative distal SRRF images of SYN in all conditions. Top left: WT control, top right: WT cLTP, bottom left: Het control, bottom right: Het cLTP. (B) SYN size for all conditions. (C) SYN fluorescent intensity for all conditions. AU stands for arbitrary units (D) SYN density (nano-objects/per μm^2) for WT control, WT cLTP, Het control, and Het cLTP. (E) Cumulative frequency graph for SYN size comparing WT control and Het control tissue. (F) Cumulative frequency graph for SYN size comparing WT control and WT cLTP conditions. (G) Cumulative frequency graph for SYN size comparing Het control and Het cLTP tissue. (H) Cumulative frequency graph for SYN intensity comparing WT control and WT cLTP tissue. (I) Cumulative frequency graph for SYN intensity comparing WT control and WT cLTP tissue. (J) Cumulative frequency graph for SYN intensity comparing Het control and Het cLTP tissue.



3-8 Nearest neighbour analysis of GluA2 and Synaptophysin along stratum radiatum in WT and heterozygous mice.

It has been shown that proteins and their associated functions at pre-synaptic terminals and at the post-synaptic density (PSD) are strongly correlated, and this correlation in protein structure and function may underlie structural and synaptic plasticity (Schikorski and Stevens, 1997; Hruska et al., 2018). Furthermore, it was recently shown that organization of NMDARs on a nanoscale level is dependent on subunit composition (Ladépêche et al., 2018). Here, in order to better understand the nanoarchitecture of the synapse and its pre and post-synaptic proteins, we used a NN analysis to determine the average distance between the AMPAR subunit GluA2 and its nearest pre-synaptic SYN neighbour in both proximal and distal (fig. 11,12) areas of hippocampus in WT control, WT cLTP, Het control, and Het cLTP tissue.

In proximal stratum radiatum, we observed a significant overall difference in GluA2 to SYN distance via NN analysis (fig. 11). We created Voronoi plots to visualize the 2D-distribution of the distance between nearest GluA2 and SYN neighbours, with cool colours (blue, black) representing closer distances and warmer colours (red, orange yellow) representing further distances (fig. 11b,12b). Specifically, cLTP significantly increased the distance between NN in het tissue, but had no effect on WT tissue (fig. 11c, d)(one-way ANOVA, $p < 0.001$. Post-hoc Tukey tests for WT control vs. WT cLTP, $p = 0.376$; WT control vs. Het Control, $p = 0.770$; WT control vs. Het cLTP, $p = 0.004$; WT cLTP vs. Het Control, $p = 0.034$; WT cLTP vs. Het cLTP, $p < 0.001$; Het Control vs. Het cLTP, $p = 0.007$; WT control: $N=3$, $n=6$, $n^1=12$, $n^2=5869$; WT cLTP: $N=3$, $n=5$, $n^1=10$, $n^2=7003$; Het control: $N=3$, $n=6$, $n^1=12$, $n^2=7319$; Het cLTP: $N=3$, $n=6$, $n^1=12$, $n=6758$).

In distal areas of hippocampus, we did not observe any significant overall differences in GluA2 to SYN distance via NN analysis (fig.12c, d)(one-way ANOVA, $p = 0.186$. Post-hoc Tukey tests for WT control vs. WT cLTP, $p = 0.669$; WT control vs. Het Control, $p = 0.797$; WT control vs. Het cLTP, $p = 0.130$; WT cLTP vs. Het Control, $p = 0.996$; WT cLTP vs. Het cLTP, $p < 0.715$; Het Control vs. Het cLTP, $p = 0.566$; WT control: $N=3$, $n=5$, $n^1=10$, $n^2=5920$; WT cLTP: $N=3$, $n=6$, $n^1=12$, $n^2=6514$; Het control: $N=3$, $n=6$, $n^1=12$, $n^2=6606$; Het cLTP: $N=3$, $n=6$, $n^1=12$, $n^2=6662$). From these data, it is evident that the changes in the distance between pre- and postsynaptic structures as detected by NN analysis of SYN and GluA2 puncta occur in proximal stratum radiatum but not in distal areas. Thus, it is possible that at this very early stage of HD, anomalies related to how the pre and post-synapse structure are only apparent in proximal stratum radiatum and have yet to propagate to distal areas.

Figure 11: NN analysis of SRRF images for GluA2 and SYN in proximal stratum radiatum in WT control, WT cLTP, Het Control, and Het cLTP conditions.

(A) Representative composite images showing GluA2 in green and SYN in red. Top left: WT control; top right: WT cLTP; bottom right: Het control; bottom left: Het cLTP. (B) Representative Voronoi plots for each condition. (C) Cumulative frequency plot for GluA2 NN-to-SYN analysis. (D) Bar graph displaying GluA2 NN-to-SYN distance (μm) for each condition.

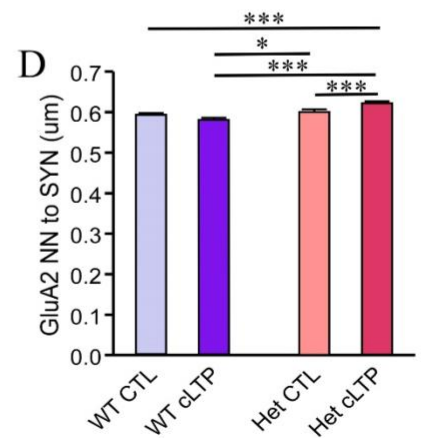
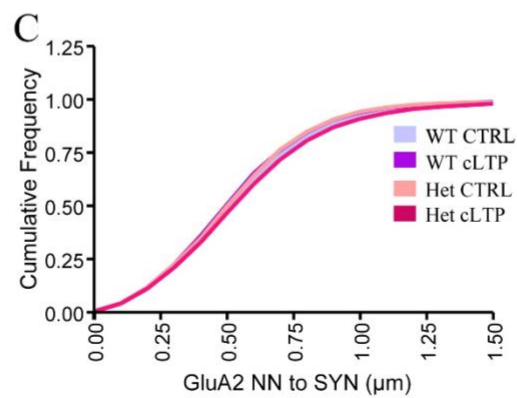
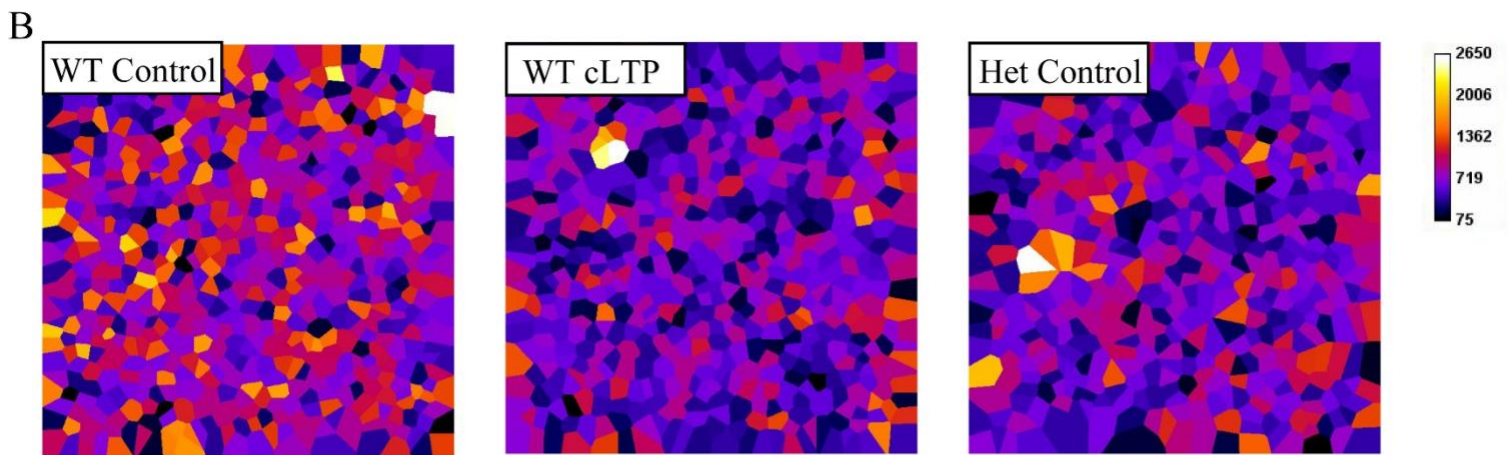
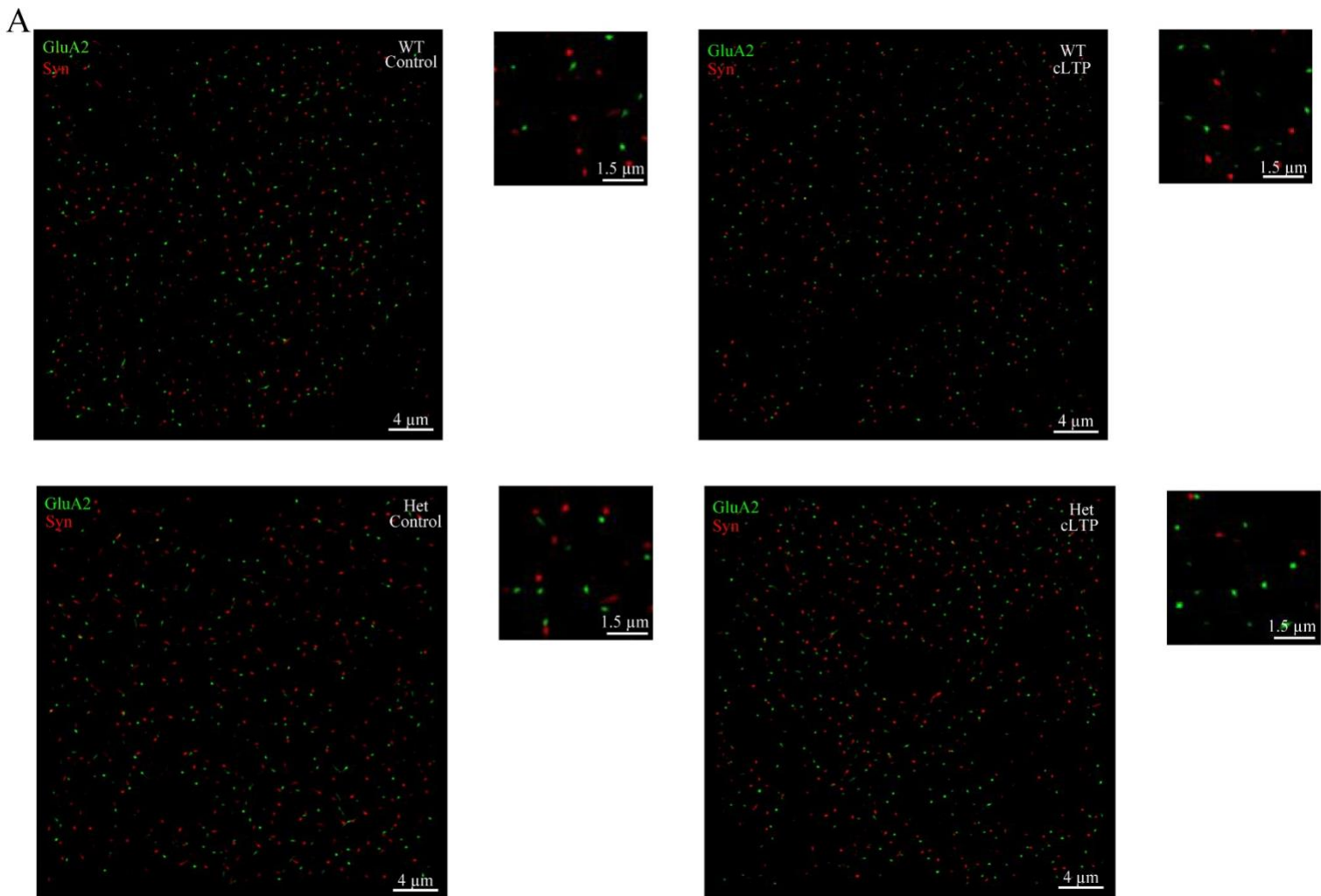
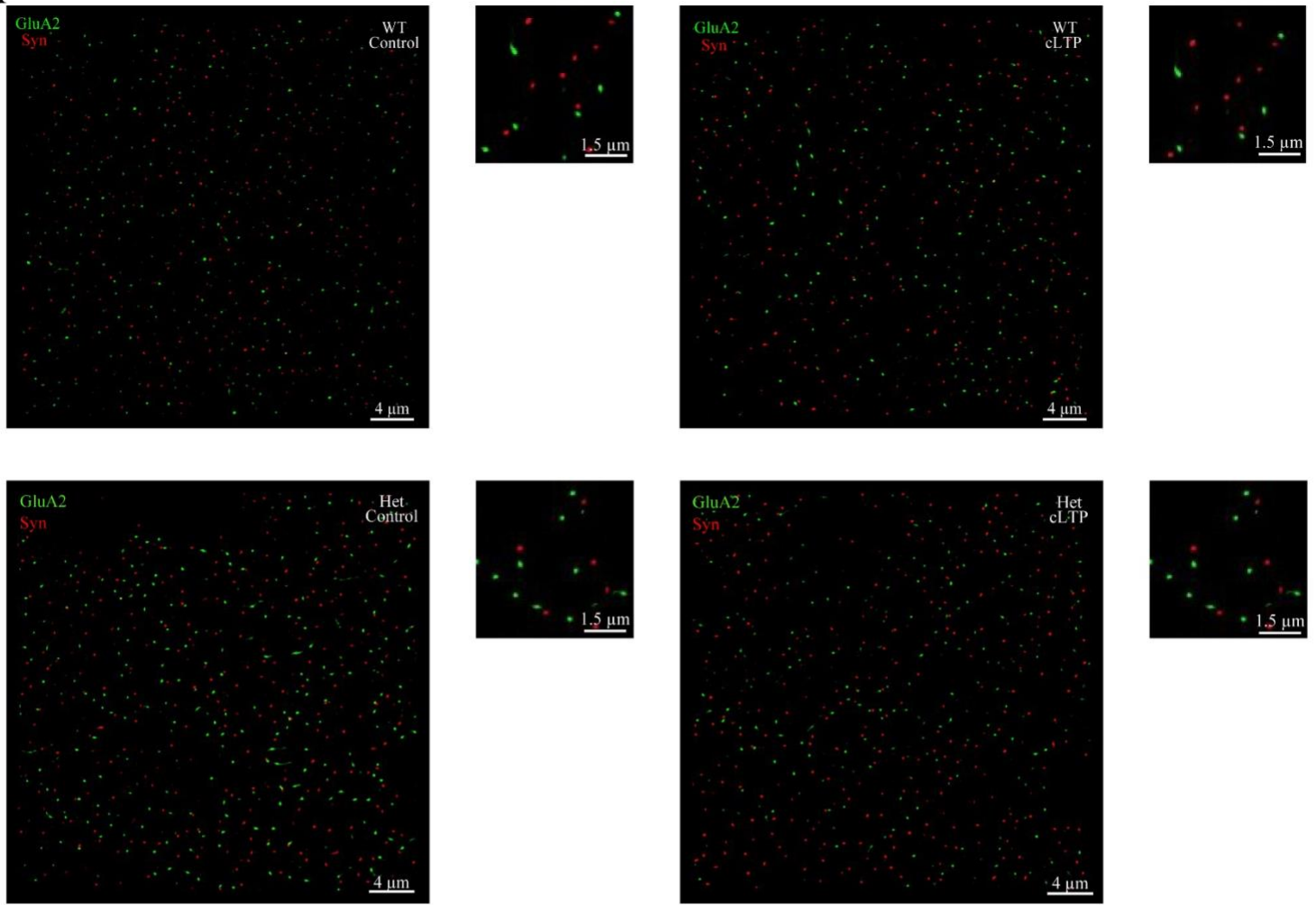


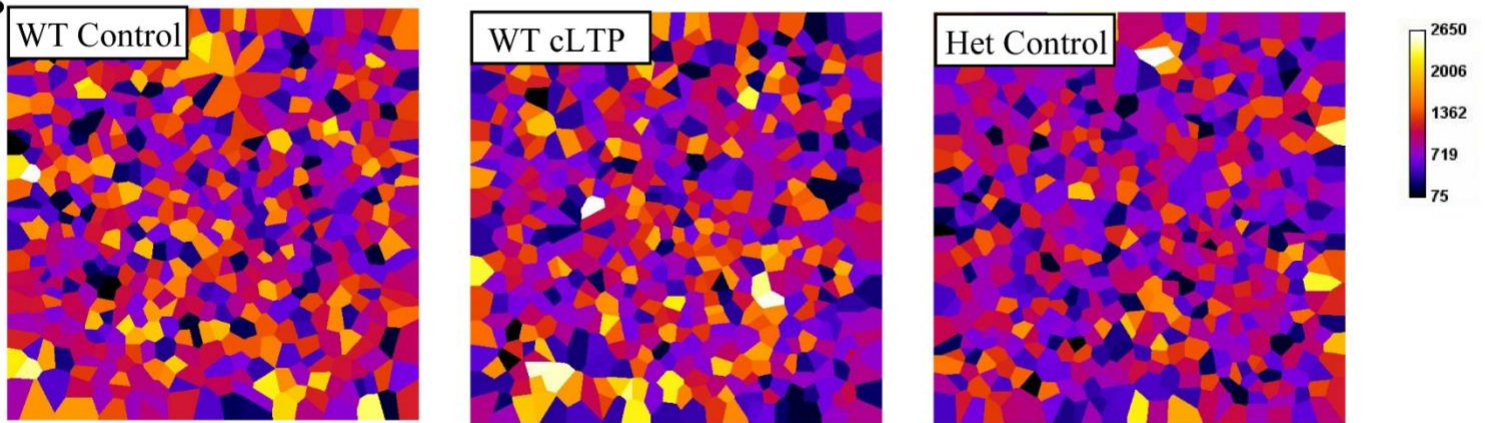
Figure 12: NN analysis of SRRF images for GluA2 and SYN in distal stratum radiatum in WT control, WT cLTP, Het Control, and Het cLTP conditions.

(A) Representative composite images showing GluA2 in green and SYN in red. Top left: WT control; top right: WT cLTP; bottom right: Het control; bottom left: Het cLTP. (B) Representative Voronoi plots for each condition. (C) Cumulative frequency plot for GluA2 NN to SYN analysis. (D) Bar graph displaying GluA2 NN to SYN distance (μm) for each condition.

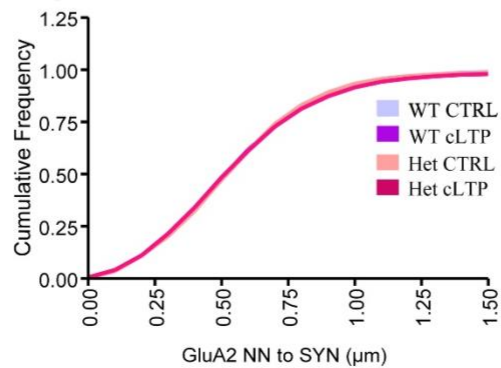
A



B



C



D

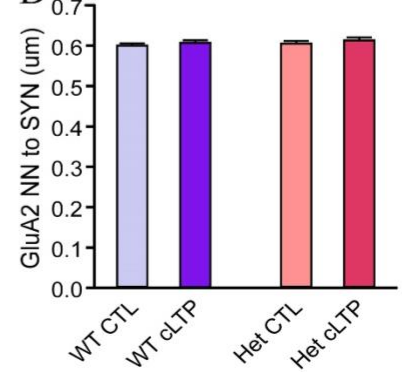
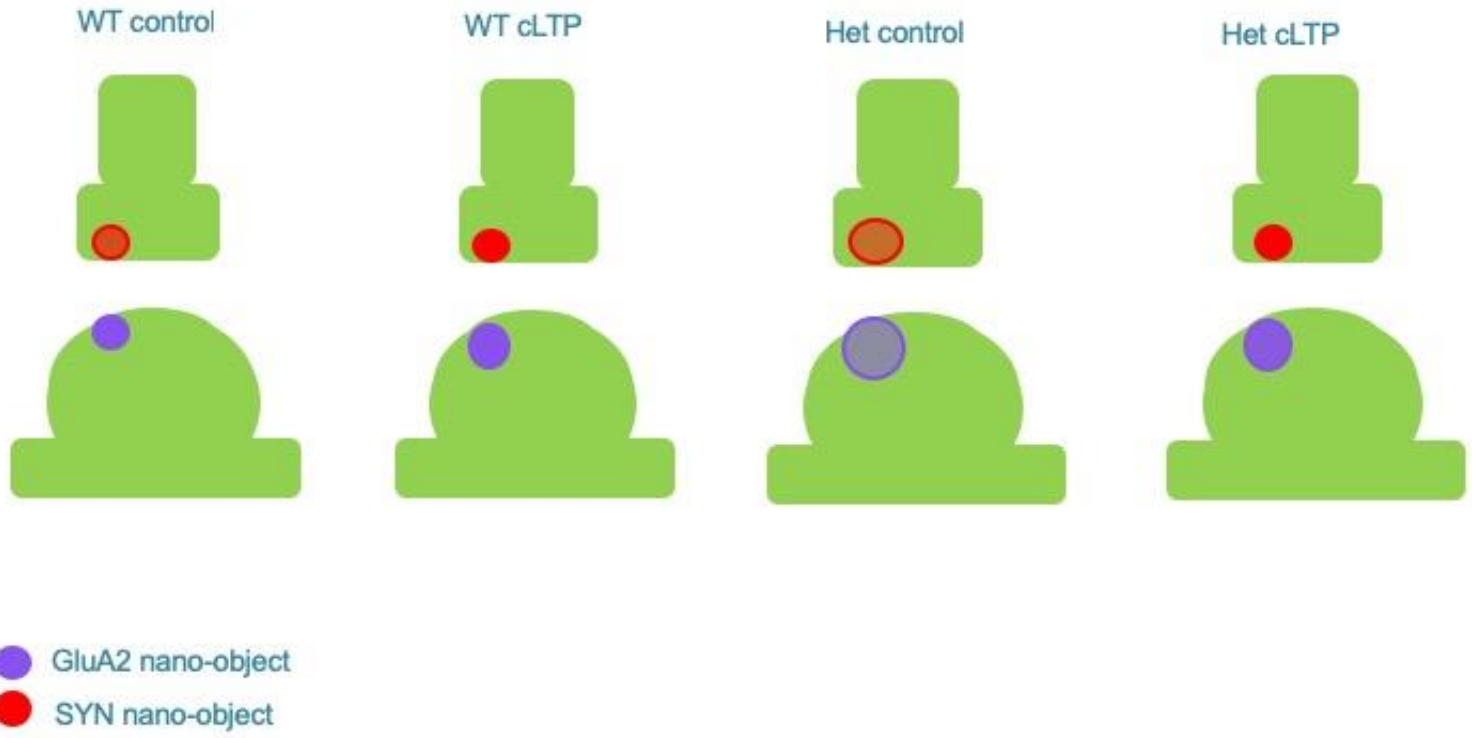


Figure 13: Summary of SRRF size, intensity, and density results.

Schematic displaying WT control, WT cLTP, Het control, and Het cLTP pre and post-synaptic terminals (green) with red circles representing SYN, and purple circles representing GluA2. Here, the size of each circle represents the change in nano-object size, and the transparency of each circle represents the fluorescent intensity. Each terminal has one representative circle to exemplify no change in nano-object density.



4-0 Discussion

4-1 Early synaptic deficits in HD

Deciphering the cellular and synaptic underpinnings of prodromal HD may allow for a breakthrough in disease treatment that has evaded clinicians and researchers alike since the beginning of HD investigation. It is already evident based on the literature that an abundance of presymptomatic aberrations in synaptic transmission and cognitive function exist in HD animal models. Specifically, at 2 months of age before the onset of behavioural symptoms that occur at around 6 months, YAC128 mice exhibited learning deficits on the rotarod test of motor coordination (Van Raamsdonk et al., 2005b). Furthermore, transgenic R6/2 HD mice, unlike controls, swam in random patterns with little to no reference to the location of the platform in a Morris water maze, indicating an impairment in spatial cognition (Murphy et al., 2000).

In conjunction with early behavioural abnormalities related to cognitive function, presymptomatic deficits in synaptic transmission have also been well documented in HD, but mostly in the striatum. For example, young R6/2 mice showed increased neuronal cell-membrane input resistance, lower stimulus intensity to evoke action potentials, and reduced paired-pulse facilitation in comparison to WT controls (Klapstein et al., 2001). Moreover, in presymptomatic 1-month old YAC128 mice, AMPAR-mediated postsynaptic currents and pre-synaptic glutamate release were significantly increased, corresponding to an increased responsiveness of MSNs to cortical stimulation. Additionally, it was recently postulated that dysregulated AMPAR surface diffusion and failure to stabilize these receptors after cLTP induction may underlie deficits in synaptic

transmission observed in a multitude of HD mouse models (Zhang et al., 2018). Presymptomatic deficits in the striatum have been well explored, however, presymptomatic deficits of the HD hippocampus have been largely understudied. Further investigation into the hippocampus in early HD could help provide more information surrounding the cellular mechanisms underlying early disease progression in cognitive function. It is important to reiterate here that all experiments conducted for the purposes of this thesis were carried out in a clinically relevant mouse model of HD, Q175FDN. This model shows slowly progressing disease phenotype, expresses human mhtt, and closely resembles the genetic mutation that causes HD. Therefore, this model is highly valuable for pre-clinical investigation (Southwell et al., 2016).

To illuminate subtle deficits at a presymptomatic stage of a disease, it is often necessary to explore the disease state at a cellular level. One method of cellular investigation that is often employed by neuroscience researchers is measuring electrical properties of neurons. It is apparent that the majority of electrophysiological evidence associated with HD has been executed via conventional methods, specifically via intracellular recording such as whole-cell patch clamping or extracellular recording by measuring field potentials. Although these techniques are accurate and utilized often, they lack the ability to examine the spatial properties of a specific brain area as a whole. We utilized multi-electrode array electrophysiology to examine the hippocampus, a brain area that has been implicated in HD and is well-known for its role in learning and memory and plays a key role in multi-modal sensory integration (Zola-Morgan and Squire, 1990; Squire and Zola-Morgan, 1991). Moreover, a high degree of transcriptional variability across the axes (Thompson et al., 2008; Cembrowski et al., 2016) of hippocampus have

been described, making simultaneous spatial investigation of its electrophysiological properties very important.

4-2 TBS and HFS LTP in presymptomatic HD

Here, using the MED64 system, we examined LTP along the stratum radiatum of hippocampus in 3-month old, presymptomatic Q175FDN HD mice. We observed a significant impairment in LTP induced by TBS in distal areas of the Schaffer collateral synapse of hippocampus. Specifically, these impairments were observed from distances of 450-750 μm away from the stimulating electrode but not in areas close by. Our electrophysiological findings are unique for a number of reasons; firstly, this deficit is observed 3 months before the onset of any quantifiable behavioural HD phenotype in the Q175FDN mice, indicating it could be among the earliest detectable synaptic aberrations associated with HD. Furthermore, it is unlikely that this impairment would have been detected as easily with conventional electrophysiology, as it was only apparent at distal electrodes in the electrode array. It is also important to note that in LTP induced by HFS, we observed no discernable differences between WT and het mice, indicating that the pattern of synaptic activity is critical. Firstly, TBS is modeled after the endogenous complex spike activity that occurs either during the positive or negative phases of hippocampal theta rhythm (Perez et al., 1999), thus arguably making it a more physiologically-relevant stimulation paradigm than HFS. Therefore, our results reflect a more physiologically-accurate deficit in LTP that would likely be observed in human HD than if our deficit was observed with HFS. Similar to our results, it was found that in an

animal model of Down syndrome, mice showed significant impairments in TBS induced LTP but not HFS (Costa and Grybko, 2005).

It is also well known that TBS and HFS rely on different intracellular signaling pathways to mediate their effects. For example, TBS requires calpain-1 activation (Zhu et al., 2015). Calpains are a family of neutral calcium-dependent proteases that have the unique ability to cleave proteins to modify the activity and/or function of their substrates (Baudry and Bi, 2016). In general, calpain-1 is required for LTP induction and is generally neuroprotective (Baudry and Bi, 2016). Thus, the deficit we observe in TBS-LTP may be mediated by deficits in calpain-1 in distal areas of presymptomatic HD mice. Furthermore, calpains, specifically calpain-2 and its targets, have been implicated in other neurodegenerative diseases such as Alzheimer Disease (Patrick et al., 1999; Kimura et al., 2014), making it likely that calpains also play a role in HD. To test this, we could investigate calpain levels in presymptomatic HD mice.

TBS-induced LTP also requires ERK activation (Selcher et al., 2003). ERKs are involved in regulation of important neuronal functions, including synaptic plasticity in basal and pathological conditions (Colucci-D'Amato et al., 2003). ERK signaling seems to be disturbed in HD, indicating another possible mechanism for our observed LTP deficit. For example, at the intercellular level ERK-dependent expression of glutamate transporters is decreased by mhTT, leading to increased glutamate signaling and excitotoxicity (Milnerwood et al., 2010; Robertson and Bottomley, 2010). Moreover, at the intracellular level, mhTT impairs glutamate-induced ERK signaling in both an upstream and downstream manner (Roze et al., 2008; Ribeiro et al., 2010). On the other hand, HFS-induced LTP requires protein kinase A (PKA) activation (Kim et al., 2010). Furthermore,

it has been shown that adenosine is released following HFS, but not TBS, to facilitate LTP (Cunha et al., 1996). From this, we can infer that intracellular signaling pathways related to TBS may be altered early on in HD progression while signaling pathways associated with HFS may remain intact.

4-3 Pre and post-synaptic aberrations in early HD

Another possible explanation for the observed deficit in LTP in this study could involve pre-synaptic abnormalities in the heterozygous Q175FDN mice. It has been shown that symptomatic HD mice show a significant reduction in LTP, but LTP could be induced by an “enhanced” tetanic stimulation paradigm (Usdin et al., 1999). This indicates that the LTP producing mechanism is intact in mutant mice, but their synapses are less able to reach the threshold for LTP induction (Usdin et al., 1999). Here, it is possible that the smaller fEPSPs observed at distal areas of hippocampus in HD mice due to the lower gain of input-output relationship are not strong enough to generate the co-operation needed to surpass the threshold required for TBS-LTP, while in WT tissue the fEPSPs are able to meet the requirements for TBS-LTP. It is possible that the smaller EPSPs are due to mutant htt acting at the synaptic terminal to inhibit neurotransmitter release. In agreement, WT htt binds to microtubules and synaptic vesicles, is enriched at the pre-synaptic terminal to enhance BDNF vesicular transport along microtubules (DiFiglia et al., 1995; Gutekunst et al., 1995; Sharp et al., 1995; Gauthier et al., 2004). In future studies, it would be interesting to investigate if increased stimulation intensity during LTP induction could help to overcome the deficit occurring at distal sites of hippocampus. Additionally, a recent study that reconstructed a HD cortico-striatal network via a

microfluidic chip showed marked changes in fast axonal transport early on in the development of the network. Furthermore, significant decreases in vesicular dynamics along with increases in mitochondrial motility were observed (Virlogeux et al., 2018). Moreover, it has been postulated that early abnormal phosphorylation of synapsin, a protein involved in regulating neurotransmitter release, may alter synaptic vesicle trafficking and cause impairments in neurotransmission in HD (Liévens et al., 2002). Similarly, downregulation of complexin II, a eukaryotic cytoplasmic neuronal protein involved in vesicle trafficking, has been observed in different models of HD (Morton and Edwardson, 2001; Edwardson et al., 2003). Although mice deficient in complexin II show no obvious phenotypical abnormalities, LTP impairments in both CA1 and CA3 regions in these mice have been observed (Reim et al., 2001). Thus, it is possible that the LTP deficit we observed at distal areas of hippocampus in HD mice is associated with pre-synaptic abnormalities of synaptic transmission.

It is also plausible that our observed deficits in LTP in the distal areas of the stratum radiatum are postsynaptic, as alterations in post-synaptic signaling in HD have been observed. Specifically, a significant reduction in phospho-ERK-immunopositive striatal neurons in response to cortical stimulation was found in *Hdh*¹⁴⁰ knock-in mice (Virlogeux et al., 2018). Additionally, in the R6/2 model of HD, *mhtt* selectively decreased the expression of NMDARs at the presymptomatic stage (Cha et al., 1998). Involvement of NMDARs in LTP is well documented (Nicoll and Malenka, 1995; Man, 2011), thus decreased expression of NMDARs could explain the impairments in LTP we observe at distal areas of hippocampus. Notably, expanded polyglutamine tracts are known to interfere with the ability of huntingtin to interact efficiently with post-synaptic

density protein 95 (PSD-95), which could influence the normal functioning of proteins anchored in the post-synaptic density, such as NMDARs and AMPARs (Sun et al., 2001). PSD-95 is neuronal scaffolding protein concentrated at excitatory synapses that is involved in synaptic transmission and synapse development (El-Husseini et al., 2000). It was also found that AMPARs have decreased ligand binding activity in the R6/2 model of HD (Cha et al., 1998). Additionally, normal receptor recycling in post-synaptic terminals is regulated by many proteins, such as endophilins, that also bind to huntingtin (Modregger et al., 2003).

4-4 Nanoscale investigation of synapses

It is evident that synaptic deficits in HD can be both pre and post-synaptic, and in all likelihood are a combination of both. A key component to understanding the therapeutic trajectory of HD patients and disease progression involves understanding synaptic dysfunction at the level of individual synapses at the earliest stages of the disease. In order to expand upon our characterization of early synaptic abnormalities in HD, we sought to visualize and examine the nanoarchitecture of the synapse via novel microscopy techniques that are more sensitive to synaptic abnormalities than population electrophysiological recordings. These techniques, currently known as super resolution imaging, have the ability to surpass the intrinsic diffraction limit associated with light, thereby allowing researchers to investigate nanoscale objects that were once deemed impossible to distinguish.

4-5 Investigation of synaptic nanoarchitecture via super-resolution imaging

Light microscopy has been a staple of scientific investigation for centuries and has allowed researchers to discover biological intricacies beyond their wildest aspirations. Until recently however, light microscopy was limited by the intrinsic diffraction limit or “spreading out” of light when it passes through a small aperture or is focused on a very small area (Huang et al., 2010). Application of super-resolution imaging presents a unique opportunity to neuroscience researchers in particular, who can now investigate nanoscale architecture, organization, and movement of components of the synaptic cleft in order to achieve a more robust understanding of the synapse in both basal and disease conditions.

Synaptic transmission is maintained by an intricate, sub-cellular molecular nanoarchitecture. Even subtle changes to synapse structure can drive functional changes during experience-dependent plasticity and pathological disorders (Fromer et al., 2014). For example, recently via stochastic optical reconstruction microscopy (STORM), trans-synaptic molecular “nanocolumns” consisting of pre-synaptic clusters of regulatory proteins were found. These proteins are tightly clustered and aligned with post-synaptic receptors and scaffolding proteins, which have higher incidences of vesicle-fusion during evoked action potentials (Tang et al., 2016). This is indicative of synaptic nano-organization that preferentially controls neurotransmitter release at sites directly opposed to post-synaptic receptors. Furthermore, NMDAR activation triggered distinct phases of plasticity in which post-synaptic reorganization was followed by nanoscale realignments trans-synaptically (Tang et al., 2016). Furthermore, via stimulated emission depletion (STED) super-resolution microscopy, it was found that spine synapses, both in vivo and

in vitro, contain discrete and aligned modules of pre and post-synaptic proteins whose number, but not size, correlates positively with spine size (Hruska et al., 2018). Moreover, it was revealed that NMDAR-dependent increases in spine size were accompanied by enhanced mobility along the synaptic cleft of both pre and post-synaptic proteins (nano-clusters) that remained aligned with one another and increased in number with increasing spine size (Hruska et al., 2018). These results indicate that pre and post-synaptic proteins maintain tight spatial and temporal nanoscale regulation with one another during activity dependent plasticity. Moreover, in one of the earliest super-resolution microscopy experiments, researchers exemplified nanoscale organization on both pre and post synaptic neurons. Specifically, on the pre-synaptic side they showed highly oriented organization of scaffolding proteins, while on the post-synaptic neuron they discovered laminar organization of PSD proteins and synapse-to-synapse variability in lateral positioning of neurotransmitter receptors (Dani et al., 2010). Furthermore, it was shown for the first time by this group that a large number of synapses in the accessory olfactory bulb (AOB) were immature when undergoing activity-dependent plasticity paradigms (Dani et al., 2010). This is indicative of the ability of super-resolution imaging to elucidate novel synaptic traits in dense scattering brain tissue with nanometer-scale precision.

4-6 Early changes in synaptic nanoarchitecture in HD via SRRF

In the present study, we utilized SRRF imaging, an open source ImageJ super-resolution plugin capable of achieving high spatial resolutions on the XY plane (Gustafsson et al., 2016) to investigate pre and post-synaptic nanoarchitecture in WT and

presymptomatic heterozygous Q175FDN HD mice. Furthermore, each genotype was also subjected to a cLTP paradigm in order to investigate the effects of activity-dependent synaptic plasticity on the nanoarchitecture of the synapse.

To assess pre-synaptic nanoarchitecture, we selected the ubiquitous neuronal protein SYN that spans the synaptic vesicle membrane four times. SYN is an integral component of pre-synaptic architecture, accounting for approximately 10% of synaptic vesicle protein content (Gordon and Cousin, 2013). To assess post-synaptic nanoarchitecture, specifically a protein closely associated with synaptic transmission, we selected the AMPAR subunit GluA2. AMPARs are primarily located at excitatory synapses, where they mediate the majority of fast synaptic transmission and play a key role in synaptic plasticity (Huganir and Nicoll, 2013). Thus, it is possible that AMPAR dysfunction is contributing to the LTP impairments we observed at distal areas of hippocampus in prodromal HD mice.

In our study, via SRRF imaging, we examined clusters of GluA2 receptors known as puncta or “nano-objects”. Specifically, we analyzed GluA2 puncta size, fluorescence intensity, and density. Our results show that in WT tissue, cLTP increases GluA2 puncta size both proximally and distally. This aligns with previous results that show enlarged dendritic spines after cLTP via STED imaging (Hruska et al., 2018). Interestingly, in het tissue, cLTP reduced the size of GluA2 puncta in both proximal and distal areas. Moreover, GluA2 puncta were much larger in het control conditions when compared to WT control. This indicates a robust basal difference in AMPAR cluster size between WT and HD tissue, possibly explaining the genotype difference we observed in I/O, as well as an opposing effect of early activity-dependent synaptic transmission between the two

genotypes. In these cLTP experiments, tissue was fixed with paraformaldehyde 10 minutes after cLTP. electrophysiological LTP experiments typically carry out measurements up to 60 minutes, making 10 min an early time point of synaptic plasticity. Although studying early phases of activity-dependent plasticity can elucidate vital results, it is also of future interest to study later time-points leading up to 60 minutes after cLTP.

Research involving changes in AMPAR localization in HD is limited, however it was recently found that the HD causing mutation leads to dysregulated AMPAR surface diffusion and AMPARs failing to stabilize after cLTP in the hippocampus of multiple rodent models of HD (Zhang et al., 2018). It is important to note that these reported changes occurred at later stages of the disease, in relation to a more overt behavioural phenotype associated with HD. In contrast, The changes we observed in the current study highlight some of the very earliest alterations in synaptic architecture associated with the presymptomatic stages of HD.

We also investigated GluA2 fluorescence intensity as another measure of synaptic architecture. It was found that in WT tissue, cLTP decreased fluorescence intensity. Taken together with the increase in GluA2 size, these results indicate that in WT animals during the early stages of activity-dependent synaptic plasticity, GluA2 puncta are migrating toward release sites in anticipation of insertion into the post-synaptic membrane (Liao et al., 1995; Bredt and Nicoll, 2003). GluA2 puncta in basal conditions (controls) are much less intense in het tissue than WT, but interestingly they show a robust increase in intensity after cLTP. This is indicative of GluA2 puncta in presymptomatic HD tissue organizing themselves and migrating in a different manner than observed in WT tissue. It is well-known that AMPAR trafficking is disturbed in

symptomatic HD (Mandal et al., 2011; Zhang et al., 2018), thus the differences we see here are likely the earliest manifestations of disturbed AMPAR trafficking and altered synaptic architecture in HD.

We also investigated GluA2 puncta density, a measure of how many puncta were present in each image, and found no significant differences between any groups in either proximal or distal areas. This indicates that although AMPARs appear to be moving around the synapse in conjunction with changes in nanoarchitecture, the number of GluA2 nano-objects remains unaltered. These findings are supported by a vast amount of research that implicates *de novo* protein synthesis as a characteristic of long-term plasticity, while here we are only measuring the early stages of LTP (Nayak et al., 1998; Dudai, 2002; Matsuo et al., 2008). It is important to note here however, that our cLTP protocol is well established (Kopec et al., 2006; Lin et al., 2008) and leads to long term synaptic changes. Overall, it is obvious that even at a very early stage of the disease, long before any detectable behavioural phenotype (Southwell et al., 2016) or overt electrophysiological deficits that can be measured conventionally, there are robust differences in AMPAR nanoarchitecture and localization in HD mice. To the best of our knowledge, these aberrations are of the earliest cellular manifestations associated with the pathophysiology of the disease.

When investigating our presynaptic marker SYN, results were markedly different than GluA2. In terms of SYN nano-object size, we observed no differences after cLTP in either proximal or distal areas in WT tissue. This result was expected, as this form of cLTP is NMDAR-dependent and known to rely largely on post-synaptic changes (Kopec et al., 2006). However, in *het* tissue SYN size was larger at basal conditions than in WT

tissue and underwent a marked increase after cLTP, potentially explaining the basal difference we observed between genotypes when measuring I/O. Taken together, it is apparent here that presynaptic alterations in nanoarchitecture are also occurring in prodromal HD, although not in the same manner as postsynaptic changes. Previous work has postulated that impairments in synapsin I phosphorylation in the striatum of R6/2 mice may alter synaptic vesicle trafficking and contribute to impaired neurotransmission in HD (Liévens et al., 2002).

When examining SYN intensity, we observed a dramatic increase in fluorescence intensity in WT tissue after cLTP. This observation indicates that SYN is clustering together following cLTP. This aligns well with research that postulates a significant role of SYN in vesicle packaging, trafficking, and release (Alder et al., 1992; Mullany and Lynch, 1998). Thus, an increase in neurotransmitter release associated with LTP would mean an increase in SYN around release sites. In HD tissue, there was an observed increase in SYN intensity at proximal sites, but it was much less dramatic. At distal sites, there was no observable increase in SYN intensity, indicating that not only is SYN trafficking impaired in HD, but this impairment seems to worsen further along stratum radiatum. Here, it is important to note that SYN intensity does not increase in distal areas of hippocampus in het tissue. This is imperative because if the physiological mechanisms underlying SYN intensity is a critical feature of early LTP, then the lack of intensity increase observed at distal sites of the HD hippocampus could help explain why TBS-LTP is impaired at distal sites of the HD hippocampus. These data also indicate that although SYN seem to be clustering around pre-synaptic release sites in HD tissue during early stages of LTP, it is not occurring as efficiently as in WT, indicating a very early pre-

synaptic nanoarchitectural anomaly in prodromal HD. Much like we observed with GluA2, there were no changes in SYN density. This indicates that despite the robust changes in nano-organization, the number of SYN nano-objects remained the same across all conditions.

In addition to the analysis parameters described above, we investigated movement of GluA2 and SYN nano-objects. This paradigm, coined “nearest neighbour” (NN) analysis allowed us to measure changes in GluA2 and SYN movement across all conditions in both proximal and distal areas of stratum radiatum. This concept was originally applied using monte-carlo simulation in combination with electron micrographs to interpret synaptic cross-talk between hippocampal neurons (Rusakov et al., 1999). From this experiment it was found that NMDAR-mediated crosstalk is likely to occur between excitatory synapses in the hippocampus, indicating that NN analysis is a useful tool for measuring synaptic communication. More recently, NN analysis was applied in conjunction with STORM super-resolution imaging to examine NMDAR nano-object localization to determine if receptors were located in synaptic or extrasynaptic areas in a model of NMDAR encephalitis, again elucidating the effectiveness of NN analysis for measuring synaptic protein migration (Ladépêche et al., 2018). With respect to our results, in proximal areas of hippocampus, we found no significant difference in nano-object migration in WT tissue after cLTP. From this we interpret that after cLTP, GluA2 and SYN puncta do not migrate away from each other along the synaptic cleft. However, in het tissue, we did observe a significant increase in NN distance after cLTP. Here, it is possible that activity-dependent transmission in HD mice is causing nanoscale pre and post-synaptic protein misalignment. It is well known that activation of extrasynaptic

NMDARs promotes pro-death gene expression and cell-death signaling (Parsons and Raymond, 2014). Furthermore, elevated extrasynaptic NMDAR activity is apparent in the pathology of HD (Hardingham and Bading, 2010; Milnerwood and Raymond, 2010). Evidence surrounding extrasynaptic AMPARs is limited, however the results observed here are again indicative of early changes in synaptic nanoarchitecture in relation to activity-dependent transmission in prodromal HD.

4-7 Caveats & Future Direction

As is the case with any scientific study, there are some drawbacks here that warrant acknowledgement. Firstly, the MEA experiments were not carried out in an equal number of male and female mice, thus sex differences could be an influencing factor. It is also important to note that the SRRF algorithm only accounts for the XY plane of images, therefore the 16 μm depth of our re-sections (Z-plane) is not accounted for during SRRF as we did not utilize confocal microscopy.

This thesis identified clear detrimental effects of mHtt on hippocampal structure and function in presymptomatic HD. Furthermore, alterations in synaptic nanoarchitecture associated with early activity-dependent plasticity were identified. In the future, executing similar cLTP experiments at different time points (i.e. 10, 60, and 180 minutes after LTP) would provide a more in-depth investigation into synaptic alterations over the course of LTP. It would also be of interest to complete similar electrophysiological and SRRF imaging experiments at different time points during the progression of HD, to measure the severity and acceleration of synaptic aberrations as the disease worsens. Furthermore, investigating intracellular Ca^{2+} pathways discussed in this

thesis such as PKA and calpain signaling, and how these pathways are affected in the early HD brain would be of great interest.

4-8 Interpretations & Conclusion

To the best of our knowledge, the present thesis has identified the earliest known synaptic anomalies in the HD hippocampus. These findings were attainable due to the increasingly diverse methodologies available in neuroscience. In combination with one another, our electrophysiological and super-resolution microscopy results suggest that there are numerous significant aberrations at the synaptic level in the hippocampus associated with presymptomatic stages of HD. Researchers and clinicians alike have long been intrigued by the cognitive and psychiatric deficits associated with HD as they likely stem from physiological abnormalities that eventually worsen as the disease progresses into its later stages. So much of the research surrounding HD is associated with the striatum, however focusing on other brain areas such as hippocampus will allow the HD research community to gain further understanding into the global nature of the disease. HD is a devastating disease that requires further investigation into specific cellular and sub-cellular aberrations associated with its early stages. As more sophisticated methodologies and subsequent development of therapeutic approaches become available, they may eventually allow us to discover and implement a viable treatment option for those living and dying with this insidious condition.

5-0 References

- Abbott LF, Nelson SB (2000) Synaptic plasticity: taming the beast. *Nat Neurosci* 3:1178–1183.
- Abraham WC, Huggett A (1997) Induction and reversal of long-term potentiation by repeated high-frequency stimulation in rat hippocampal slices. *Hippocampus* 7:137–145.
- Agster KL, Fortin NJ, Eichenbaum H (2002) The hippocampus and disambiguation of overlapping sequences. *J Neurosci* 22:5760–5768.
- Albensi BC, Oliver DR, Toupin J, Odero G (2007) Electrical stimulation protocols for hippocampal synaptic plasticity and neuronal hyper-excitability: Are they effective or relevant? *Exp Neurol* 204:1–13.
- Albin RL, Young AB, Penney JB (1989) The functional anatomy of basal ganglia disorders. *Trends Neurosci* 12:366–375.
- Alder J, Lu B, Valtorta F, Greengard P, Poo MM (1992) Calcium-dependent transmitter secretion reconstituted in *Xenopus* oocytes: requirement for synaptophysin. *Science* 257:657–661.
- Alexander GE, DeLong MR, Strick PL (1986) Parallel Organization of Functionally Segregated Circuits Linking Basal Ganglia and Cortex. *Annu Rev Neurosci* 9:357–381.
- Andrew SE, Paul Goldberg Y, Kremer B, Telenius H, Theilmann J, Adam S, Starr E, Squitieri F, Lin B, Kalchman MA, Graham RK, Hayden MR (1993) The relationship between trinucleotide (CAG) repeat length and clinical features of Huntington's

- disease. *Nat Genet* 4:398–403.
- Aylward EH, Li Q, Stine OC, Ranen N, Sherr M, Barta PE, Bylsma FW, Pearlson GD, Ross CA (1997) Longitudinal change in basal ganglia volume in patients with Huntington's disease. *Neurology* 48:394–399.
- Aylward EH, Nopoulos PC, Ross CA, Langbehn DR, Pierson RK, Mills JA, Johnson HJ, Magnotta VA, Juhl AR, Paulsen JS, PREDICT-HD Investigators and Coordinators of Huntington Study Group (2011) Longitudinal change in regional brain volumes in prodromal Huntington disease. *J Neurol Neurosurg Psychiatry* 82:405–410.
- Barria A, Malinow R (2002) Subunit-specific NMDA receptor trafficking to synapses. *Neuron* 35:345–353.
- Bates G (2003) Huntingtin aggregation and toxicity in Huntington's disease. *Lancet* (London, England) 361:1642–1644.
- Baudry M, Bi X (2016) Calpain-1 and Calpain-2: The Yin and Yang of Synaptic Plasticity and Neurodegeneration. *Trends Neurosci* 39:235–245.
- Beaumont V, Park L, Rassoulpour A, Dijkman U, Heikkinen T, Lehtimäki K, Kontkanen O, Al Nackkash R, Bates GP, Gleyzes M, Steidl E, Ramboz S, Murphy C, Beconi MG, Dominguez C, Muñoz-Sanjuan I (2014) The PDE1/5 Inhibitor SCH-51866 Does Not Modify Disease Progression in the R6/2 Mouse Model of Huntington's Disease. *PLoS Curr* 6.
- Begeti F, Schwab LC, Mason SL, Barker RA (2016) Hippocampal dysfunction defines disease onset in Huntington's disease. *J Neurol Neurosurg Psychiatry* 87:975–981.
- Bergles DE, Dzubay JA, Jahr CE (1997) Glutamate transporter currents in bergmann glial cells follow the time course of extrasynaptic glutamate. *Proc Natl Acad Sci U S A*

94:14821–14825.

- Berrios GE, Wagle AC, Markova IS, Wagle SA, Rosser A, Hodges JR (2002) Psychiatric symptoms in neurologically asymptomatic Huntington's disease gene carriers: a comparison with gene negative at risk subjects. *Acta Psychiatr Scand* 105:224–230.
- Betzig E, Patterson GH, Sougrat R, Lindwasser OW, Olenych S, Bonifacino JS, Davidson MW, Lippincott-Schwartz J, Hess HF (2006) Imaging Intracellular Fluorescent Proteins at Nanometer Resolution. *Science* (80-) 313:1642–1645.
- Bird CM, Burgess N (2008) The hippocampus and memory: insights from spatial processing. *Nat Rev Neurosci* 9:182–194.
- Bliss TVP, Collingridge GL (1993) A synaptic model of memory: long-term potentiation in the hippocampus. *Nature* 361:31–39.
- Bliss TVP, Lømo T (1973) Long-lasting potentiation of synaptic transmission in the dentate area of the anaesthetized rabbit following stimulation of the perforant path. *J Physiol* 232:331–356.
- Bogaard SJA, Dumas EM, Acharya TP, Johnson H, Langbehn DR, Scahill RI, Tabrizi SJ, Buchem MA, Grond J, Roos RAC, Group T-HI (2011) Early atrophy of pallidum and accumbens nucleus in Huntington's disease. *J Neurol* 258:412–420.
- Bredt DS, Nicoll RA (2003) AMPA receptor trafficking at excitatory synapses. *Neuron* 40:361–379.
- Brooks SP, Dunnett SB (2013) Mouse Models of Huntington's Disease. In: *Current topics in behavioral neurosciences*, pp 101–133.
- Brooks SP, Janghra N, Higgs G V., Bayram-Weston Z, Heuer A, Jones L, Dunnett SB (2012) Selective cognitive impairment in the YAC128 Huntington's disease mouse.

- Brain Res Bull 88:121–129.
- Buzsáki G (2002) Theta oscillations in the hippocampus. *Neuron* 33:325–340.
- Cattaneo E, Zuccato C, Tartari M (2005) Normal huntingtin function: an alternative approach to Huntington's disease. *Nat Rev Neurosci* 6:919–930.
- Cembrowski MS, Wang L, Sugino K, Shields BC, Spruston N (2016) Hipposeq: a comprehensive RNA-seq database of gene expression in hippocampal principal neurons. *Elife* 5:e14997.
- Cha JH, Kosinski CM, Kerner JA, Alsdorf SA, Mangiarini L, Davies SW, Penney JB, Bates GP, Young AB (1998) Altered brain neurotransmitter receptors in transgenic mice expressing a portion of an abnormal human huntington disease gene. *Proc Natl Acad Sci U S A* 95:6480–6485.
- Clarke HF, Robbins TW, Roberts AC (2008) Lesions of the Medial Striatum in Monkeys Produce Perseverative Impairments during Reversal Learning Similar to Those Produced by Lesions of the Orbitofrontal Cortex. *J Neurosci* 28:10972–10982.
- Colucci-D'Amato L, Perrone-Capano C, di Porzio U (2003) Chronic activation of ERK and neurodegenerative diseases. *BioEssays* 25:1085–1095.
- Costa ACS, Grybko MJ (2005) Deficits in hippocampal CA1 LTP induced by TBS but not HFS in the Ts65Dn mouse: A model of Down syndrome. *Neurosci Lett* 382:317–322.
- Crook ZR, Housman DE (2012) Dysregulation of dopamine receptor D2 as a sensitive measure for Huntington disease pathology in model mice. *Proc Natl Acad Sci* 109:7487–7492.
- Cunha RA, Vizi ES, Ribeiro JA, Sebastião AM (1996) Preferential release of ATP and its

- extracellular catabolism as a source of adenosine upon high- but not low-frequency stimulation of rat hippocampal slices. *J Neurochem* 67:2180–2187.
- Dalley JW, Cardinal RN, Robbins TW (2004) Prefrontal executive and cognitive functions in rodents: neural and neurochemical substrates. *Neurosci Biobehav Rev* 28:771–784.
- Dani A, Huang B, Bergan J, Dulac C, Zhuang X (2010) Superresolution Imaging of Chemical Synapses in the Brain. *Neuron* 68:843–856.
- DiFiglia M, Sapp E, Chase K, Schwarz C, Meloni A, Young C, Martin E, Vonsattel J-P, Carraway R, Reeves SA, Boyce FM, Aronin N (1995) Huntingtin is a cytoplasmic protein associated with vesicles in human and rat brain neurons. *Neuron* 14:1075–1081.
- Dudai Y (2002) Molecular bases of long-term memories: a question of persistence. *Curr Opin Neurobiol* 12:211–216.
- Edwardson JM, Wang C-T, Gong B, Wyttenbach A, Bai J, Jackson MB, Chapman ER, Morton AJ (2003) Expression of Mutant Huntingtin Blocks Exocytosis in PC12 Cells by Depletion of Complexin II. *J Biol Chem* 278:30849–30853.
- El-Husseini AE, Schnell E, Chetkovich DM, Nicoll RA, Brecht DS (2000) PSD-95 involvement in maturation of excitatory synapses. *Science* 290:1364–1368.
- Epping EA, Kim J-I, Craufurd D, Brashers-Krug TM, Anderson KE, McCusker E, Luther J, Long JD, Paulsen JS, PREDICT-HD Investigators and Coordinators of the Huntington Study Group the P-HI and C of the HS (2016) Longitudinal Psychiatric Symptoms in Prodromal Huntington’s Disease: A Decade of Data. *Am J Psychiatry* 173:184–192.

- Favaron M, Manev RM, Rimland JM, Candeo P, Beccaro M, Manev H (1993) NMDA-stimulated expression of BDNF mRNA in cultured cerebellar granule neurones. *Neuroreport* 4:1171–1174.
- Fisher ER, Hayden MR (2014) Multisource ascertainment of Huntington disease in Canada: Prevalence and population at risk. *Mov Disord* 29:105–114.
- Fortin NJ, Agster KL, Eichenbaum HB (2002) Critical role of the hippocampus in memory for sequences of events. *Nat Neurosci* 5:458–462.
- Fromer M et al. (2014) De novo mutations in schizophrenia implicate synaptic networks. *Nature* 506:179–184.
- Gauthier LR, Charrin BC, Borrell-Pagès M, Dompierre JP, Rangone H, Cordelières FP, De Mey J, MacDonald ME, Leßmann V, Humbert S, Saudou F (2004) Huntingtin Controls Neurotrophic Support and Survival of Neurons by Enhancing BDNF Vesicular Transport along Microtubules. *Cell* 118:127–138.
- Gil JMAC, Mohapel P, Araújo IM, Popovic N, Li J-Y, Brundin P, Petersén Å (2005) Reduced hippocampal neurogenesis in R6/2 transgenic Huntington's disease mice. *Neurobiol Dis* 20:744–751.
- Giralt A, Puigdellivol M, Carreton O, Paoletti P, Valero J, Parra-Damas A, Saura CA, Alberch J, Gines S (2012) Long-term memory deficits in Huntington's disease are associated with reduced CBP histone acetylase activity. *Hum Mol Genet* 21:1203–1216.
- Giralt A, Rodrigo T, Martín ED, Gonzalez JR, Milà M, Ceña V, Dierssen M, Canals JM, Alberch J (2009) Brain-derived neurotrophic factor modulates the severity of cognitive alterations induced by mutant huntingtin: Involvement of phospholipaseC γ

- activity and glutamate receptor expression. *Neuroscience* 158:1234–1250.
- Giralt A, Saavedra A, Carretón O, Xifró X, Alberch J, Pérez-Navarro E (2011) Increased PKA signaling disrupts recognition memory and spatial memory: role in Huntington's disease. *Hum Mol Genet* 20:4232–4247.
- Gordon SL, Cousin MA (2013) X-Linked Intellectual Disability-Associated Mutations in Synaptophysin Disrupt Synaptobrevin II Retrieval. *J Neurosci* 33:13695–13700.
- Gray M, Shirasaki DI, Cepeda C, André VM, Wilburn B, Lu X-H, Tao J, Yamazaki I, Li S-H, Sun YE, Li X-J, Levine MS, Yang XW (2008) Full-length human mutant huntingtin with a stable polyglutamine repeat can elicit progressive and selective neuropathogenesis in BACHD mice. *J Neurosci* 28:6182–6195.
- Gustafsson N, Culley S, Ashdown G, Owen DM, Pereira PM, Henriques R (2016) Fast live-cell conventional fluorophore nanoscopy with ImageJ through super-resolution radial fluctuations. *Nat Commun* 7:12471.
- Gutekunst CA, Levey AI, Heilman CJ, Whaley WL, Yi H, Nash NR, Rees HD, Madden JJ, Hersch SM (1995) Identification and localization of huntingtin in brain and human lymphoblastoid cell lines with anti-huntingtin protein antibodies. *Proc Natl Acad Sci U S A* 92:8710–8714.
- Hampshire A, Chaudhry AM, Owen AM, Roberts AC (2012) Dissociable roles for lateral orbitofrontal cortex and lateral prefrontal cortex during preference driven reversal learning. *Neuroimage* 59:4102–4112.
- Hansen HH, Briem T, Dzierko M, Sifringer M, Voss A, Rzeski W, Zdzisinska B, Thor F, Heumann R, Stepulak A, Bittigau P, Ikonomidou C (2004) Mechanisms leading to disseminated apoptosis following NMDA receptor blockade in the developing rat

- brain. *Neurobiol Dis* 16:440–453.
- Hardingham GE, Arnold FJL, Bading H (2001) A calcium microdomain near NMDA receptors: on switch for ERK-dependent synapse-to-nucleus communication. *Nat Neurosci* 4:565–566.
- Hardingham GE, Bading H (2010) Synaptic versus extrasynaptic NMDA receptor signalling: implications for neurodegenerative disorders. *Nat Rev Neurosci* 11:682–696.
- Hardingham GE, Fukunaga Y, Bading H (2002) Extrasynaptic NMDARs oppose synaptic NMDARs by triggering CREB shut-off and cell death pathways. *Nat Neurosci* 5:405–414.
- Harjes P, Wanker EE (2003) The hunt for huntingtin function: Interaction partners tell many different stories. *Trends Biochem Sci* 28:425–433.
- Heng MY, Detloff PJ, Wang PL, Tsien JZ, Albin RL (2009) In Vivo Evidence for NMDA Receptor-Mediated Excitotoxicity in a Murine Genetic Model of Huntington Disease. *J Neurosci* 29:3200–3205.
- Hogarth P, Kayson E, Kieburz K, Marder K, Oakes D, Rosas D, Shoulson I, Wexler NS, Young AB, Zhao H (2005) Interrater agreement in the assessment of motor manifestations of Huntington's disease. *Mov Disord* 20:293–297.
- Hruska M, Henderson N, Le Marchand SJ, Jafri H, Dalva MB (2018) Synaptic nanomodules underlie the organization and plasticity of spine synapses. *Nat Neurosci* 21:671–682.
- Huang B, Babcock H, Zhuang X (2010) Breaking the Diffraction Barrier: Super-Resolution Imaging of Cells. *Cell* 143:1047–1058.

- Huganir RL, Nicoll RA (2013) AMPARs and Synaptic Plasticity: The Last 25 Years. *Neuron* 80:704–717.
- Huntington G (1872) On chorea.
- Huntington Study Group (1996) Unified Huntington’s disease rating scale: Reliability and consistency. *Mov Disord* 11:136–142.
- Ivanov A, Pellegrino C, Rama S, Dumalska I, Salyha Y, Ben-Ari Y, Medina I (2006) Opposing role of synaptic and extrasynaptic NMDA receptors in regulation of the extracellular signal-regulated kinases (ERK) activity in cultured rat hippocampal neurons. *J Physiol* 572:789–798.
- Johnson SA et al. (2007) Beyond disgust: impaired recognition of negative emotions prior to diagnosis in Huntington’s disease. *Brain* 130:1732–1744.
- Joshi PR, Wu N-P, André VM, Cummings DM, Cepeda C, Joyce JA, Carroll JB, Leavitt BR, Hayden MR, Levine MS, Bamford NS (2009) Age-Dependent Alterations of Corticostriatal Activity in the YAC128 Mouse Model of Huntington Disease. *J Neurosci* 29:2414–2427.
- Julien CL, Thompson JC, Wild S, Yardumian P, Snowden JS, Turner G, Craufurd D (2007) Psychiatric disorders in preclinical Huntington’s disease. *J Neurol Neurosurg & Psychiatry* 78:939–943.
- Kafitz KW, Rose CR, Thoenen H, Konnerth A (1999) Neurotrophin-evoked rapid excitation through TrkB receptors. *Nature* 401:918–921.
- Kanterewicz BI, Urban NN, McMahon DB, Norman ED, Giffen LJ, Favata MF, Scherle PA, Trzskos JM, Barrionuevo G, Klann E (2000) The extracellular signal-regulated kinase cascade is required for NMDA receptor-independent LTP in area CA1 but not

- area CA3 of the hippocampus. *J Neurosci* 20:3057–3066.
- Kawamoto Y, Nakamura S, Nakano S, Oka N, Akiguchi I, Kimura J (1996) Immunohistochemical localization of brain-derived neurotrophic factor in adult rat brain. *Neuroscience* 74:1209–1226.
- Kim J-S, Reading SA., Brashers-Krug T, Calhoun VD, Ross CA, Pearlson GD (2004) Functional MRI study of a serial reaction time task in Huntington’s disease. *Psychiatry Res Neuroimaging* 131:23–30.
- Kim M, Huang T, Abel T, Blackwell KT (2010) Temporal sensitivity of protein kinase a activation in late-phase long term potentiation. Nowotny T, ed. *PLoS Comput Biol* 6:e1000691.
- Kimura T, Ishiguro K, Hisanaga S (2014) Physiological and pathological phosphorylation of tau by Cdk5. *Front Mol Neurosci* 7:65.
- Klanker M, Post G, Joosten R, Feenstra M, Denys D (2013) Deep brain stimulation in the lateral orbitofrontal cortex impairs spatial reversal learning. *Behav Brain Res* 245:7–12.
- Klapstein GJ, Fisher RS, Zanjani H, Cepeda C, Jokel ES, Chesselet M-F, Levine MS (2001) Electrophysiological and Morphological Changes in Striatal Spiny Neurons in R6/2 Huntington’s Disease Transgenic Mice. *J Neurophysiol* 86:2667–2677.
- Klar TA, Hell SW (1999) Subdiffraction resolution in far-field fluorescence microscopy. *Opt Lett* 24:954.
- Klar TA, Jakobs S, Dyba M, Egnér A, Hell SW (2000) Fluorescence microscopy with diffraction resolution barrier broken by stimulated emission. *Proc Natl Acad Sci U S A* 97:8206–8210.

- Komatsu Y, Nakajima S, Toyama K (1991) Induction of long-term potentiation without participation of N-methyl-D-aspartate receptors in kitten visual cortex. *J Neurophysiol* 65:20–32.
- Kopec CD, Li B, Wei W, Boehm J, Malinow R (2006) Glutamate receptor exocytosis and spine enlargement during chemically induced long-term potentiation. *J Neurosci* 26:2000–2009.
- Ladépêche L, Planagumà J, Thakur S, Suárez I, Hara M, Borbely JS, Sandoval A, Laparra-Cuervo L, Dalmau J, Lakadamyali M (2018) NMDA Receptor Autoantibodies in Autoimmune Encephalitis Cause a Subunit-Specific Nanoscale Redistribution of NMDA Receptors. *Cell Rep* 23:3759–3768.
- Landwehrmeyer GB, Standaert DG, Testa CM, Penney JB, Young AB (1995) NMDA receptor subunit mRNA expression by projection neurons and interneurons in rat striatum. *J Neurosci* 15:5297–5307.
- Larson J, Munkácsy E (2015) Theta-burst LTP. *Brain Res* 1621:38–50.
- Lawrence A, Weeks RA, Brooks DJ, Andrews TC, Watkins LH, Harding AE, Robbins TW, Sahakian BJ (1998) The relationship between striatal dopamine receptor binding and cognitive performance in Huntington’s disease. *Brain* 121:1343–1355.
- Lawrence AD, Watkins LHA, Sahakian BJ, Hodges JR, Robbins TW (2000) Visual object and visuospatial cognition in Huntington’s disease: implications for information processing in corticostriatal circuits. *Brain* 123:1349–1364.
- Lazic SE, Grote HE, Blakemore C, Hannan AJ, van Dellen A, Phillips W, Barker RA (2006) Neurogenesis in the R6/1 transgenic mouse model of Huntington’s disease: effects of environmental enrichment. *Eur J Neurosci* 23:1829–1838.

- Li L, Fan M, Icton CD, Chen N, Leavitt BR, Hayden MR, Murphy TH, Raymond LA (2003) Role of NR2B-type NMDA receptors in selective neurodegeneration in Huntington disease. *Neurobiol Aging* 24:1113–1121.
- Liao D, Hessler NA, Malinow R (1995) Activation of postsynaptically silent synapses during pairing-induced LTP in CA1 region of hippocampal slice. *Nature* 375:400–404.
- Liévens J-C, Woodman B, Mahal A, Bates GP (2002) Abnormal phosphorylation of synapsin I predicts a neuronal transmission impairment in the R6/2 Huntington's disease transgenic mice. *Mol Cell Neurosci* 20:638–648.
- Lin MT, Luján R, Watanabe M, Adelman JP, Maylie J (2008) SK2 channel plasticity contributes to LTP at Schaffer collateral–CA1 synapses. *Nat Neurosci* 11:170–177.
- Lu W-Y, Man H-Y, Ju W, Trimble WS, MacDonald JF, Wang YT (2001) Activation of Synaptic NMDA Receptors Induces Membrane Insertion of New AMPA Receptors and LTP in Cultured Hippocampal Neurons. *Neuron* 29:243–254.
- MacDonald ME et al. (1993) A novel gene containing a trinucleotide repeat that is expanded and unstable on Huntington's disease chromosomes. *Cell* 72:971–983.
- Makino H, Malinow R (2009) AMPA Receptor Incorporation into Synapses during LTP: The Role of Lateral Movement and Exocytosis. *Neuron* 64:381–390.
- Malenka RC, Nicoll RA (1999) Long-term potentiation--a decade of progress? *Science* 285:1870–1874.
- Man H-Y (2011) GluA2-lacking, calcium-permeable AMPA receptors — inducers of plasticity? *Curr Opin Neurobiol* 21:291–298.
- Mandal M, Wei J, Zhong P, Cheng J, Duffney LJ, Liu W, Yuen EY, Twelvetrees AE, Li

- S, Li X-J, Kittler JT, Yan Z (2011) Impaired alpha-amino-3-hydroxy-5-methyl-4-isoxazolepropionic acid (AMPA) receptor trafficking and function by mutant huntingtin. *J Biol Chem* 286:33719–33728.
- Marder K, Zhao H, Myers RH, Cudkowicz M, Kayson E, Kieburz K, Orme C, Paulsen J, Penney JB, Siemers E, Shoulson I, Bodner T (2000) Rate of functional decline in Huntington's disease. Huntington Study Group. *Neurology* 54:452–458.
- Matsuo N, Reijmers L, Mayford M (2008) Spine-type-specific recruitment of newly synthesized AMPA receptors with learning. *Science* 319:1104–1107.
- Mazarakis NK, Cybulska-Klosowicz A, Grote H, Pang T, Van Dellen A, Kossut M, Blakemore C, Hannan AJ (2005) Deficits in Experience-Dependent Cortical Plasticity and Sensory-Discrimination Learning in Presymptomatic Huntington's Disease Mice. *J Neurosci* 25:3059–3066.
- McEchron MD, Disterhoft JF (1997) Sequence of Single Neuron Changes in CA1 Hippocampus of Rabbits During Acquisition of Trace Eyeblink Conditioned Responses. *J Neurophysiol* 78:1030–1044.
- McEchron MD, Tseng W, Disterhoft JF (2003) Single neurons in CA1 hippocampus encode trace interval duration during trace heart rate (fear) conditioning in rabbit. *J Neurosci* 23:1535–1547.
- Menalled LB et al. (2012) Comprehensive Behavioral and Molecular Characterization of a New Knock-In Mouse Model of Huntington's Disease: zQ175 Okazawa H, ed. *PLoS One* 7:e49838.
- Menalled LB, Chesselet M-F (2002) Mouse models of Huntington's disease. *Trends Pharmacol Sci* 23:32–39.

- Milner B, Squire LR, Kandel ER (1998) Cognitive neuroscience and the study of memory. *Neuron* 20:445–468.
- Milnerwood AJ, Gladding CM, Pouladi MA, Kaufman AM, Hines RM, Boyd JD, Ko RWY, Vasuta OC, Graham RK, Hayden MR, Murphy TH, Raymond LA (2010) Early Increase in Extrasynaptic NMDA Receptor Signaling and Expression Contributes to Phenotype Onset in Huntington's Disease Mice. *Neuron* 65:178–190.
- Milnerwood AJ, Raymond LA (2007) Corticostriatal synaptic function in mouse models of Huntington's disease: early effects of huntingtin repeat length and protein load. *J Physiol* 585:817–831.
- Milnerwood AJ, Raymond LA (2010) Early synaptic pathophysiology in neurodegeneration: insights from Huntington's disease. *Trends Neurosci* 33:513–523.
- Mink JW (1996) The Basal Ganglia: Focused selection and inhibition of competing motor programs. *Prog Neurobiol* 50:381–425.
- Modregger J, Schmidt AA, Ritter B, Huttner WB, Plomann M (2003) Characterization of Endophilin B1b, a brain-specific membrane-associated lysophosphatidic acid acyl transferase with properties distinct from endophilin A1. *J Biol Chem* 278:4160–4167.
- Morton AJ, Edwardson JM (2001) Progressive depletion of complexin II in a transgenic mouse model of Huntington's disease. *J Neurochem* 76:166–172.
- Morton AJ, Lagan MA, Skepper JN, Dunnett SB (2000) Progressive formation of inclusions in the striatum and hippocampus of mice transgenic for the human Huntington's disease mutation. *J Neurocytol* 29:679–702.

- Mullany PM, Lynch MA (1998) Evidence for a role for synaptophysin in expression of long-term potentiation in rat dentate gyrus. *Neuroreport* 9:2489–2494.
- Murphy KP, Carter RJ, Lione LA, Mangiarini L, Mahal A, Bates GP, Dunnett SB, Morton AJ (2000) Abnormal synaptic plasticity and impaired spatial cognition in mice transgenic for exon 1 of the human Huntington's disease mutation. *J Neurosci* 20:5115–5123.
- Nasir J, Floresco SB, O'Kusky JR, Diewert VM, Richman JM, Zeisler J, Borowski A, Marth JD, Phillips AG, Hayden MR (1995) Targeted disruption of the Huntington's disease gene results in embryonic lethality and behavioral and morphological changes in heterozygotes. *Cell* 81:811–823.
- Nayak A, Zastrow DJ, Lickteig R, Zahniser NR, Browning MD (1998) Maintenance of late-phase LTP is accompanied by PKA-dependent increase in AMPA receptor synthesis. *Nature* 394:680–683.
- Nehl C, Paulsen JS, Huntington Study Group (2004) Cognitive and Psychiatric Aspects of Huntington Disease Contribute to Functional Capacity. *J Nerv Ment Dis* 192:72–74.
- Nicoll RA, Malenka RC (1995) Contrasting properties of two forms of long-term potentiation in the hippocampus. *Nature* 377:115–118.
- Novak JL, Wheeler BC (1988) Multisite hippocampal slice recording and stimulation using a 32 element microelectrode array. *J Neurosci Methods* 23:149–159.
- O'Keefe J, Dostrovsky J (1971) The hippocampus as a spatial map. Preliminary evidence from unit activity in the freely-moving rat. *Brain Res* 34:171–175.
- Oka H, Shimono K, Ogawa R, Sugihara H, Taketani M (1999) A new planar multielectrode array for extracellular recording: application to hippocampal acute

- slice. *J Neurosci Methods* 93:61–67.
- Okamoto S, Pouladi MA, Talantova M, Yao D, Xia P, Ehrnhoefer DE, Zaidi R, Clemente A, Kaul M, Graham RK, Zhang D, Vincent Chen H-S, Tong G, Hayden MR, Lipton SA (2009) Balance between synaptic versus extrasynaptic NMDA receptor activity influences inclusions and neurotoxicity of mutant huntingtin. *Nat Med* 15:1407–1413.
- Otmakhov N, Khibnik L, Otmakhova N, Carpenter S, Riahi S, Asrican B, Lisman J (2004) Forskolin-induced LTP in the CA1 hippocampal region is NMDA receptor dependent. *J Neurophysiol* 91:1955–1962.
- Papadia S, Soriano FX, Léveillé F, Martel M-A, Dakin KA, Hansen HH, Kaindl A, Sifringer M, Fowler J, Stefovská V, McKenzie G, Craigon M, Corriveau R, Ghazal P, Horsburgh K, Yankner BA, Wyllie DJA, Ikonomidou C, Hardingham GE (2008) Synaptic NMDA receptor activity boosts intrinsic antioxidant defenses. *Nat Neurosci* 11:476–487.
- Parsons MP, Raymond LA (2014) Extrasynaptic NMDA Receptor Involvement in Central Nervous System Disorders. *Neuron* 82:279–293.
- Parsons MP, Vanni MP, Woodard CL, Kang R, Murphy TH, Raymond LA (2016) Real-time imaging of glutamate clearance reveals normal striatal uptake in Huntington disease mouse models. *Nat Commun* 7:11251.
- Patrick GN, Zukerberg L, Nikolic M, de la Monte S, Dikkes P, Tsai L-H (1999) Conversion of p35 to p25 deregulates Cdk5 activity and promotes neurodegeneration. *Nature* 402:615–622.
- Paulsen JS (2011) Cognitive Impairment in Huntington Disease: Diagnosis and

- Treatment. *Curr Neurol Neurosci Rep* 11:474–483.
- Paulsen JS, Butters N, Sadek JR, Johnson SA, Salmon DP, Swerdlow NR, Swenson MR (1995) Distinct cognitive profiles of cortical and subcortical dementia in advanced illness. *Neurology* 45:951–956.
- Paulsen JS, Zhao H, Stout JC, Brinkman RR, Guttman M, Ross CA, Como P, Manning C, Hayden MR, Shoulson I, Huntington Study Group (2001) Clinical markers of early disease in persons near onset of Huntington's disease. *Neurology* 57:658–662.
- Perez Y, Chapman CA, Woodhall G, Robitaille R, Lacaille J-C (1999) Differential induction of long-lasting potentiation of inhibitory postsynaptic potentials by theta patterned stimulation versus 100-Hz tetanization in hippocampal pyramidal cells in vitro. *Neuroscience* 90:747–757.
- Phillips W, Morton AJ, Barker RA (2005) Abnormalities of neurogenesis in the R6/2 mouse model of Huntington's disease are attributable to the in vivo microenvironment. *J Neurosci* 25:11564–11576.
- Pouladi MA, Morton AJ, Hayden MR (2013) Choosing an animal model for the study of Huntington's disease. *Nat Rev Neurosci* 14:708–721.
- Ravikumar B, Vacher C, Berger Z, Davies JE, Luo S, Oroz LG, Scaravilli F, Easton DF, Duden R, O'Kane CJ, Rubinsztein DC (2004) Inhibition of mTOR induces autophagy and reduces toxicity of polyglutamine expansions in fly and mouse models of Huntington disease. *Nat Genet* 36:585–595.
- Reim K, Mansour M, Varoquaux F, McMahon HT, Südhof TC, Brose N, Rosenmund C (2001) Complexins regulate a late step in Ca²⁺-dependent neurotransmitter release. *Cell* 104:71–81.

- Reiner A, Albin RL, Anderson KD, D'Amato CJ, Penney JB, Young AB (1988)
Differential loss of striatal projection neurons in Huntington disease. *Proc Natl Acad Sci U S A* 85:5733–5737.
- Ribeiro FM, Paquet M, Ferreira LT, Cregan T, Swan P, Cregan SP, Ferguson SSG (2010)
Metabotropic Glutamate Receptor-Mediated Cell Signaling Pathways Are Altered in a Mouse Model of Huntington's Disease. *J Neurosci* 30:316–324.
- Rigamonti D, Bauer JH, De-Fraja C, Conti L, Sipione S, Sciorati C, Clementi E, Hackam A, Hayden MR, Li Y, Cooper JK, Ross CA, Govoni S, Vincenz C, Cattaneo E (2000) Wild-Type Huntingtin Protects from Apoptosis Upstream of Caspase-3. *J Neurosci* 20:3705–3713.
- Robertson AL, Bottomley SP (2010) Towards the treatment of polyglutamine diseases: the modulatory role of protein context. *Curr Med Chem* 17:3058–3068.
- Rosas HD, Koroshetz WJ, Chen YI, Skeuse C, Vangel M, Cudkowicz ME, Caplan K, Marek K, Seidman LJ, Makris N, Jenkins BG, Goldstein JM (2003) Evidence for more widespread cerebral pathology in early HD: an MRI-based morphometric analysis. *Neurology* 60:1615–1620.
- Rosenblatt A, Liang K-Y, Zhou H, Abbott MH, Gourley LM, Margolis RL, Brandt J, Ross CA (2006) The association of CAG repeat length with clinical progression in Huntington disease. *Neurology* 66:1016–1020.
- Ross CA, Aylward EH, Wild EJ, Langbehn DR, Long JD, Warner JH, Scahill RI, Leavitt BR, Stout JC, Paulsen JS, Reilmann R, Unschuld PG, Wexler A, Margolis RL, Tabrizi SJ (2014) Huntington disease: natural history, biomarkers and prospects for therapeutics. *Nat Rev Neurol* 10:204–216.

- Roze E, Betuing S, Deyts C, Marcon E, Brami-Cherrier K, Pagès C, Humbert S, Mérienne K, Caboche J (2008) Mitogen- and stress-activated protein kinase-1 deficiency is involved in expanded-huntingtin-induced transcriptional dysregulation and striatal death. *FASEB J* 22:1083–1093.
- Rusakov DA, Kullmann DM, Stewart MG (1999) Hippocampal synapses: do they talk to their neighbours? *Trends Neurosci* 22:382–388.
- Rust MJ, Bates M, Zhuang X (2006) Sub-diffraction-limit imaging by stochastic optical reconstruction microscopy (STORM). *Nat Methods* 3:793–796.
- Schikorski T, Stevens CF (1997) Quantitative ultrastructural analysis of hippocampal excitatory synapses. *J Neurosci* 17:5858–5867.
- Selcher JC, Weeber EJ, Christian J, Nekrasova T, Landreth GE, Sweatt JD (2003) A role for ERK MAP kinase in physiologic temporal integration in hippocampal area CA1. *Learn Mem* 10:26–39.
- Selkoe DJ (2002) Alzheimer's disease is a synaptic failure. *Science* 298:789–791.
- Sepers MD, Raymond LA (2014) Mechanisms of synaptic dysfunction and excitotoxicity in Huntington's disease. *Drug Discov Today* 19:990–996.
- Sharp AH, Loev SJ, Schilling G, Li S-H, Li X-J, Bao J, Wagster M V, Kotzuk JA, Steiner JP, Lo A, Hedreen J, Sisodia S, Snyder SH, Dawson TM, Ryugo DK, Ross CA (1995) Widespread expression of Huntington's disease gene (IT15) protein product. *Neuron* 14:1065–1074.
- Shentu Y-P, Huo Y, Feng X-L, Gilbert J, Zhang Q, Liuyang Z-Y, Wang X-L, Wang G, Zhou H, Wang X-C, Wang J-Z, Lu Y-M, Westermarck J, Man H-Y, Liu R (2018) CIP2A Causes Tau/APP Phosphorylation, Synaptopathy, and Memory Deficits in

- Alzheimer's Disease. *Cell Rep* 24:713–723.
- Smith MA, Brandt J, Shadmehr R (2000) Motor disorder in Huntington's disease begins as a dysfunction in error feedback control. *Nature* 403:544–549.
- Snell RG, MacMillan JC, Cheadle JP, Fenton I, Lazarou LP, Davies P, MacDonald ME, Gusella JF, Harper PS, Shaw DJ (1993) Relationship between trinucleotide repeat expansion and phenotypic variation in Huntington's disease. *Nat Genet* 4:393–397.
- Snowden JS, Craufurd D, Thompson J, Neary D (2002) Psychomotor, Executive, and Memory Function in Preclinical Huntington's Disease. *J Clin Exp Neuropsychol* 24:133–145.
- Southwell AL, Smith-Dijak A, Kay C, Sepers M, Villanueva EB, Parsons MP, Xie Y, Anderson L, Felczak B, Waltl S, Ko S, Cheung D, Dal Cengio L, Slama R, Petoukhov E, Raymond LA, Hayden MR (2016) An enhanced Q175 knock-in mouse model of Huntington disease with higher mutant huntingtin levels and accelerated disease phenotypes. *Hum Mol Genet* 25:3654–3675.
- Squire LR, Zola-Morgan S (1991) The medial temporal lobe memory system. *Science* 253:1380–1386.
- Starling AJ, André VM, Cepeda C, de Lima M, Chandler SH, Levine MS (2005) Alterations in N-methyl-D-aspartate receptor sensitivity and magnesium blockade occur early in development in the R6/2 mouse model of Huntington's disease. *J Neurosci Res* 82:377–386.
- Stout JC, Paulsen JS, Queller S, Solomon AC, Whitlock KB, Campbell JC, Carlozzi N, Duff K, Beglinger LJ, Langbehn DR, Johnson SA, Biglan KM, Aylward EH (2011) Neurocognitive signs in prodromal Huntington disease. *Neuropsychology* 25:1–14.

- Stout JC, Weaver M, Solomon AC, Queller S, Hui S, Johnson SA, Gray J, Beristain X, Wojcieszek J, Foroud T (2007) Are Cognitive Changes Progressive in Prediagnostic HD? *Cogn Behav Neurol* 20:212–218.
- Sun Y, Savanenin A, Reddy PH, Liu YF (2001) Polyglutamine-expanded huntingtin promotes sensitization of N-methyl-D-aspartate receptors via post-synaptic density 95. *J Biol Chem* 276:24713–24718.
- Swerdlow NR, Paulsen J, Braff DL, Butters N, Geyer MA, Swenson MR (1995) Impaired prepulse inhibition of acoustic and tactile startle response in patients with Huntington's disease. *J Neurol Neurosurg Psychiatry* 58:192–200.
- Tabrizi SJ, Langbehn DR, Leavitt BR, Roos RA, Durr A, Craufurd D, Kennard C, Hicks SL, Fox NC, Scahill RI, Borowsky B, Tobin AJ, Rosas HD, Johnson H, Reilmann R, Landwehrmeyer B, Stout JC (2009) Biological and clinical manifestations of Huntington's disease in the longitudinal TRACK-HD study: cross-sectional analysis of baseline data. *Lancet Neurol* 8:791–801.
- Tabrizi SJ, Scahill RI, Durr A, Roos RA, Leavitt BR, Jones R, Landwehrmeyer GB, Fox NC, Johnson H, Hicks SL, Kennard C, Craufurd D, Frost C, Langbehn DR, Reilmann R, Stout JC (2011) Biological and clinical changes in premanifest and early stage Huntington's disease in the TRACK-HD study: the 12-month longitudinal analysis. *Lancet Neurol* 10:31–42.
- Tabrizi SJ, Scahill RI, Owen G, Durr A, Leavitt BR, Roos RA, Borowsky B, Landwehrmeyer B, Frost C, Johnson H, Craufurd D, Reilmann R, Stout JC, Langbehn DR (2013) Predictors of phenotypic progression and disease onset in premanifest and early-stage Huntington's disease in the TRACK-HD study: analysis

- of 36-month observational data. *Lancet Neurol* 12:637–649.
- Tang A-H, Chen H, Li TP, Metzbower SR, MacGillavry HD, Blanpied TA (2016) A trans-synaptic nanocolumn aligns neurotransmitter release to receptors. *Nature* 536:210–214.
- Thompson CL, Pathak SD, Jeromin A, Ng LL, MacPherson CR, Mortrud MT, Cusick A, Riley ZL, Sunkin SM, Bernard A, Puchalski RB, Gage FH, Jones AR, Bajic VB, Hawrylycz MJ, Lein ES (2008) Genomic Anatomy of the Hippocampus. *Neuron* 60:1010–1021.
- Tu W, Xu X, Peng L, Zhong X, Zhang W, Soundarapandian MM, Belal C, Wang M, Jia N, Zhang W, Lew F, Chan SL, Chen Y, Lu Y (2010) DAPK1 Interaction with NMDA Receptor NR2B Subunits Mediates Brain Damage in Stroke. *Cell* 140:222–234.
- Usdin MT, Shelbourne PF, Myers RM, Madison D V. (1999) Impaired Synaptic Plasticity in Mice Carrying the Huntington’s Disease Mutation. *Hum Mol Genet* 8:839–846.
- van Duijn E, Kingma EM, van der Mast RC (2007) Psychopathology in Verified Huntington’s Disease Gene Carriers. *J Neuropsychiatry Clin Neurosci* 19:441–448.
- Van Raamsdonk JM, Pearson J, Rogers DA, Bissada N, Vogl AW, Hayden MR, Leavitt BR (2005a) Loss of wild-type huntingtin influences motor dysfunction and survival in the YAC128 mouse model of Huntington disease. *Hum Mol Genet* 14:1379–1392.
- Van Raamsdonk JM, Pearson J, Slow EJ, Hossain SM, Leavitt BR, Hayden MR (2005b) Cognitive dysfunction precedes neuropathology and motor abnormalities in the YAC128 mouse model of Huntington’s disease. *J Neurosci* 25:4169–4180.
- Virlogeux A, Moutaux E, Christaller W, Genoux A, Bruyère J, Fino E, Charlot B,

- Cazorla M, Saudou F (2018) Reconstituting Corticostriatal Network on-a-Chip Reveals the Contribution of the Presynaptic Compartment to Huntington's Disease. *Cell Rep* 22:110–122.
- Vonsattel J-P, Myers RH, Stevens TJ, Ferrante RJ, Bird ED, Richardson EP (1985) Neuropathological Classification of Huntington's Disease. *J Neuropathol Exp Neurol* 44:559–577.
- Wang X, Liu D, Huang H-Z, Wang Z-H, Hou T-Y, Yang X, Pang P, Wei N, Zhou Y-F, Dupras M-J, Calon F, Wang Y-T, Man H-Y, Chen J-G, Wang J-Z, Hébert SS, Lu Y, Zhu L-Q (2018) A Novel MicroRNA-124/PTPN1 Signal Pathway Mediates Synaptic and Memory Deficits in Alzheimer's Disease. *Biol Psychiatry* 83:395–405.
- Wexler NS et al. (2004) Venezuelan kindreds reveal that genetic and environmental factors modulate Huntington's disease age of onset. *Proc Natl Acad Sci* 101:3498–3503.
- Wood ER, Dudchenko PA, Eichenbaum H (1999) The global record of memory in hippocampal neuronal activity. *Nature* 397:613–616.
- Zhang H, Zhang C, Vincent J, Zala D, Benstaali C, Sainlos M, Grillo-Bosch D, Daburon S, Coussen F, Cho Y, David DJ, Saudou F, Humeau Y, Choquet D (2018) Modulation of AMPA receptor surface diffusion restores hippocampal plasticity and memory in Huntington's disease models. *Nat Commun* 9:4272.
- Zhen J, Qian Y, Weng X, Su W, Zhang J, Cai L, Dong L, An H, Su R, Wang J, Zheng Y, Wang X (2017) Gamma rhythm low field magnetic stimulation alleviates neuropathologic changes and rescues memory and cognitive impairments in a mouse model of Alzheimer's disease. *Alzheimer's Dement Transl Res Clin Interv* 3:487–

497.

- Zhou Z, Liu A, Xia S, Leung C, Qi J, Meng Y, Xie W, Park P, Collingridge GL, Jia Z (2018) The C-terminal tails of endogenous GluA1 and GluA2 differentially contribute to hippocampal synaptic plasticity and learning. *Nat Neurosci* 21:50–62.
- Zhu G, Liu Y, Wang Y, Bi X, Baudry M (2015) Different patterns of electrical activity lead to long-term potentiation by activating different intracellular pathways. *J Neurosci* 35:621–633.
- Zola-Morgan S, Squire LR, Amaral DG (1986) Human amnesia and the medial temporal region: enduring memory impairment following a bilateral lesion limited to field CA1 of the hippocampus. *J Neurosci* 6:2950–2967.
- Zola-Morgan SM, Squire LR (1990) The primate hippocampal formation: evidence for a time-limited role in memory storage. *Science* 250:288–290.
- Zuccato C, Ciammola A, Rigamonti D, Leavitt BR, Goffredo D, Conti L, MacDonald ME, Friedlander RM, Silani V, Hayden MR, Timmusk T, Sipione S, Cattaneo E (2001) Loss of Huntingtin-Mediated BDNF Gene Transcription in Huntington's Disease. *Science* (80-) 293:493–498.
- Zuccato C, Tartari M, Crotti A, Goffredo D, Valenza M, Conti L, Cataudella T, Leavitt BR, Hayden MR, Timmusk T, Rigamonti D, Cattaneo E (2003) Huntingtin interacts with REST/NRSF to modulate the transcription of NRSE-controlled neuronal genes. *Nat Genet* 35:76–83.

